PERFORMANCE CHARACTERIZATION OF A MEDIUM-DUTY DIESEL ENGINE WITH BIO-DIESEL AND PETROLEUM DIESEL FUELS

A Thesis

by

JASON ESQUIVEL

Submitted to the Office of Graduate Studies of
Texas A&M University
in partial fulfillment of the requirements for the degree of

MASTER OF SCIENCE

December 2008

Major Subject: Mechanical Engineering

PERFORMANCE CHARACTERIZATION OF A MEDIUM-DUTY DIESEL ENGINE WITH BIO-DIESEL AND PETROLEUM DIESEL FUELS

A Thesis

by

JASON ESQUIVEL

Submitted to the Office of Graduate Studies of
Texas A&M University
in partial fulfillment of the requirements for the degree of

MASTER OF SCIENCE

Approved by:

Chair of Committee,	Timothy J. Jacobs
Committee Members,	N.K. Anand
	Yassin A.Hassan
Head of Department,	Dennis O'Neal

December 2008

Major Subject: Mechanical Engineering

ABSTRACT

Performance Characterization of a Medium-Duty Diesel Engine with Bio-Diesel and Petroleum Diesel Fuels. (December 2008)

Jason Esquivel, B.S., The Florida State University

Chair of Advisory Committee: Dr. Timothy J. Jacobs

In the wake of global warming and fossil fuel depletion, renewed attention has been paid to shifting away from the use of petroleum based fuels. The world's energy demand is commencing its dependency on alternative fuels. Such alternative fuels in use today consist of bio-alcohols (such as ethanol), hydrogen, biomass, and natural oil/fat derived fuels. However, in this study, the focus will be on the alternative fuel derived from natural oils and fats, namely biodiesel.

The following study characterizes the performance of a medium-duty diesel engine fuelled with biodiesel and conventional diesel. The objective is accomplished by taking measurements of manifold pressure and temperature, fuel flow, air flow, and torque. The study first characterizes a John Deere 4.5 liter 4 cylinder direct injection engine with exhaust gas recirculation (EGR), common rail fuel injection, and variable turbo-charging with conventional petroleum diesel to set a reference for comparison. The study then proceeds to characterize the differences in engine performance as a result of using biodiesel relative to conventional diesel.

The results show that torque decreases with the use of biodiesel by about 10%. The evaluation of engine performance parameters shows that torque is decreased because of the lower heating value of biodiesel compared to conventional diesel. The insignificant difference between the other performance parameters shows that the ECM demands the same performance of the engine regardless of the fuel being combusted by the engine.

DEDICATION

This thesis is in dedication to my parents, Candy and Carlos Esquivel, who have always supported me in my journey through life. Thanks Mom and Dad for the guidance, confidence, and means to proceed with my dreams.

ACKNOWLEDGEMENTS

This thesis has been a long time coming and a lot of work has been put in to getting to this point. I could not have done this by myself and I would like to thank those people who have made it possible.

I would first like to thank Dr. Tim Jacobs for taking a chance on me and letting me work in his research group. Your mentorship has meant a great deal and I have learned a lot.

I want to thank my partner in crime, Brandon Tompkins. We built the non-existent lab at Texas A&M University in 103 Thompson Hall from the ground up. The lab space we came into had nothing but an old dyno, a big resistor bank, and a test bed. The lab you see today is through our efforts.

I would also like to thank several professors along the way who have helped me succeed. First, I would like to thank Dr. Annamalai for helping to further my studies both as his TA for Thermal Fluid Sciences and help with course materials. Second I would like to Dr. Anand and Dr. Lau for helping me when I had academic troubles and seeing me through. Last but not least, I would like to thank Dr. Alvarado for sitting in on my committee on such short notice.

Special thanks go to the guys in the shop, Johnny Hallford and Mike Walker, for their help in giving us guidance in setting up and building the lab. Last but not least comes all my friends who have been there along the way. There are too many to list but you are always in my heart, thanks to everyone for their support.

ABBREVIATIONS/NOMENCLATURE

AERL	Advanced Engine Research Laboratory
BSFC	Brake Specific Fuel Consumption
CO	Carbon Monoxide
CO_2	Carbon Dioxide
CPO	Compressor Pressure Out
cSt	Centistokes
CTO	Compressor Temperature Out
DC	Direct Current
Dyno	Dynamometer
ECM	Engine Control Module
EES	Engineering Equation Solver
EGR	Exhaust Gas Recirculation
EMP	Exhaust Manifold Pressure
F/A	Fuel-Air Ratio
H_2O	Water
HC	Hydrocarbons
HHV	Higher Heating Value
IMP	Intake Manifold Pressure
IMT	Intake Manifold Temperature
LFE	Laminar Flow Element
LHV	Lower Heating Value

M_{air}	Molecular Weight of Air
M_f	Molecular Weight of the Fuel
NDIR	Non-Dispersive Infrared
NO	Nitric Monoxide
NO_2	Nitric Dioxide
O_2	Oxygen
O_3	Ozone
PMEP	Pumping Mean Effective Pressure
PPM	Parts Per Million
PTO	Power Take Off
Q_{LHV}	Lower Heating Value of Fuel
TPO	Turbine Pressure Out
TTI	Turbine Temperature In
TTO	Turbine Temperature Out
VGT	Variable Geometry Turbo-Charger
V_d	Displacement Volume
$\rho_{a,i}$	Density of Air at Intake Manifold
η_{fc}	Fuel Conversion Efficiency
η_v	Volumetric Efficiency

TABLE OF CONTENTS

Page

Page

LIST OF FIGURES

Page

Page

Page

Page

Page

Page

LIST OF TABLES

Page

1. INTRODUCTION

The purpose of the internal combustion engine is to take chemical energy stored in a fuel and convert it to mechanical energy. This mechanical energy can be used in many different forms from propelling a vehicle forward to generating electricity. The internal combustion engine as it is known today was first developed in the 1860's. J.J.E. Lenoir developed the first marketable commercial engine burning coal-gas air mixtures [1]. Nicolaus Otto improved on this idea with an "atmospheric engine" which used the pressure rise resulting from combustion of a fuel-air charge in the outward stroke to accelerate a free piston and rack assembly [1]. The free piston would create a vacuum in its cylinder where then atmospheric pressure would force the piston inward while engaged to the output shaft [1]. This engine also had its shortcomings and to overcome them Otto proposed an engine cycle with four piston strokes. Of course, this engine cycle is still used today in modern internal combustion engines.

In 1892, a German engineer named Rudolf Diesel developed an internal combustion engine that uses compression ignition to combust fuel. His engine consisted of drawing air into a chamber which was solely heated by the compression of the piston in the cylinder. The fuel is then introduced near the end of the compression stroke into the high temperature and pressure air and mixes. Auto-ignition commences at different points in the mixture of vaporized fuel and high temperature air when the appropriate

---

This thesis follows the style of Journal of Engineering for Gas Turbines and Power.

composition is attained for combustion. Fuel-air mixing therefore plays an important role in diesel fuel combustion. This type of combustion in an engine is known as compression ignition. The fuel-air charge is compressed in order to start combustion hence "compression ignition". This type of internal combustion engine which uses compression ignition is called a diesel engine after its developer Rudolf Diesel.

In the wake of global warming and fossil fuel depletion, renewed attention has been paid to shifting away from the use of petroleum based fuels. The world's energy demand is commencing its dependency on alternative fuels. Such alternative fuels in use today consist of bio-alcohols (such as ethanol), hydrogen, biomass, and natural oil/fat derived fuels (such as biodiesel). Other alternative means of energy production come from using the earth's natural phenomena such as wind, tidal flow, river flow, and geothermal activity to generate power. However, in this study, the focus will be on the alternative fuel derived from natural oils and fats, namely biodiesel. Biodiesel is the alternative fuel in this country and Europe receiving attention for use in compression ignition engines.

Oils and fats from different feedstocks can be used in compression ignition engines. A feedstock is the raw material from which oils and fats are derived. Rapeseed, soybean, cottonseed, linseed, and peanut are common feedstocks. Complications do come with the direct use of these oils and fats within an engine. They can cause severe injector coking, piston ring sticking, and engine deposits which will render the engine inoperable [2]. The oils or fats can be chemically converted so that their properties are viable for use within a diesel engine. This process of conversion is called

transesterification. Transesterification is a reaction between one ester (triglyceride) of one alcohol (glycerin) and a second alcohol (methanol) to form an ester of the second alcohol (methyl ester) [3,4]. The oils or fats now can be classified as a biodiesel after the transesterification process.

Biodiesel has different fuel properties compared to its petroleum diesel counterpart. Examples of these fuel properties are cetane number, heating value, density, viscosity, and bulk modulus. Each respective fuel property changes the combustion and performance characteristics of biodiesel compared to diesel. However, this study will focus on the change of performance characteristics compared to conventional diesel fuel.

The first fuel property impacting the performance characteristics of biodiesel used to fuel a diesel engine is its heating value. The heating value of a fuel is defined as the energy released from the complete combustion of a fuel which is returned to the standard reference state. Complete combustion refers to all the carbon in the fuel being converted to carbon dioxide (CO_2) and all the hydrogen converted to water (H_2O). Basically, the heating value is how much energy is stored in the fuel, before combustion, for a unit mass of fuel. The heating value of a fuel affects the combustion of the fuel in the cylinder; thus affecting the temperature and pressure that an air-fuel charge produces inside the cylinder. Furthermore, the pressure in the cylinder affects the performance of the engine, characterized by its torque. Increased in-cylinder pressure will produce higher amounts of torque. In-cylinder pressures developed from biodiesel combustion are generally lower than that from petroleum diesel combustion [3]. Thus biodiesel produces lower torque, and thus power, compared to petroleum diesel [5]. Along with

torque, the brake specific fuel consumption (BSFC) of the bio-fuelled engine increases to compensate for the lower heating value of the fuel to maintain the same level of torque [2,5,6,7,8].

Fuel cetane number is a measure of the ignition quality or how readily the fuel will ignite. A higher cetane number indicates a shorter ignition delay for the fuel. Ignition delay is the time between the start of fuel injection and the start of combustion. Cetane numbers for biodiesel have been found to be higher than diesel fuel. This translates to shorter ignition delays for biodiesel [3,6,9]. The shorter ignition delay of the fuel corresponds to an advanced start of combustion.

The bulk modulus of a fuel has an effect on the injection characteristics of the fuel. The bulk modulus of compressibility is a measure of how much a unit of the fluid volume can be decreased when increasing the pressure working on it [6]; a higher bulk modulus indicates a lower change in volume with increase in pressure (less compression). Biodiesel has a higher bulk modulus than conventional diesel [6,9], meaning it is more incompressible than diesel. Therefore, biodiesel reaches the injection pressure sooner than diesel. This results in an earlier start of fuel injection. In turn, this will advance the start of combustion in comparison to diesel.

The combination of both shorter ignition delays and advanced fuel injection will advance the start of combustion. These two fuel property effects control when the peak pressure will occur. The pressure curve is shifted to the left and diminishes the in-cylinder peak pressure effects that manifest the torque of the engine.

The objective of this research is to compare the performance characteristics of biodiesel and a petroleum based diesel fuel in a medium-duty diesel engine. Previous studies have given fuel properties and their possible effect on performance. They have given a qualitative view of lower power, higher fuel consumption, and lower peak torque compared to diesel [2,3,4,5,9,10]. One study gives a reduction in power of 5% for biodiesel compared to petroleum diesel at rated power [5]. Other studies have given a range of 5-10% decrease in torque using different types of biodiesel [3,11]. The objective of this research will be accomplished by taking measurements of manifold pressure, temperature, fuel flow, air flow, and torque to characterize the differences in performance of each fuel within a John Deere 4.5 liter 4 cylinder direct injection engine with exhaust gas recirculation (EGR), common rail fuel injection, and variable turbo-charging.

2. EXPERIMENTAL SETUP AND METHODOLOGY

2.1 Test Engine

The Advanced Engine Research Laboratory (AERL) at Texas A&M University has been newly commissioned for engine experimental research. The facility is equipped with a medium-duty diesel engine, the specifications of which are shown in Table 1. The medium-duty diesel engine is a John Deere 4.5 liter in-line 4 cylinder direct injection engine with exhaust gas recirculation (EGR), common rail fuel injection, and variable geometry turbo-charging (VGT). The layout of the engine can be seen in Figure 5.

Table 1: Specifications of John Deere 4045 DI Diesel Engine

Designer / Manufacturer	John Deere
Number of Cylinders	4
Displacement – L (cu.in.)	4.5 (275)
Bore – mm (in)	106 (4.19)
Stroke – mm (in)	127 (5.00)
Compression Ratio	17.0 : 1
Rated Power – kW (hp) @ 2400 rpm	115 (154)
Peak Torque – N-m (ft-lb) @ 1400 rpm	575 (424)
Number of Valves / Cylinder	4
Fuel System	High pressure common rail, direct injection
Air System	Variable geometry turbo-charger (VGT) with exhaust gas recirculation (EGR)

2.1.1 Engine Fuel System

The fuel system of the engine commences with a pre-filter which screens particles from the incoming fuel. The pre-filter is located on the suction side of the mechanical transfer pump which uses an eccentric lobe on the engine camshaft to

operate. A pushrod between the lobe and the pump lever transfers a linear up and down motion causing fuel to flow through the transfer pump. The fuel exiting the mechanical transfer pump enters a second filter element further filtering the fuel with a 5-micron filter and exits to the high pressure fuel pump. At the Denso HP3 high pressure fuel pump, the fuel is pressurized and delivered to the high pressure common rail. The pressurized common rail is now available to deliver fuel to each of the electronic injectors located inside the cylinder head demanded by the engine control module (ECM).

The electronic fuel injector is shown in Figure 1 for the engine in this study. The amount of fuel delivered to the cylinder is in direct proportion to the amount of time current is supplied to the injector electromagnetic valve. Fuel enters the electronic injector at the fuel inlet (identified as Item C). During a non-injection period, the fuel enters the control chamber (Item G) causing the hydraulic pressure of the fuel to push the needle down to close the nozzle. The high pressure fuel from the common rail is held inside the nozzle (Item F) until injection.

Injection begins when a signal from the ECM supplies a current to the injector electromagnetic valve. The electromagnetic force pulls the solenoid valve (Item B) up, causing the orifice seat (Item D) to open. The fuel in the control chamber (Item G) is released and flows out the fuel leak off line (Item E) to the engine fuel return line. The hydraulic pressure has been released off of the piston allowing the nozzle to open with the upward force of the valve spring (Item H). The fuel now flows through the nozzle at the pressure of the common rail.

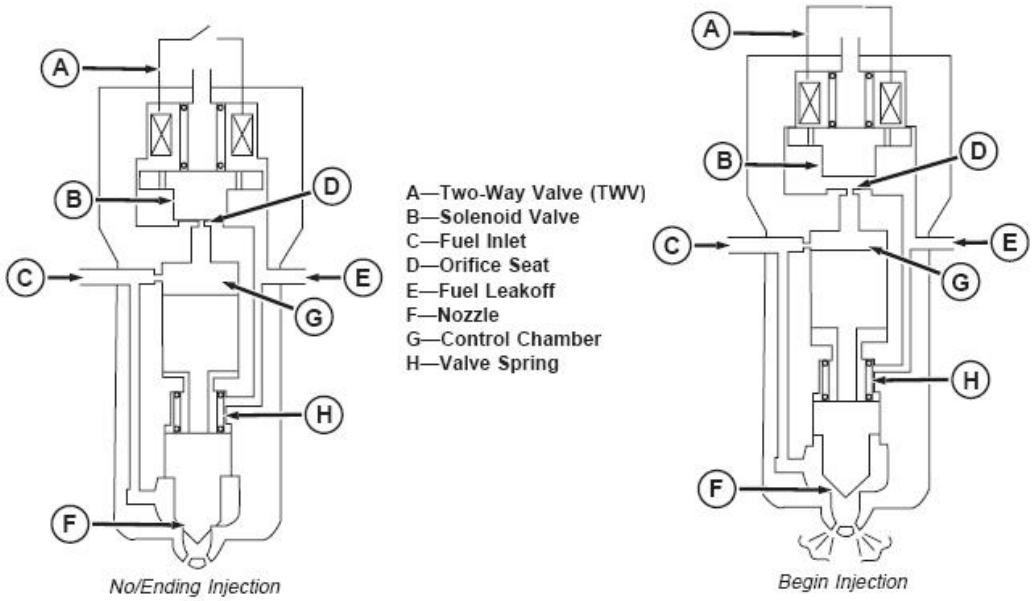

Figure 1: Cross-sectional drawing of typical injector used in John Deere 4045 Diesel Engine for (left) non-injecting and (right) injecting actions [12].

Injection ends when the signal from the ECM and the current supplied to the injector electromagnetic valve ceases. The solenoid valve (Item B) is forced down causing the orifice seat (Item D) to close. The control chamber (Item G), again, fills with high pressure fuel causing the hydraulic piston to push the needle down and close the nozzle (Item F). This completes the injection process.

2.1.2 Variable Geometry Turbo (VGT)

The engine in this study employs two features to enhance both performance and emissions control. These two features are EGR and VGT. The description of the turbocharger being variable is due to the fact that adjustable vanes change flow kinetics

across the turbine blades based on engine speed and load demand. Adjustment of vane position serves a dual purpose, not only to drive the compressor, but to drive the EGR and fresh air mixing. Figure 2 shows a sketch of the VGT and EGR system accomplishing this dual purpose.

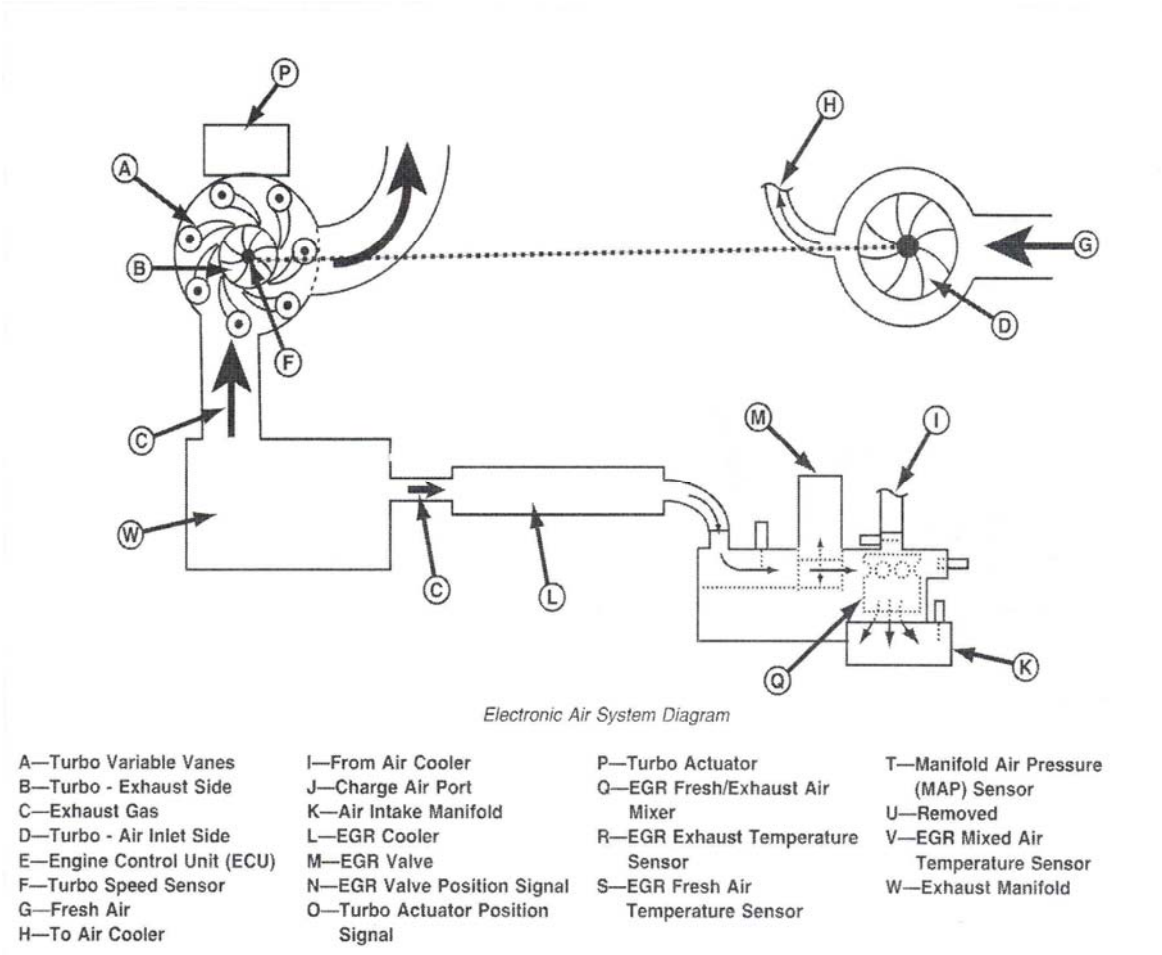

Figure 2: Schematic of VGT and EGR system of the John Deere 4045 DI Engine [12].

As the engine's load and speed demands increase, the ECM sends a signal to the VGT actuator to rotate the vanes located on pins on the outside diameter of the turbine

wheel. As these vanes close, the flow kinetics change across the turbine blades increasing the momentum from the exhaust gases to drive the compressor. The compressor is now able to increase engine boost or pressure of the incoming air to increase the power output of the engine. Another consequence of the vanes closing is an increase in exhaust manifold pressure. The flow past the vanes is hindered thus creating a pressure increase in the manifold. The pressure increase in the exhaust manifold is the driving force of EGR flow to the intake manifold. An EGR valve, located in the intake manifold, controls the mixture of the cooled exhaust gases with intake air. The EGR flow passes through a heat exchanger surrounded by engine coolant before arriving at the EGR valve. The EGR valve is operational only when the engine is under load and at a predetermined engine coolant operating temperature.

2.2 Test Fuels

The objective of this study is characterizing the differences in performance of the John Deere 4045 engine with two different fuels. The two fuels used for comparison in this study are biodiesel and a petroleum based certification fuel which is representative of conventional diesel fuel. The known properties of these two fuels are given in Table 2. The biodiesel manufacturer did not disclose the methyl ester feedstock or any other property that can distinguish the fuel from conventional diesel. Therefore, a determination of biodiesel fuel properties is needed to characterize the biodiesel fuel. The properties obtained for this study are the density and heating value of the biodiesel. These two properties will be discussed later and their importance to this study.

The heating value is obtained by a constant volume bomb calorimeter at the Bio Energy Testing and Analysis Laboratory at Texas A&M University. The gross heating value analysis of both the biodiesel and conventional diesel is shown in Table 5 of Appendix B. A constant volume bomb calorimeter is used to determine the gross heating value of both fuels. The fuel is placed in a stainless steel container which is immersed in water. The temperature rise of the water and calorimeter is measured. A sufficient amount of water is used to condense all the water produced in the chemical reaction. Thus, the gross heating value or the heating value measured has water in the products of combustion condensed to a liquid. A more useful property is the net heating value of the fuel which is used to calculate engine performance characteristics such as fuel conversion efficiency. The net heating value of the fuel, or the heating value of which the water in the products of combustion is in vapor form, is determined by subtracting the product of water latent heat of vaporization and the ratio of mass of water to mass of fuel from the gross heating value. The calculation of the net heating value can be seen in Appendix A and is explained later in the data analysis section.

The density is obtained at the Advanced Engine Research Laboratory (AERL) at Texas A&M University. Samples of different volumes are taken with a graduated cylinder and weighed where an average can then be taken to obtain the biodiesel density.

Table 2: Ultra Low Sulfur 2007 Diesel and Biodiesel Properties

Properties	Diesel 2007 ULS	Biodiesel
Density (kg/m^3)	845.1	874
Net Heating Value (MJ/kg)	42.240	37.691
Gross Heating Value (MJ/kg)	45.095	40.287
Sulfur (ppm)	8.2	-
Viscosity (cSt)	2.1	-
Cetane #	44	-
Hydrogen (wt%)	13.1	-
Carbon (wt%)	86.9	-

2.3 Test Cell Instrumentation

Instrumentation in the research facility includes test cell ambient conditions (barometric pressure, temperature, and humidity), engine manifold pressures and temperatures, fuel and air flow rates, gaseous exhaust and intake speciation, and engine speed and torque. A schematic of the test cell layout is shown in Figure 3.

Engine fueling commences at the fuel storage cabinet where 55-gallon drums of fuel of both biodiesel and conventional diesel are stored. A pump provides the necessary head to deliver the fuel in the drums to the fuel metering system. An inline fuel filter is downstream of the fuel pump to filter out any foreign bodies from entering the fuel metering system. The fuel proceeds to enter the fuel metering system. A schematic of the fuel metering system is provided in Figure 4.

The fuel metering system consists of a Max Machinery vapor eliminator, fuel meter, and a level controller. The fuel first enters the vapor eliminator. The vapor eliminator eliminates any bubbles entrained in the fuel from the pumping of fuel into the metering system. The bubbles can come from air in the lines or fuel that has vaporized in

the lines. These bubbles cause measurement errors as they pass through the flow meter. Second, the fuel flow enters the flow meter. The flow meter is a positive displacement meter with four pistons and cylinders arranged in a radial fashion around a central crankshaft. The piston's movement, due to the pumping of the fuel in and out of the cylinder, is converted to a circular motion at the central crankshaft. The central crankshaft is coupled to a magnet and the motion is sensed and converted into a signal. The fuel meter's stated accuracy is 0.5% of the reading. A maximum fuel flow rate measured in testing is about 6 g/s. The fuel flow measurement is therefore within a maximum of .03 g/s of the true value. After the fuel flow meter, the fuel flows into the level controller. The level controller is a vented recirculation tank which collects fuel returning from the engine and routes it back to the engine. The level controller maintains its level through a float valve that controls the fuel flow through the flow meter.

The dynamometer (dyno) measures the amount of mechanical work produced by the engine, namely torque. A few types of dynamometers can be used to obtain torque measurements; the AERL uses a direct current (DC) electric dyno. The dyno obtains torque measurements by applying a braking force or load on the engine shaft connected to the dyno. The dyno controller applies a current to the dyno, setting the applied braking force on the rotor by the housing or stator of the dyno. The amount of current supplied to the dyno controls the amount of braking force applied to the rotor. The force induced on the stator by braking the rotor is measured with a load cell connected to the dyno housing. The load cell force is then multiplied by the distance from the applied force to the center of the rotor giving the measured torque produced by the engine.

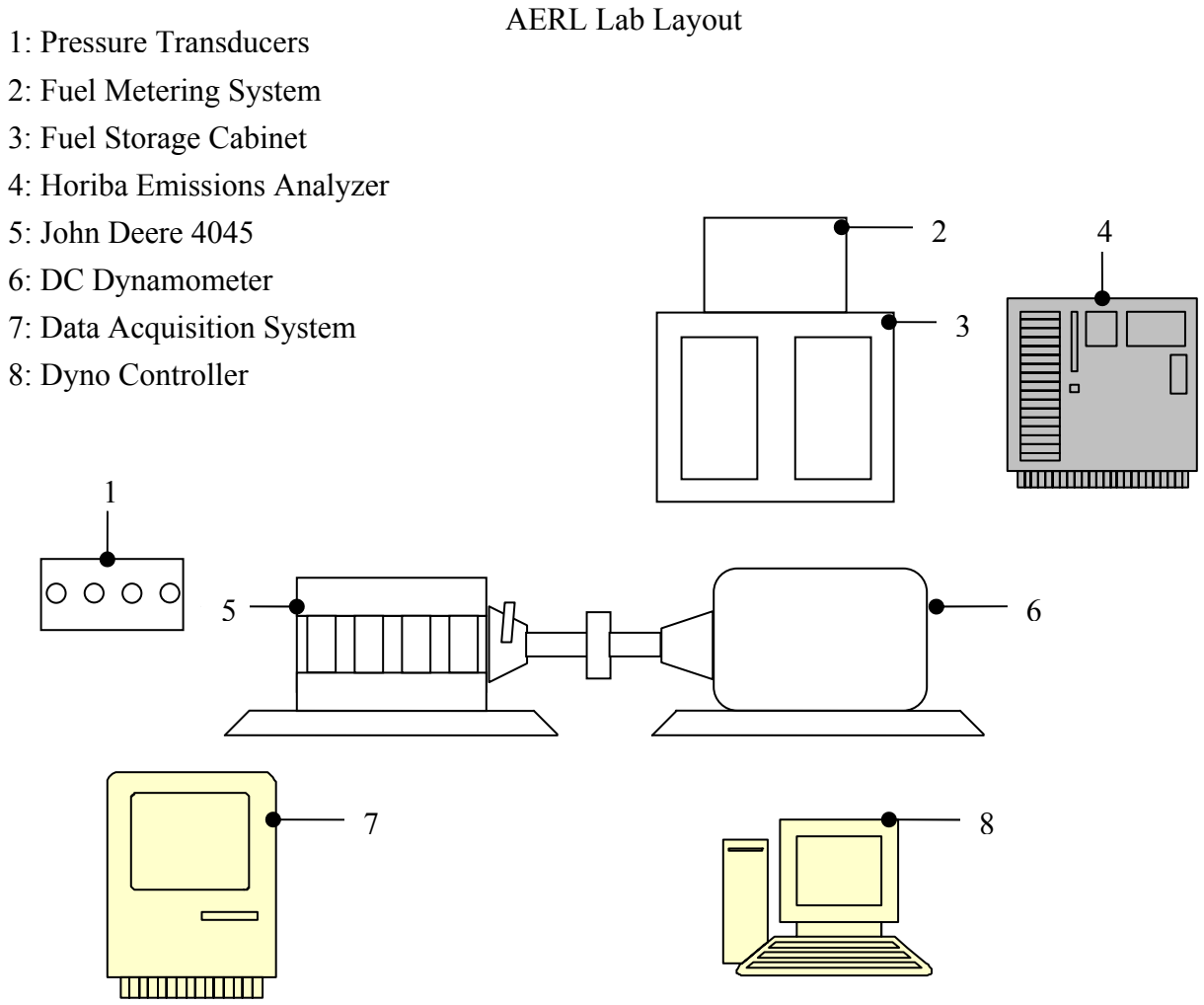

Figure 3: Schematic of AERL engine lab layout.

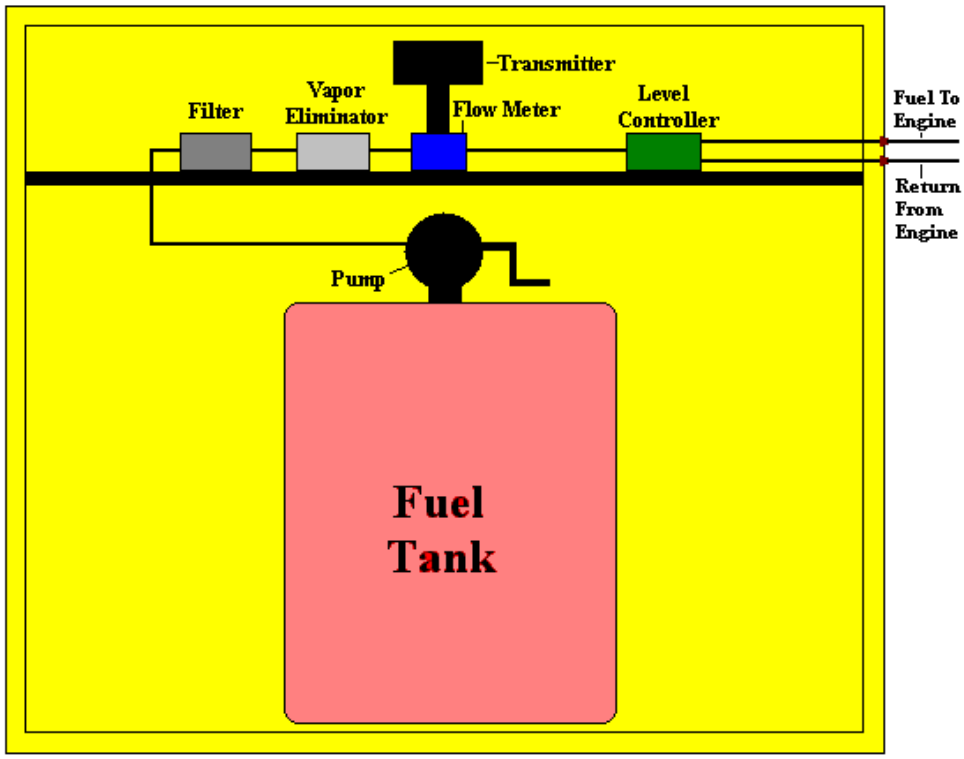

Figure 4: Schematic of fuel metering system including fuel storage tank and fuel filter.

Engine load and speed are controlled by the dyno, therefore engaging the engine driveshaft to the dyno rotor is critical. The engine is coupled to the DC electric dyno through a driveshaft and power take off (PTO) system. The PTO, basically a clutch system, engages the engine drive shaft to the dyno rotor and is disengaged for engine startup and warm-up.

Air flow induced by the VGT to the engine is determined from a Meriam laminar flow element (LFE) model 50MC2-4. A bundle of capillary tubes is housed within the LFE and pressure difference measurements are taken at the inlet and exit of the bundle of capillary tubes. The capillary tubes induce a laminar flow condition within each of the

tubes. The Hagen-Poiseuille formula gives the relationship between the pressure drop across the laminar flow in capillary tubes and the volumetric flow rate. The pressure drop is directly proportional to the volumetric air flow rate passing through the LFE. The air flow rate also depends on the viscosity of the air which is a strong function of temperature. Air temperature is taken at the air filter intake, shown in Figure 5, to capture the temperature directly at the point of entry into the air system. The calibration curve of the flow rate of this particular LFE is integrated into Lab View taking the pressure differential and temperature inputs to give a mass flow rate.

Pressure measurements are critical to characterizing engine operation between the two fuels used in this study. Four points on the engine are modified for pressure transducer placement. The placement of the pressure transducers consist of post-compressor, pre- and post-turbine, and the intake manifold.

Figure 5 shows the engine layout and the pressure transducer placement on the engine. Pressure measurements are taken with an Omega strain gauge pressure transducer model PX309-050A5V which gives pressure measurements in absolute pressure units. The stated accuracy of the pressure transducer is 2% of the full scale output, where the full scale output of this transducer is 50 psi. Thus, the pressure of the transducer is within 1 psi or .0689 bar of the true value.

Temperature measurements also characterize engine operating conditions. Temperature, as pressure, plays an important role in the VGT performance providing the necessary charging effect demanded by the ECM. Temperatures are measured by a Temprel shielded K-type thermocouple at roughly the same aforementioned locations as

pressure which is shown in Figure 5. The stated accuracy of the thermocouple is .4% of the reading. The greatest temperature taken was about 600 °C, thus giving the greatest temperature to be within 2.4 °C of the true value.

The Horiba emissions bench measures the gaseous emissions of the engine both from the exhaust and the intake manifold. The intake manifold gaseous emissions characterize the use of EGR for the engine in this study. The emissions bench houses analyzers for the measurement of CO, CO_2, O_2, and NO.

Emission gases CO and CO_2 are measured with a non-dispersive infrared (NDIR) analyzer. This analyzer uses the infrared absorption principle of gases. An infrared light source emits infrared energy into the sample of gas. The sample gas of interest absorbs a particular frequency of the infrared spectrum. An infrared detector is set to detect a specific infrared wavelength matching the gas of interest. The amount of infrared light that enters the detector is then compared to the light detected in the reference cell to give a concentration from the absorption characteristics of that gas.

NO is measured with a chemiluminescence detector. Chemiluminescence is the emission of light as the result of a chemical reaction between ozone (O_3) and NO. The reaction produces NO_2 in the excited state and as NO_2 returns to its normal state, light photons are emitted. The emitted light photons are counted by a photomultiplier and are proportional to the NO concentration.

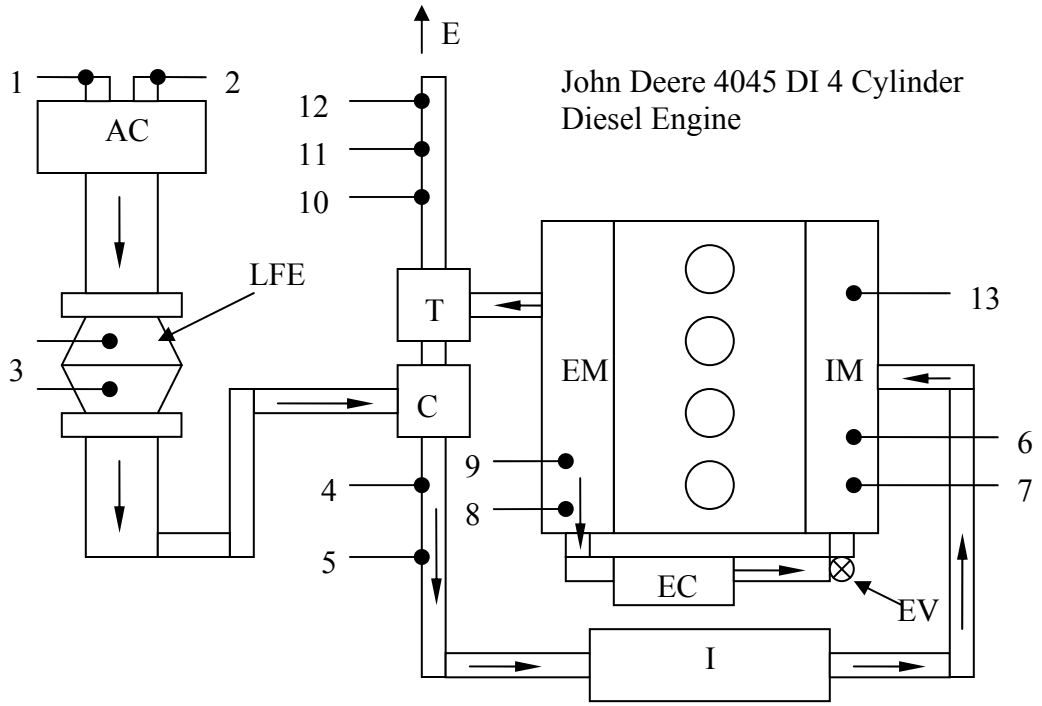

AC: Air Cleaner
LFE: Laminar Flow Element
C: Compressor of VGT
I: Intercooler
EC: EGR Cooler
EV: EGR Valve
T: Turbine of VGT
E: Exhaust
EM: Exhaust Manifold
IM: Intake Manifold

1: Temperature and Humidity
2: Barometer
3: LFE Pressure Sensor
4: Compressor Temperature Out
5: Compressor Pressure Out
6: Intake Manifold Temperature
7: Intake Manifold Pressure
8: Exhaust Manifold Temperature
9: Exhaust Manifold Pressure
10: Turbine Temperature Out
11: Turbine Pressure Out
12: Emission Sample Point
13: Intake CO2 Measurement

Figure 5: Schematic of engine layout and location of measurements

A magneto pneumatic analyzer is used to measure the O_2 concentration. Oxygen is a paramagnetic gas and when placed in a magnetic field oxygen becomes magnetized. An uneven magnetic field is applied as the sample of gas enters the analyzer. Oxygen, being magnetized in the magnetic field, is pulled to the stronger side of the magnetic field and pressure rises on that side. A non-magnetic gas is used to produce a pressure rise outside the magnetic field. The difference in pressure is proportional to the concentration of the oxygen.

2.4 Test Procedure

As mentioned previously, the objective of this research is to compare the performance characteristics of biodiesel and diesel fuels in a medium-duty diesel engine. A nine-point test matrix, summarized in Table 3, serves as the base set of engine conditions for the assessment of fuel performance characteristics. All the aforementioned measurement capabilities are recorded while conducting this test matrix repeatedly several times. The points were chosen to give several load conditions at each operating speed; a low load case and two mid load cases.

The inconsistent loads between study operating speeds, shown in Table 3, are due to poor dyno performance at low speed high load conditions, EGR induction transition points, and the engine load seen at the high engine speed with no load from the dyno. The first inconsistent operating point of the test matrix is due to the dyno not holding an engine load of 75% at the low engine speed which leads to the operating point being tested at 70% load. At mid load points, a transition point is seen where the engine operating point reaches a coolant temperature in which EGR either flows or is

discontinued to flow. The point switches back and forth leading to different air flow rates. This transition point at high speed gives inconsistent data, thus the load increase at this operating point. Lastly, the engine load starts above 20% for the high speed case leading to an operating point of 30%. Therefore, these points are chosen to give the study consistency in comparing engine performance trends.

Table 3: Engine Study Operating Points

Speed	Load %
1400	20, 60, 70
1900	20, 60, 75
2400	30, 65, 75

The emissions bench is calibrated before commencement of any engine testing or recalibration after one full test matrix has been completed. This ensures the emission bench acquires repeatable data. The emission bench calibration starts with setting all emission analyzers to zero on the control board. Zero is the flow of nitrogen gas through the analyzers. The nitrogen gas is inert and effectively cleans out the analyzer to give a true reading of zero. Once the analyzers are at zero, a span gas is sent through each analyzer. The span gas is specific to each analyzer and with a known concentration calibration is completed by dialing in the known concentration. After the analyzers are calibrated the emissions bench is set to take samples of the engine's emissions and take data of the set stabilized engine point.

After the dyno and dyno controller procedure is followed to prepare for engine testing (procedure is located in Appendix) and the test facility prepared to take data, the

engine warm up is started. Engine warm up commences with a 2-3 minute idle period. After the idle period, the engine is brought up to 1200 rpm and 30% load. This speed and load is set for about 20 minutes or until the coolant temperature of 130°F is reached.

After engine warm up is completed, the engine study points are set according to the test matrix in Table 3. Before taking data, the study point has to stabilize. Stabilization comes with steady coolant and exhaust manifold temperatures. The data is then taken when these parameters stabilize. A data log is set up to record 150 sample points and done twice at each study point. Two data logs are taken to get both the gaseous emissions from the exhaust and the intake manifold. Two data logs have to be taken because exhaust emissions and intake manifold gas speciation cannot be done at the same time. The gaseous emissions from the intake are taken for indication of EGR in the manifold at a particular operating point. After data logging is completed, a review of the data is taken to verify the stabilization of the test operating point. If large fluctuations occur this indicates that the engine was not fully stabilized, the data point is retaken. The full test matrix is completed in the same manner. Full engine test matrices are performed twice a day to test in changing atmospheric conditions.

After all data logging is completed, the test facility is shutdown. The engine is disengaged from the dyno and allowed to cool down to protect the VGT. The turbine temperatures are monitored until they reach a suitable temperature for engine shut off. All systems are now able to be taken offline and turned off to ensure proper shutdown of the facility.

2.5 Data Analysis

2.5.1 Uncertainty Analysis

As with any experimentation, uncertainty is associated with any measured performance of an experiment. Thus, a determination of the true value is seldom known and an estimate of its uncertainty is required. The sources of measurement uncertainty come from bias and precision error. The bias error is an estimate of the magnitude of the fixed error or constant error. The precision error is an estimate of the scatter of the measurements from its true value by random errors.

The bias error or an error introduced because of calibration is known from the manufacturer's stated specification of accuracy for each of the instruments. Table 4 shows the known specifications of accuracy given by the manufacturer. The accuracy of these instruments is the difference between the measured and true value as seen by the manufacturer. Another source of bias error comes from systematic errors of the data acquisition system. This error is always present and as the name states is biased and will give uncertainty from the true value. Another bias error that is seen, especially for the laminar flow element air flow measurement, is from human error. The difference in pressure had to be measured and the value taken from a water manometer. Thus, this was a bias error due to the measurement being taken from a single operator each time.

The precision error or random errors can be caused from many different sources for each of the parameters measured and calculated. The torque measurements of the engine are influenced by the ambient conditions in the cell (ie. humidity, barometric pressure, temperature). Temperature measurements are influenced by the spatial

variations of temperature in the intake or exhaust manifold, sensor location, or a combination of both. Another error is the repeatability of the engine operating condition. In other words, the engine operating point was not repeated either by not getting the exact engine speed or load of previous points. These are all examples of precision errors seen in this study. All these errors and the capabilities of this facility have been previously documented. It was demonstrated that the measurement capabilities of this facility are repeatable and have low uncertainty [13].

Table 4: Accuracy Specifications of Instrumentation Stated by Manufacturer

Instrumentation	Accuracy
Max Machinery Fuel Flow Meter	0.5% of reading
Omega Strain Gauge Pressure Transducer	2% of full scale output
Temprel K-type Thermocouple	0.4% of reading

As mentioned earlier, a data log is set to take data from a stabilized study point. All of the test cell instrumentation previously mentioned is logged in the data test log. The data collected for each parameter over the 150 points taken is averaged. The standard deviation of these 150 points is also taken. The standard deviation measures the spread from the average of the 150 points. As mentioned earlier, the stabilized study point was said to be stabilized by having a small standard deviation. The average of each test performed is then averaged to get a final average of the parameters for a particular study point. The uncertainty of a parameter for a study is calculated by taking the standard deviation of the four tests and multiplying it by two. This gives a 95% probability that a large number of readings for the parameter of interest will lie within

the uncertainty band of the true value. The reported uncertainty is shown in each graph by uncertainty bars placed on each corresponding study point. The max uncertainty is reported in the figure caption and denotes the maximum uncertainty seen on the graph. The other study point's uncertainties are less than this maximum uncertainty.

2.5.2 Calculated Parameters

Helping to further characterize the differences between biodiesel and conventional diesel, the collected data is used to calculate parameters that measure engine performance. These engine performance parameters consist of brake specific fuel consumption (BSFC), fuel conversion efficiency, volumetric efficiency, power and pumping mean effective pressure (PMEP).

The first calculated parameter discussed is power. Power is a measure of the rate at which work is produced by the engine. It is calculated by multiplying a factor of 2π to the product of torque and rotational engine speed. The power calculated in kilowatts is further used in other calculated engine performance parameters. One such parameter is BSFC. BSFC is a measure of how efficiently an engine is using the fuel supplied to produce work. BSFC is calculated by taking the mass flow rate of fuel in grams per second and dividing it by the power produced by the engine in kilowatts. BSFC is given in units of grams per kilowatt-hour.

A second parameter that uses power in its calculation is the fuel conversion efficiency. Fuel conversion efficiency measures how well the energy supplied to the engine is being released by combustion in the cylinder. It is calculated by dividing the power produced by the multiplication of fuel mass flow rate and the lower heating value

of the fuel. The lower heating value of the fuel is determined from a bomb calorimeter as explained earlier in this methodology section. The bomb calorimeter gives the higher heating value of the fuel as explained earlier. Thus, the lower heating value (LHV) of the fuel has to be calculated.

The LHV calculation for the reference fuel, known as conventional diesel in this study, takes a few steps to accomplish. First, the conventional diesel fuel used in this study is a certification fuel and its composition was provided to us from the fuel manufacturer. Although the composition of the fuel is given, it is given in weight percentage of hydrogen and carbon. Thus, the chemical formula of the reference fuel needs calculation from these two weight percentages. A detailed version of the calculation is provided in Appendix A. Once the chemical formula is determined, a balance of the chemical reaction is performed. Knowing the molar value of each of the products, the ratio of the mass of water to the mass of fuel is determined. This ratio can now be placed in the following equation with the gross heating value (HHV).

$$LHV\left(\frac{Btu}{lb}\right) = HHV\left(\frac{Btu}{lb}\right) - 1050\left(\frac{m_{H_2O}}{m_{fuel}}\right)$$

The LHV calculation of biodiesel is done in the same manner as the conventional diesel. The exception being that the fuel chemical formula is not known. A chemical analysis was not done of the fuel that could have given, as with conventional diesel, its chemical makeup in weight percentage. This calculation, therefore, assumes a chemical formula of $C_{18.74}H_{34.34}O_2$. Literature states that this chemical formula is a good approximation for biodiesel fuel [2,10].

A fourth parameter, PMEP, is calculated from data taken of the engine. Work is done on or by the piston as the engine intakes and exhausts gases from the cylinder. The net work done whether it's to the piston or by the piston is PMEP or the pumping work of the engine. The lack of in cylinder pressure traces to give such a parameter leads to an approximation of PMEP. The approximation can be calculated by taking the difference of EMP and IMP. This value is given as a positive number but this parameter takes away from the work done by combustion to the piston. On the other hand, if the IMP was larger than EMP, PMEP would add to the work done by combustion.

A fifth parameter, volumetric efficiency, is also calculated from the logged data. Volumetric efficiency is a measure of how well an engine can induct air. The parameter is calculated by the following equation:

$$\eta_v = \frac{2\dot{m}_a}{\rho_{a,i} V_d N}$$

The density of air for this calculation is taken to be at the intake manifold and is calculated from known logged parameters taken of the engine. Further explanation of the intake manifold density calculation will follow. The air flow rate of the engine, as given by the laminar flow element, was verified by calculating the air flow rate from exhaust emissions data for each of the study points. Further explanation of this calculation will also follow.

The intake manifold density calculation is calculated using engineering equation solver (EES). This program is used for its thermo-physical property functions that aid in solving for the density using logged data of atmospheric conditions at the testing time.

First an equation is set up taking the barometric pressure, humidity, and temperature at the inlet of the air cleaner to obtain the humidity ratio using the thermo-physical property functions of EES. After calculating the humidity ratio given atmospheric conditions, an equation is set up to solve for the saturation pressure of water at the inlet temperature. The following equation is used

$$\omega = 0.622 \frac{\phi p_g}{P - \phi p_g}$$

where ϕ is relative humidity, p_g is vapor saturation pressure at the inlet temperature, and P is the barometric pressure in bar. Next, an equation is set up to calculate the vapor pressure knowing the relative humidity logged and saturation pressure of the vapor at the inlet temperature using the definition of relative humidity. Relative humidity is the ratio of the water vapor pressure to the saturation pressure at the same temperature. Knowing the vapor pressure, an equation for the mole fraction of water vapor in the air is setup. The mole fraction is the ratio of the vapor pressure calculated at inlet conditions to the barometric pressure. The mole fraction of water vapor in the air is inserted in an equation set up to calculate for pressure of just air in the intake manifold. This equation will also take into account EGR flow into the intake manifold when demanded by the ECM. This equation is the multiplication of the water vapor mole fraction in the air to the IMP and the multiplication of the CO_2 mole fraction to the IMP both subtracted from the IMP. The pressure of air in the intake manifold is then used to setup an equation using the thermo-physical properties of EES to obtain the density of air in the intake

along with the temperature logged of the intake manifold. A sample of the calculation in EES is provided in Appendix A.

The air flow rate of the engine is calculated using an oxygen balance air-fuel ratio [14,15]. The equation to calculate the oxygen balance air-fuel ratio is

$$\frac{A}{F} = 4.773\left(\frac{M_{air}}{M_f}\right)\frac{(CO_2)+\frac{(CO)}{2}+\frac{(H_2O)}{2}+\frac{(NO)}{2}+(NO_2)+(O_2)}{(HC)+(CO)+(CO_2)}$$

where ( ) are percent molar concentrations, M_{air} is 28.96, $M_f = 12.01 + 1.008y$ where y is the H/C ratio of the fuel, and (H_2O) is calculated from the following equation

$$(H_2O) = 0.5y\frac{(CO_2)+(CO)}{\frac{(CO)}{[K(CO_2)]}+1}$$

The (HC), (NO), and (NO_2) of the air-fuel equation above are neglected in calculation of the air-fuel ratio. A carbon balance air-fuel ratio was also calculated using the following equation [14,15]:

$$\frac{A}{F} = \left(\frac{M_{air}}{M_f}\right)\frac{100+(HC)-\frac{(CO)}{2}+\frac{3(H_2O)}{2}-(H_2O)_a}{(HC)+(CO)+(CO_2)}-\frac{y}{2}$$

The $(H_2O)_a$ term is neglected due the analyzers using an ice bath to chill the exhaust sample to effectively remove the water vapor at the analyzers. The (HC) term is also neglected in the carbon balance air-fuel ratio calculation. Once the air-fuel is calculated, the air flow rate of the engine is calculated from the air-fuel ratio. The air-fuel ratio is a mass ratio of air to fuel. Knowing the mass fuel flow rate of the engine and calculating

the air-fuel ratio, the air flow rate of the engine is calculated by multiplying the calculated air-fuel ratio by the fuel flow rate.

Another method for calculating the air flow rate of the engine is performed due to the previous two methods being for fuels comprised of only carbon and hydrogen. Biodiesel is comprised of carbon, hydrogen and oxygen, thus the previous two equations cannot be used to calculate the air flow rate of the engine. The following equation can be used with oxygenated fuels ($C_nH_mO_r$):

$$\phi = \frac{2n_{O_2}}{n_p x_{H_2O} + n_p\left(1 - x_{H_2O}\right)\left(x_{CO} + 2x_{CO_2} + 2x_{O_s} + x_{NO} + 2x_{NO_2}\right) - r}$$

where x_i is the dry mole fraction of species i, K is 3.8, and the following equations calculate the rest of the parameters of the equation [15].

$$x_{H_2O} = \frac{m}{2n}\frac{x_{CO} + x_{CO_2}}{[1 + \frac{x_{co}}{Kx_{co_2}} + (\frac{m}{2n})(x_{CO} + x_{CO_2})]}$$

$$n_p = \frac{n}{x_{HC} + (1 - x_{H_2O})(x_{CO} + x_{CO_2})}$$

$$n_{O_2} = (n + m/4 - r/2)$$

Once the equivalence ratio is calculated, the stoichiometric air-fuel ratio is divided by the equivalence ratio to give the actual air-fuel ratio of the engine at a particular study point. The actual air-fuel ratio is multiplied by the mass fuel rate to give the air flow rate at a particular study point as described previously for the oxygen and carbon balance air-fuel ratio calculations.

Another calculated parameter is the EGR dilution ratio. This parameter is not a true measurement of the EGR percentage in the intake, but it gives evidence that EGR is flowing to the intake manifold. The EGR dilution ratio is calculated by taking the intake percentage concentration of CO_2 and dividing it by the percentage concentration of CO_2 from the exhaust.

A final two parameters calculated both pertain to the fuel flow of the engine. These two parameters are cycle fuel flow and volumetric flow rate. The cycle fuel flow gives insight into fuel flow per cycle of the engine instead of with engine speed. It is calculated by multiplying the fuel flow rate and the number of revolutions per cycle and dividing it by the engine speed. Cycle fuel flow is given in units of grams per cycle. The volumetric flow rate of the engine is calculated by taking the fuel flow rate and dividing it by the density of the fuel being used. The volumetric flow rate is given in units of liters per hour. Both these calculations can be seen in the Appendix A.

3. RESULTS AND DISCUSSION

3.1 Introduction

This section presents the performance characterization of a John Deere 4.5 liter 4 cylinder direct injection engine with exhaust gas recirculation (EGR), common rail fuel injection, and variable turbo-charging. The discussion will be divided into two discrete parts. The first section presents the characterization of the engine with conventional petroleum diesel. The second section presents the characterization of the differences in engine performance as a result of using biodiesel relative to petroleum diesel.

3.2 Characterization of Engine with Conventional Diesel Fuel

3.2.1 Performance

An engine produces work by converting the stored chemical energy of a fuel into mechanical energy. The output of mechanical energy from an engine is called torque. Torque is a measure of an engine's ability to do work. In a perfect world, an engine produces the same torque throughout its speed range. The work done on the piston by combustion is not all converted to useful mechanical energy, therefore, rendering actual torque to be less than the ideal torque. This reduction in actual torque relative to ideal torque, shown conceptually in Figure 6, is mostly attributed to friction, volumetric efficiency, and heat transfer of an engine.

Friction is inevitable in an engine with parts that continuously interact with each other. Parts rotate and slide within or past each other dissipating the engine's torque. The

total friction work of an engine can be separated further into pumping work, rubbing friction, and accessory work [16]. The pumping work of an engine is defined by the net work per cycle done by the piston on the in-cylinder gases during the inlet and exhaust strokes. Rubbing friction is the work required to overcome the friction due to the relative motion of all moving parts in an engine. Last is the accessory work or work to drive the engine accessories such as the water pump, alternator, and other accessories. The total friction work is dominated by the rubbing friction but for this discussion it will be taken as a whole. Frictional effects increase linearly with engine speed, thus at the high speed ranges more of an effect will act to diminish torque [16].

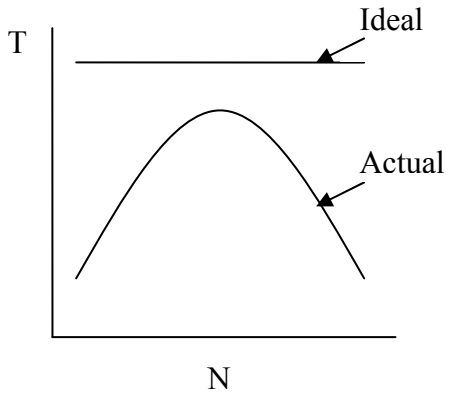

Figure 6: Ideal and actual torque curves versus engine speed.

Volumetric efficiency is another factor that affects torque production of an engine. The volumetric efficiency is a measure of how well an engine inducts air into the volume of a cylinder. In other words, volumetric efficiency is the ratio of mass inducted into the cylinder to the mass ideally inducted into the cylinder, based on displaced cylinder volume at the intake density [17]. The amount of air inducted gives the amount

of fuel that will be injected into the cylinder for proper combustion. A larger mass of inducted air allows for a larger mass of fuel to be injected into the cylinder, thus allowing more torque production at a particular speed and load. It is said that torque curves follow the trend of the volumetric efficiency curve of an engine because of the fact stated above [17]. Because the engine used in this study is enhanced with a turbo-charger, the volumetric efficiency can be over one hundred percent; the efficiency curve, seen in Figure 7, will still have the same trend as the torque curve. Thus, at low engine speeds volumetric efficiency is lower, increasing to a maximum, and then decreasing as engine speeds increase past the maximum point.

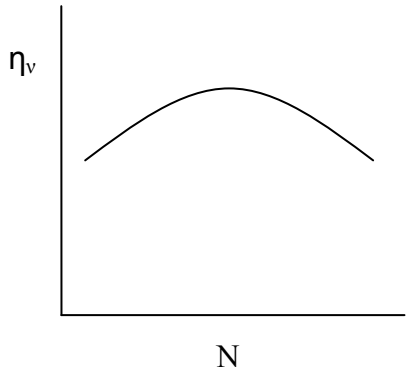

Figure 7: Volumetric efficiency curve versus engine speed.

Heat transfer is a complicated topic for an engine. Heat can flow out of an engine in various ways affecting performance, efficiency, and emissions. This energy flow out of the engine can be divided into its respective parts [17]. The major energy flow as heat is transferred out with the coolant flow. This heat flow includes heat transfer to the

combustion chamber walls and friction work. Another major part of the energy flow out of the engine is the sensible energy from the exhaust gases. The energy loss due to the exhaust flow is hard to eliminate but one such way to recover a part of this energy is to integrate a turbo-charger to the engine and use this flow energy to compress the incoming air flow. Being that a major flow of energy is carried off by the coolant, this will be the driving force of how heat transfer affects engine performance [17].

The heat transfer to the combustion chamber wall is affected by speed. Increasing the engine speed decreases the time in which heat can transfer to the wall, therefore decreasing the heat transfer per cycle. Heat transfer lowers the average combustion temperature and pressure reducing work transferred to the piston predominantly at the lower engine speeds.

Figure 8 presents the torque curve at full load of the engine used in this study. The performance reducing parameters can be seen in action as you follow the curve. At low engine speeds, the volumetric efficiency and heat transfer is limiting the torque production of the engine. As the engine speed increases, the volumetric efficiency is increased and heat transfer effects are diminished while friction effects are starting to take effect. This is seen with the first part of the torque curve increasing in torque to a peak at 1400 rpm. The speed further increases and friction becomes the dominant parameter of torque reduction with the added effect of a lower volumetric efficiency with any further engine speed increase.

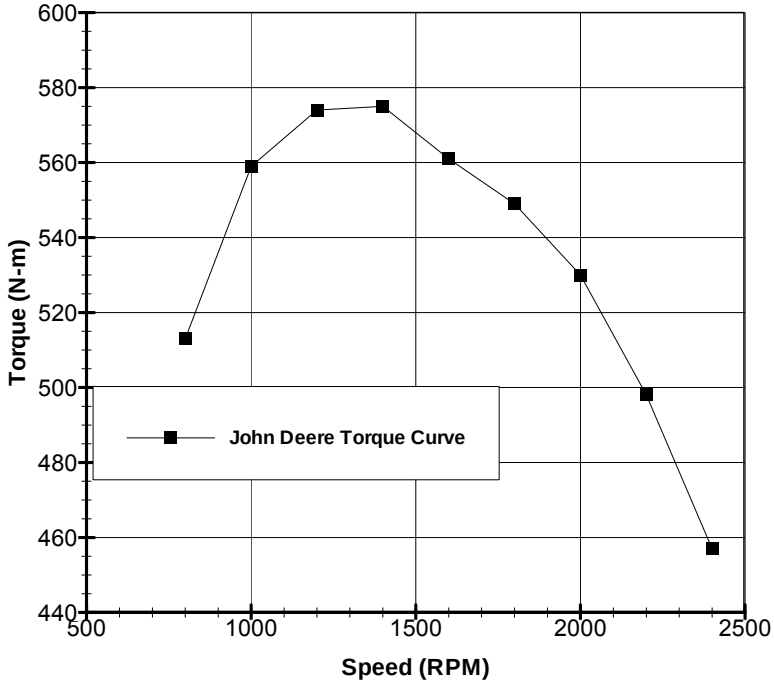

Figure 8: John Deere 4045 DI Diesel Engine Torque Performance Curve.

The torque produced over the tested engine speed and load ranges of conventional fuel is shown in Figure 9. The load cases reported throughout this study are nominal due to several factors. The first factor is due to dyno constraints. At 1400 rpm, the dynamometer could not brake the engine to reach a load of 75%, thus the test point is taking at 70% load which produces less torque. A second factor is the engine control system. The ECM actuates exhaust gas recirculation (EGR) at a set coolant temperature and air flow is observed to change at this transition point. The transition point made it hard to take consistent data due to coolant temperatures varying around the set EGR actuation point. Thus, the test point of 2400 rpm 60% load was replaced by a load of 65% which gives an increased torque production. The third factor is the engine idle load at 2400 rpm. The idle load is about 23% restricting the ability of taking data at 20% load,

therefore the point was tested at 30% load. The last factor is holding of a certain load percentage consistently. At all test points the load is not consistently held, even though the idea is to hold the exact load and speed as data is taken, changes occur during the data logging process. Therefore, torque trends seen in Figure 9 are skewed from the trends expected because of nominal load values.

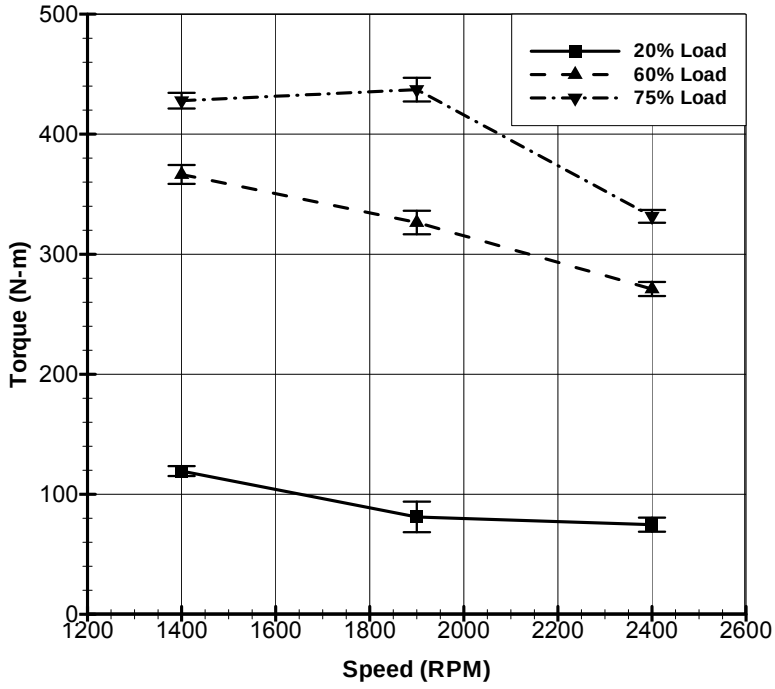

Figure 9: Torque versus engine speed for conventional diesel fuel for 20%, 60%, and 75% loads. Max uncertainty ± 12.7 N-m.

Torque production varies in an engine with a change in load. The engine injects more fuel into the compressed air in the cylinder to keep the engine's speed at its set point. The increased fuel in the cylinder increases the peak pressure in the cylinder therefore increasing the torque produced. Figure 9 shows the torque at each speed

increasing with an increase in applied load to the engine, as would be expected from the discussion just presented. The 20% load case shows torque production decreasing from 1400 rpm. This trend correlates well with the effect of performance reducing parameters as speed increases. The volumetric efficiency is highest at 1400 rpm, heat transfer is not as significant, and friction is yet to fully take effect. As speed increases, friction effects become dominant coupled with decreasing volumetric efficiency. Therefore, the torque production trend should decrease from 1400 rpm as speed increases for all loads. At 60 and 70% load, the same trend is seen as the 20% load.

As mentioned above, torque production varies in an engine with a change in load. An increase in applied load to the engine at a particular engine speed causes an increase in fuel flow. Figure 10 shows the fuel flow of the engine per cycle at each speed increasing with an increase in load, thus increasing torque production. Also in Figure 10, notice that the trend at each respective load follows closely the trends of torque seen in Figure 9. The amount of fuel supplied controls the amount of torque produced by the engine, thus the fuel flow and torque trends should closely follow each other.

A parameter measuring the efficiency of how well the engine uses the fuel supplied to produce work is break specific fuel consumption (BSFC). In other words, the fuel flow rate per unit power output. Figure 11 shows the BSFC for the points tested on the engine in this study. The increase in friction as speed increases is clearly shown in BSFC with it increasing as the speed increases at each respective load. The friction lowers the power that could be produced for the same amount of fuel increasing the BSFC. This is especially seen at 20% load. The other trend to notice is the increasing

BSFC as load decreases. The mechanical efficiency or the ratio of brake power produced to the indicated power is decreasing as load is decreased. Again, the power that could be produced is being reduced, thus increasing the BSFC as load is decreased.

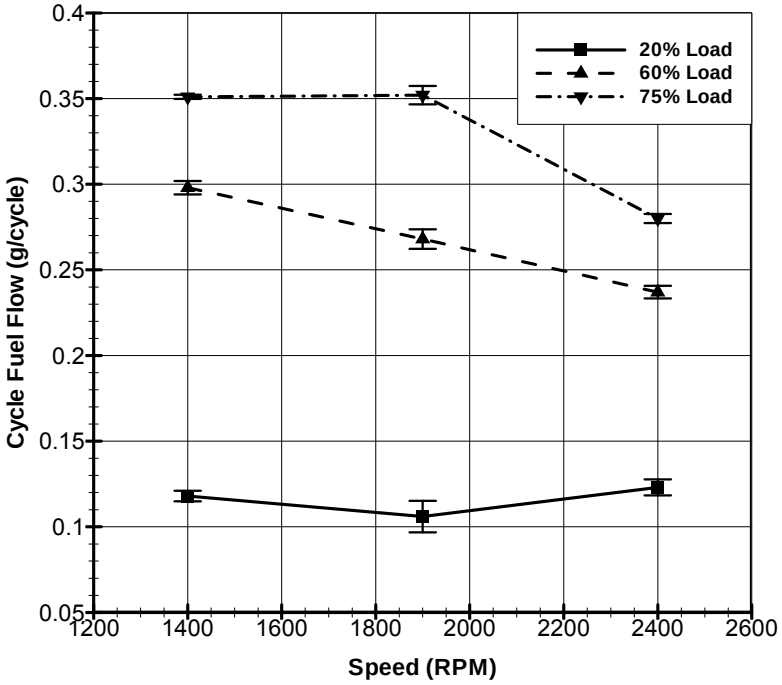

Figure 10: Cycle fuel flow versus engine speed for conventional diesel fuel for 20%, 60%, and 75% loads. Max uncertainty ± 0.0092 g/cycle.

Another characteristic of engine performance is the work done per unit time. The characteristic is power and is calculated by converting torque to work per cycle and dividing by engine speed in revolutions per second. Figure 12 shows the full load power curve of the engine in this study. If torque were constant throughout the speed range the power would increase linearly. Looking at Figure 12, we do not see this trend. The increase in power steadily decreases as the speed increases giving rise to a curve that

comes to a peak. The engine power curve shows this peak power at both 2300 and 2400 rpm. Peak power being at both engine speed points arises because of the torque difference at these respective speeds, since power is a multiplication of these two values.

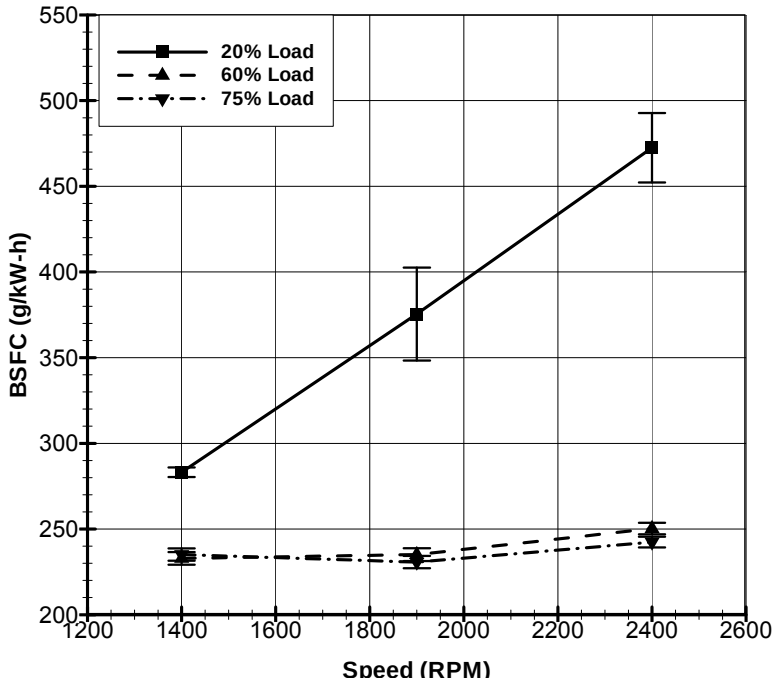

Figure 11: BSFC versus engine speed for conventional diesel fuel for 20%, 60%, and 75% load. Max uncertainty ± 27.13 g/kW-h.

The power produced over the tested engine speed and load ranges of conventional fuel are shown in Figure 13. The power production at 20% load is linear due to the fact of how power is calculated. Being that torque is low, the product of speed and torque does not change a significant amount as speed increases. Although at higher torque productions, the significance of speed increases in the calculation of engine power. The 60% load case illustrates this very well. As speed increases the torque

decreases but power production increases. At the 75% load case, this can be seen with a power increase compared to the torque decrease between 1400 and 1900 rpm. Between 1900 and 2400 rpm, there is a slight decrease in power production due to the reduction in torque production.

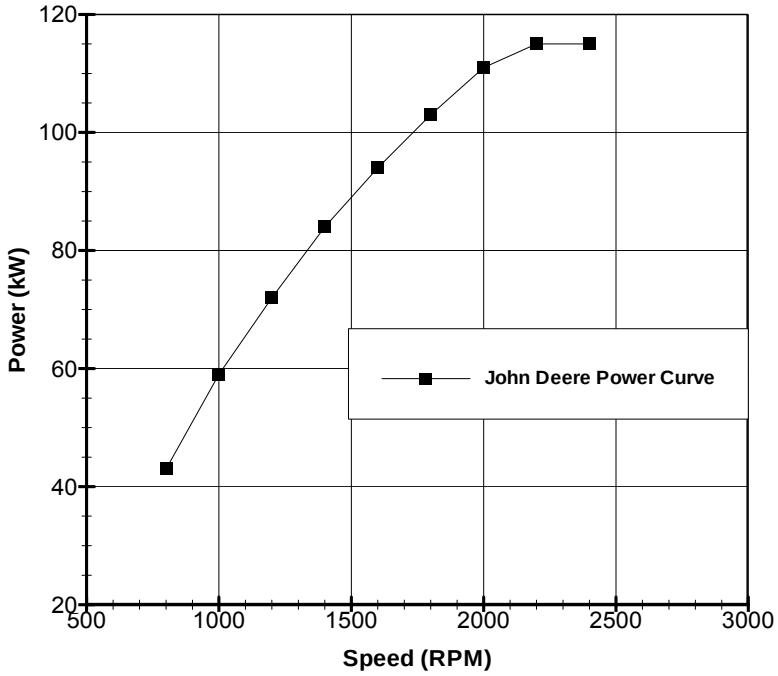

Figure 12: John Deere 4045 DI Diesel Engine Power Performance Curve.

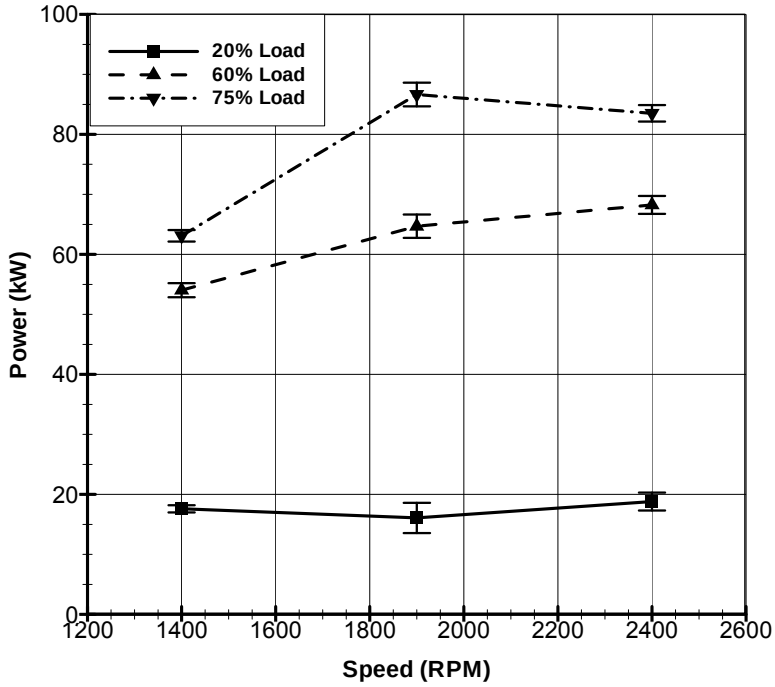

Figure 13: Power versus engine speed for conventional diesel fuel for 20%, 60%, and 75% loads. Max uncertainty ± 2.521 kW.

3.2.2 Breathing of the Engine

Air induction into an engine is vital to the performance of an engine. An air induction system has the ability to increase or decrease the performance of an engine. As discussed above, the ability of the induction system to fill the cylinder volume with air is called the volumetric efficiency. The more air inducted into the cylinder the more fuel that can be injected into the cylinder, thus a turbocharger is integrated into the engine to "boost" its performance.

A turbocharger is a device that transfers exhaust flow energy to the intake flow. The turbocharger accomplishes this by passing the exhaust through its turbine. The turbine extracts the exhaust energy and produces useful work. The work is transferred by

a shaft which drives a compressor. The compressor increases the mass air flow rate into its volume, thus increasing its density. The increased density of the air increases the mass that fills the volume of the cylinder, thus allowing an increase in fuel flow to increase torque.

The variable geometry turbo (VGT) is a turbocharger with the ability of changing its turbine geometry with vane position. The vanes are located on the outside diameter of the turbine wheel. The adjustable vanes change the velocity trajectory of the incoming exhaust gases and control the pressure in the exhaust manifold. An increase in exhaust velocity translates to an increase in turbine speed, thus increasing air mass flow rate, density, and pressure at the intake manifold. Pressure control inside the exhaust manifold provides for a suitable pressure difference for EGR flow into the intake.

Three exhaust gas analysis based calculations of air flow and the air flow given by the LFE are represented in Figure 14 through Figure 16. They show a comparison of the air flow rates the VGT is inducting at the tested engine speeds and loads of conventional diesel fuel. The figures show a carbon balance, oxygen balance, inorganic gas analysis (which is referred to on the graphs as “calculated”), and an LFE based air flow. The calculated exhaust based calculations are shown with the measured LFE air flow as a check to see if the air flow measured by the LFE is correct. The comparison shows that the LFE air flow measurement is high compared the exhaust based calculations of air flow. Further, a comparison is made between the three calculated air flows to determine the difference in magnitude of each method to determine the air flow rate of the engine.

Figure 14 shows the mass air flow rate versus engine speed for 20% load. The mass air flow rate increases as engine speed increases with a greater increase from 1900 to 2400 rpm. The three calculated air flow rates show this trend with the calculated and oxygen balance air flow rates being virtually the same. The carbon balance calculated air flow rate is lower than the two previously mentioned. Figure 15 shows the mass air flow rate versus engine speed for 60% load. As with 20% load, the mass air flow rate increases as engine speed increases. The increase in air flow rate is virtually linear as engine speed increases. Again, as in 20% load, the oxygen balance and calculated air flow rates are virtually the same with the carbon balance being lower. Similarly, the same trend is seen at 75% load with the carbon balance calculation being lower than both the calculated and oxygen balance calculations. Also, seen in Figure 16 is the increase in air flow rate as engine speed increases but with a smaller increase from 1900 to 2400 rpm.

The difference seen with the carbon balance calculation of mass air flow rate can be due to the fact that hydrocarbons were not measured. Being that it is a carbon balance and the hydrocarbons are not measured can alter the result of this method. Also, with diesel combustion being fuel lean there is more oxygen in the exhaust products lending itself to the oxygen balance calculation. The oxygen balance calculation provides improved accuracy and reduced sensitivity to the carbon balance which is useful for lean engine operation as with the diesel engine used in this study [14].

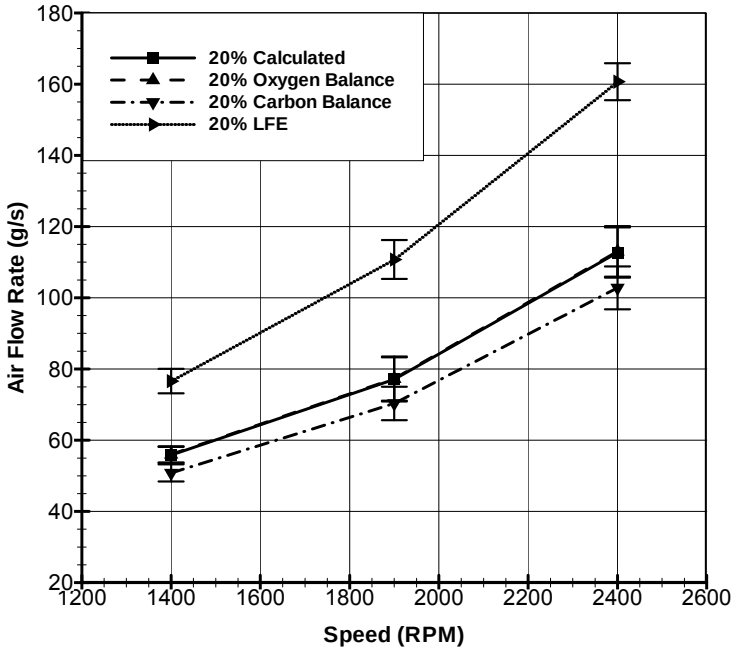

Figure 14: Comparison of calculated air flow rates versus engine speed for conventional diesel fuel from exhaust emissions at 20% load. Max uncertainty ± 7.06 g/s.

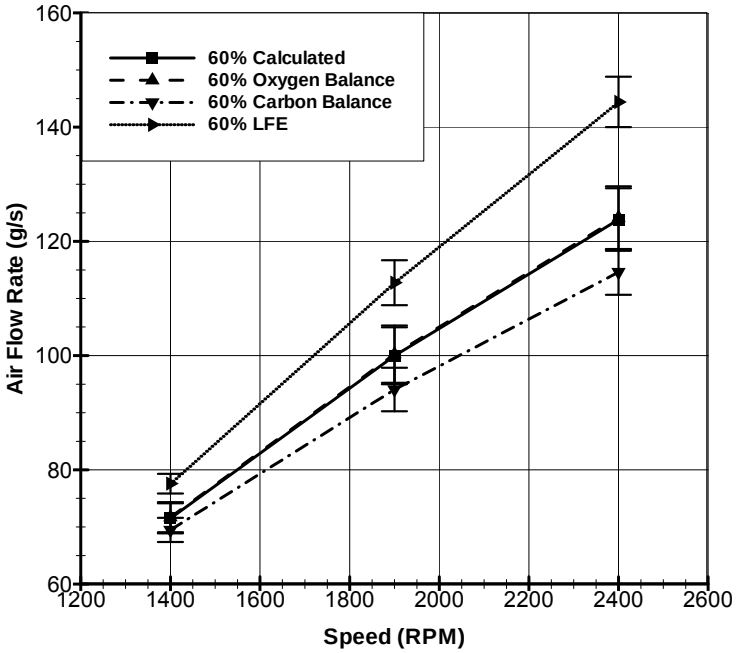

Figure 15: Comparison of calculated air flow rates versus engine speed for conventional diesel fuel from exhaust emissions at 60% load. Max uncertainty ± 5.48 g/s.

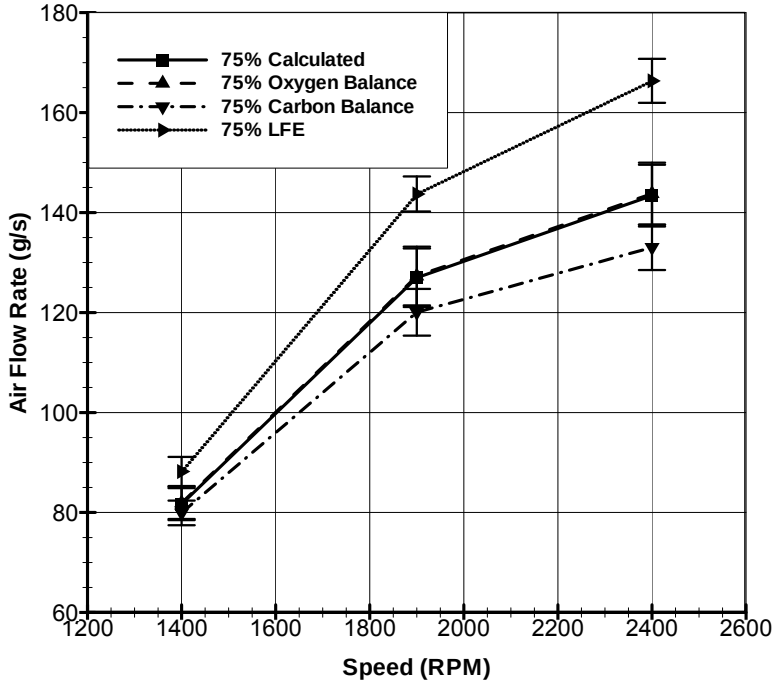

Figure 16: Comparison of calculated air flow rates versus engine speed for conventional diesel fuel from exhaust emissions at 75% load. Max uncertainty ± 6.2 g/s.

EGR is used in an engine to reduce certain emissions, such as nitric oxides, by reducing the peak combustion temperatures. CO_2 concentration was measured from the intake manifold at all engine test points. These measurements are shown in Figure 17 as the EGR dilution ratio. The measure given in this figure does not give the exact percentage of EGR in the intake but for the purposes of this study it verifies the use of EGR at each load and speed. Figure 17 confirms the introduction of EGR into the intake manifold at the mid-load points of 60 and 70%. The EGR at 1400 rpm is comparable at both loads, but increases slightly from the 60% load at 1900 rpm. At 2400 rpm EGR is again comparable for both load cases. Figure 17 also shows that EGR is not introduced at 20% load for all tested engine speeds.

Observation on engine performance while testing shed some light into the EGR use demanded by the ECM. The introduction of EGR for this engine is dependent on two conditions, the load and coolant temperature of the engine. At the mid-load points the coolant temperature would reach 170°F causing a change in air flow rate. The air flow rate before the introduction of EGR at these mid-load points was higher. The lowering of the air flow rate is inferred to be induced by the ECM to prepare for the introduction of EGR to give a certain intake pressure.

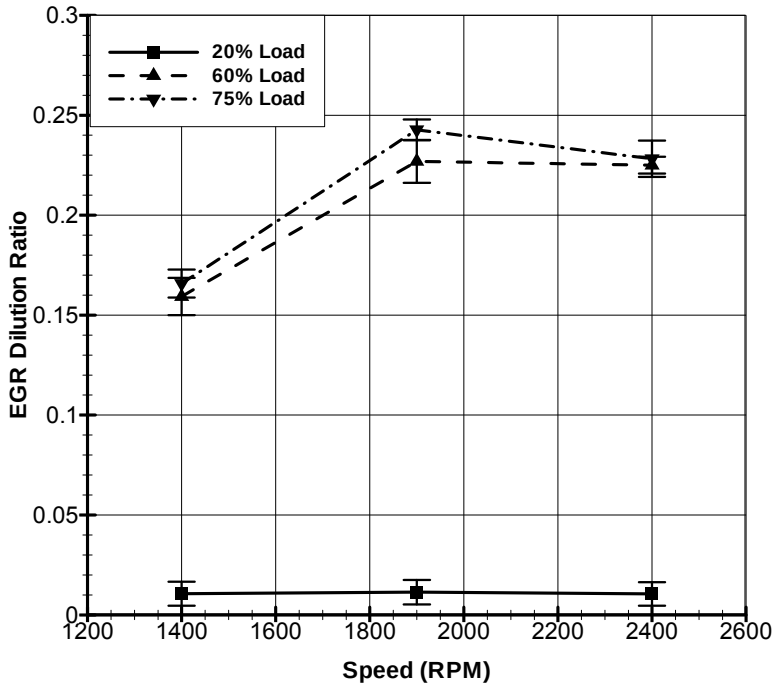

Figure 17: EGR dilution ratio versus engine speed for conventional diesel fuel for 20%, 60%, and 75% loads. Max uncertainty ± .011.

Figure 18 shows the absolute compressor pressure out (CPO) over ambient conditions of the inducted air. CPO behaves similarly to the trend seen with the air flow

rate at 20% load. The pressure increases as the engine speed increases with a greater increase in pressure from 1900 to 2400 rpm. At the two mid-load points, as discussed above, EGR is flowing into the intake. Therefore, the pressure in the intake system is a combination of the inducted air and EGR. At 60% load, the pressures increase from 20% load at their respective speeds with 2400 rpm having a slight increase. The slight increase in pressure at 2400 rpm 60% load is attributed to the EGR flow being comparable to the 1900 rpm case in combination with a comparable flow of fresh air compared to 20% load. At 75% load, the pressure significantly increases from 1400 to 1900 rpm with a drop in pressure for the 2400 rpm case. The drop in pressure can be attributed to the ECM demand of EGR not being fulfilled or the ECM demand of exhaust manifold pressure not being reached.

The increase in pressure also gives rise to an increase in air temperature. Figure 19 shows the temperature of the air after it exits the compressor. The trends in temperature follow closely the trends in pressure after the compressor. Once the air exits the compressor, the above ambient pressure and temperature air flows from the compressor through the intercooler and into the intake manifold as shown in Figure 5. The air flow passes through the intercooler lowering the raised air temperature caused by the compression effects of the turbo-charger.

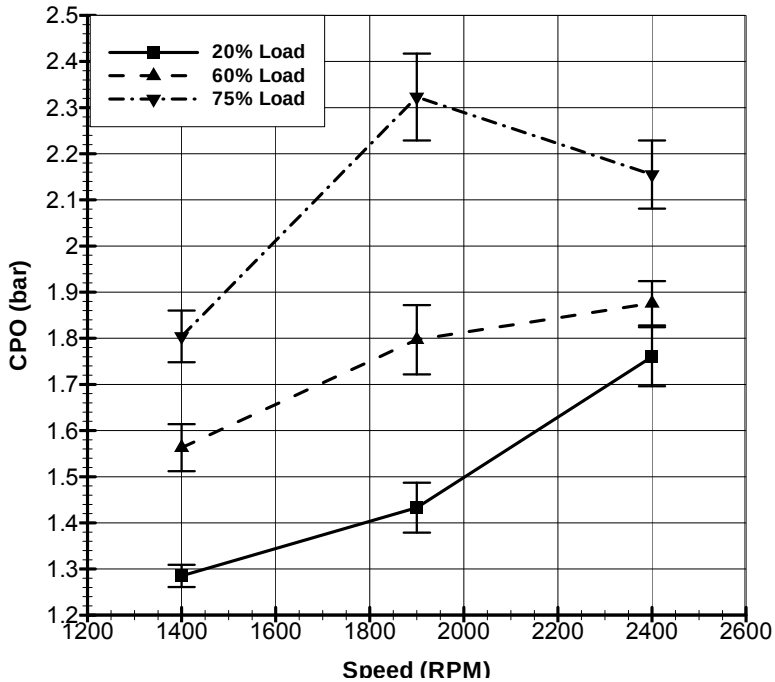

Figure 18: The exiting pressure of the compressor versus engine speed for conventional diesel fuel for 20%, 60%, and 75% loads. Max uncertainty ± .094 bar.

The advantage of lowering the air temperature is to raise its density; in other words more mass per volume can be inducted into the cylinder than higher temperature air. This increases volumetric efficiency. Figure 20 shows the intake manifold temperature (IMT) of the air after passing through the intercooler. The 20% load case is solely dependant on the air flow through the intercooler. The difference of CTO and IMT, shown in Figure 21, clearly shows with an increase in engine speed the greater reduction in air temperature. As engine speed increases, the transfer of heat from the intercooler to the ambient air increases giving the increasing difference in temperature at 20% load. This can be attributed to an increase in fan speed forcing a higher flow rate over the intercooler fins.

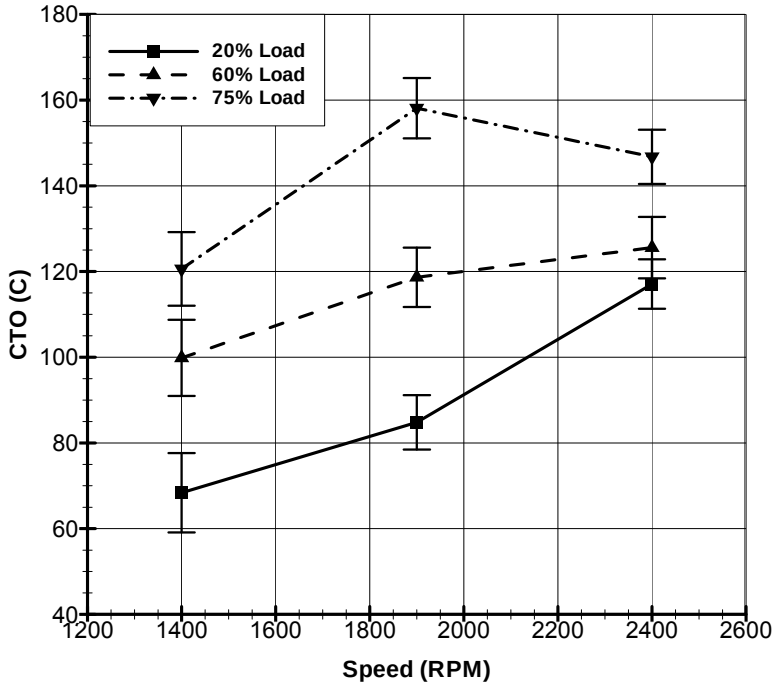

Figure 19: The temperature exiting the compressor versus engine speed for conventional diesel fuel for 20%, 60%, and 75% loads. Max uncertainty ± 9.272 °C.

At the mid-load points the gas in the intake manifold is a mixture of EGR and air. IMT is therefore a function of heat loss through the intercooler and the temperature of the EGR mass. Looking at Figure 21, the temperature difference increases as load increases at each respective speed except at 2400 rpm. Knowing that at 60 and 75% load EGR is being mixed with fresh air; one could infer that the temperature difference of CTO and IMT can be greater. Thus, the intercooler heat transfer to the ambient has increased to increase the temperature difference through the intercooler as the load is increased.

At 60% load, IMT is significantly higher than 20% load at all engine speeds. This is due to the initial compressor out temperatures being higher compared to the 20%

load and EGR flow into the intake. The EGR mixing with the fresh air gives a smaller difference between CTO and IMT indicating that the EGR temperature is relatively higher. The IMT at 75% load is increased from 60% load at each respective engine speed, 1400 and 2400 rpm being a slight increase. The EGR dilution is comparable except at 1900 rpm suggesting that EGR induction is smaller at these two points.

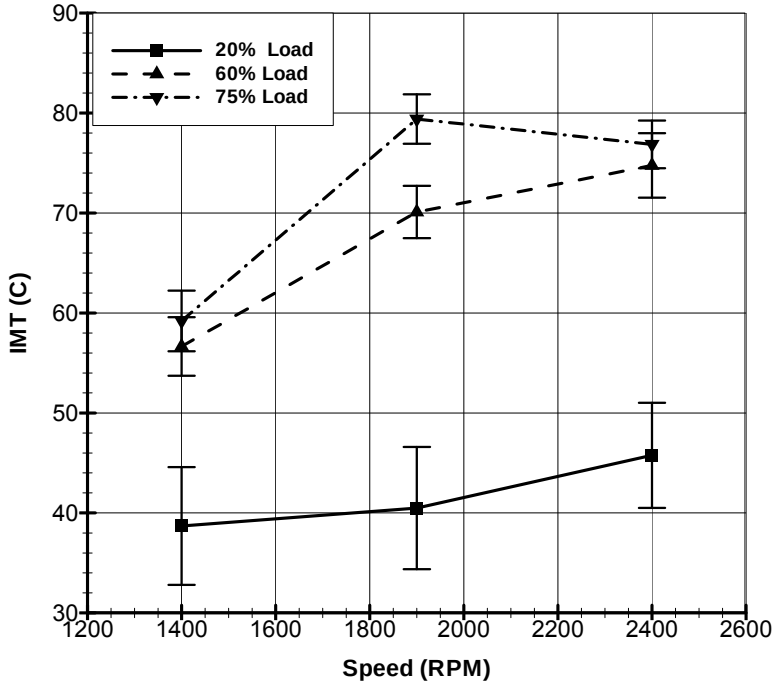

Figure 20: The temperature in the intake manifold versus engine speed for conventional diesel fuel for 20%, 60%, and 75% loads. Max uncertainty ± 6.109 °C.

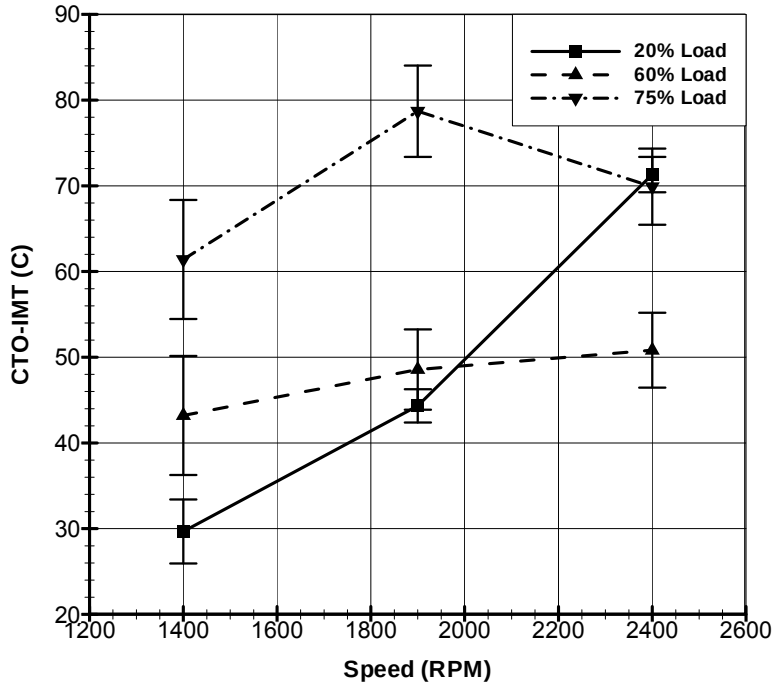

Figure 21: Difference of CTO and IMT versus engine speed for conventional diesel fuel for 20%, 60%, and 75% loads. Max uncertainty ± 6.949 °C.

The intake manifold pressure plays an important role in the combustion work of an engine. Fundamentally, a higher initial pressure of the cylinder at the start of combustion will increase the pressures throughout the cycle. The work done on the piston is calculated from the pressure-volume relationship, where higher pressures throughout the cycle enlarge the area under the curve giving an increase of work done on the piston. Figure 22 shows the intake manifold pressures (IMP) for the tested engine points. The intake pressure at 20% load increases for each respective speed with a greater increase in pressure from 1900 to 2400 rpm. At 60% load, the pressure increases from 20% load at their respective speeds with 2400 rpm having a slight increase. The slight increase in pressure can be attributed to the EGR and fresh air flow being similar

to the 1900 rpm case. At 75% load, a similar trend seen with CPO, the pressure significantly increases from 1400 to 1900 rpm with a drop in pressure for the 2400 rpm case. The drop in pressure can be attributed to the ECM demand of EGR not being fulfilled or VGT not fulfilling the required air flow rate.

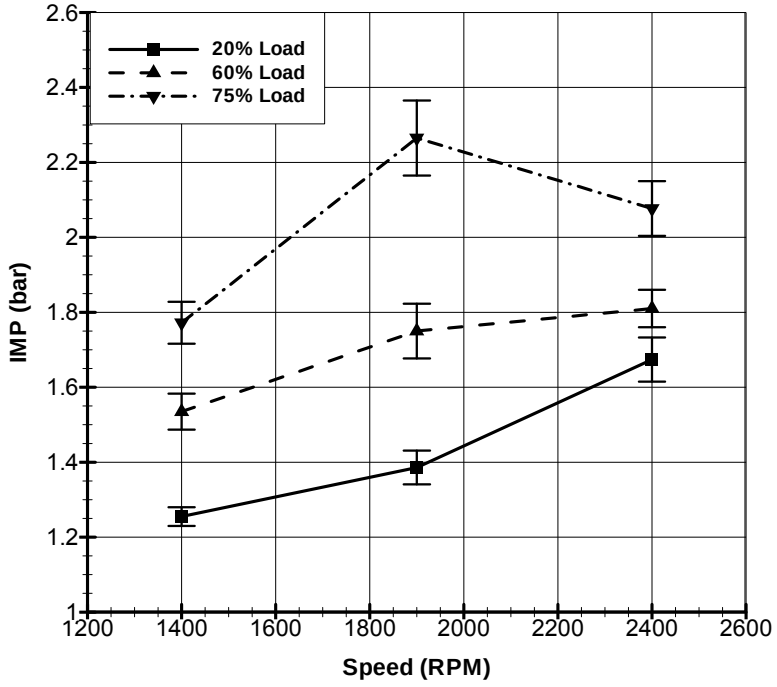

Figure 22: Intake manifold pressure (IMP) versus engine speed for conventional diesel fuel for 20%, 60%, and 75% loads. Max uncertainty ± .1 bar.

The pressure of the intake manifold would ideally be the same as CPO, but as air flows through the intake system pressure losses occur. Figure 23 shows the difference between CPO and IMP. At 20% load, as the engine speed increases the pressure difference increases. This correlates well with the fact that as air flow rate increases through pipes friction increases, thus a greater pressure difference. At 60% load, the air

flow rate has increased from 20% load, thus an increase in pressure difference should be seen. This trend is not seen at 60% load. A similar difference in pressure to 20% load is seen except at 2400 rpm. A reason for the similarity can be the combination of fresh air and EGR at 60 and 75% load. As EGR flows into the intake manifold the pressure is raised decreasing the pressure difference. The EGR flow can also explain the expected higher difference in pressure not seen at 75% load.

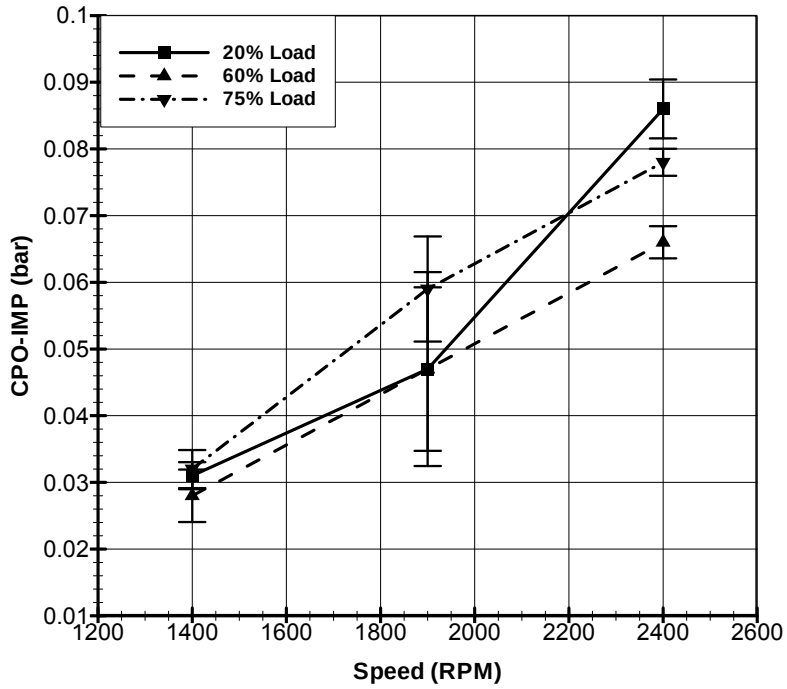

Figure 23: CPO-IMP versus engine speed for conventional diesel fuel for 20%, 60%, and 75% load. Max uncertainty ± .0145

The exhaust manifold pressure is affected by the VGT as the ECM of the engine demands both the need to flow EGR and performance from the engine. The need to flow EGR is set by the ECM when a particular load and coolant temperature is reached. The

pressure difference between the exhaust and intake manifold is the driving force for EGR flow. As the pressure in the exhaust manifold increases over the intake pressure and the EGR valve opens, EGR will flow to the intake manifold as shown in Figure 2. The VGT vanes open and close to control the exhaust manifold pressure and exhaust velocity to increase momentum transfer to the turbine. Figure 24 shows a schematic of the VGT vanes at their fully open position. As the vanes close, they decrease the area of flow to the turbine vanes and increase the pressure of the exhaust manifold.

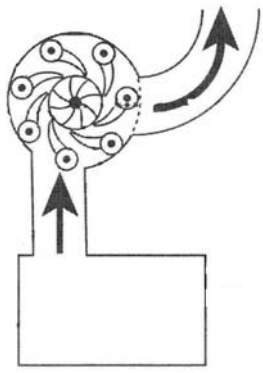

Figure 24: Variable Geometry Turbo (VGT) schematic showing orientation of fully open vanes and exhaust flow through them [12].

Figure 25 shows the exhaust manifold pressure (EMP) versus engine speed. EMP at 20% load increases as the engine speed increases. The trend correlates with the IMP at 20% load. Although, the increase in EMP as engine speed increases is greater than that of IMP leading to believe that the greater increase in EMP is needed to achieve the specific IMP at each engine speed. At 60% load, EMP is similar to 20% load at 1400 and 1900 rpm even though that at 20% load no EGR flows into the intake manifold. Figure

25 also shows EMP following very similar trends to IMP at the 60 and 75% loads. The similarity of this trend with IMP can be due to the fact that EGR is being used at the two mid-load points.

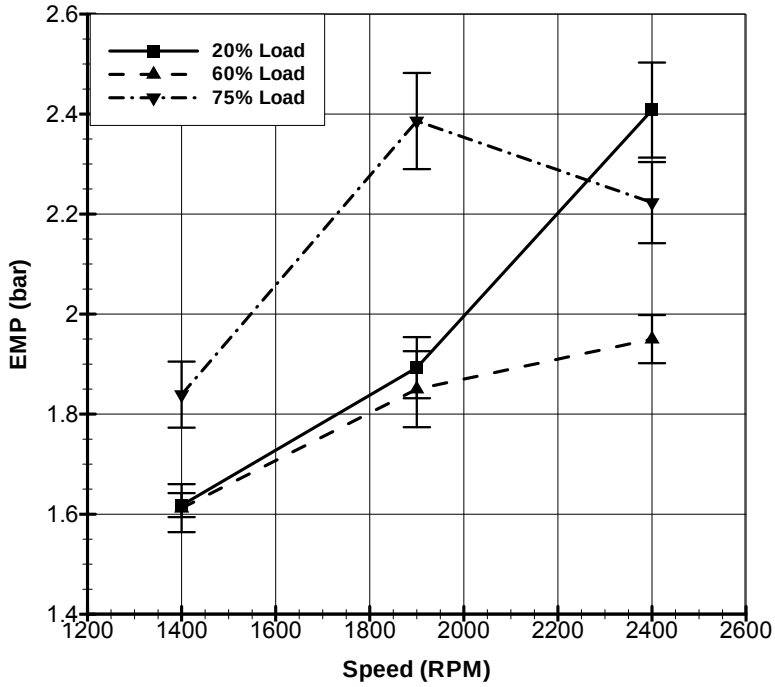

Figure 25: Exhaust manifold pressure versus engine speed for conventional diesel fuel for 20%, 60%, and 75% loads. Max uncertainty ± .096 bar.

Figure 26 shows the difference of EMP and IMP which is the driving force for EGR to flow to the intake manifold at 60 and 75% loads. At 60% load, the difference increases as the engine speed increases. The increase in pressure difference is not great from speed to speed but it gives an increased driving force for EGR flow as the engine speed increases. A similar trend is seen at 75% load with the 1900 rpm speed having a slight increase in pressure difference from 60% load. This could be a reason for the

slight increase of EGR dilution from 60 to 70% load seen in Figure 17. The other two engine speeds at 75% load have a similar pressure difference as 60% load.

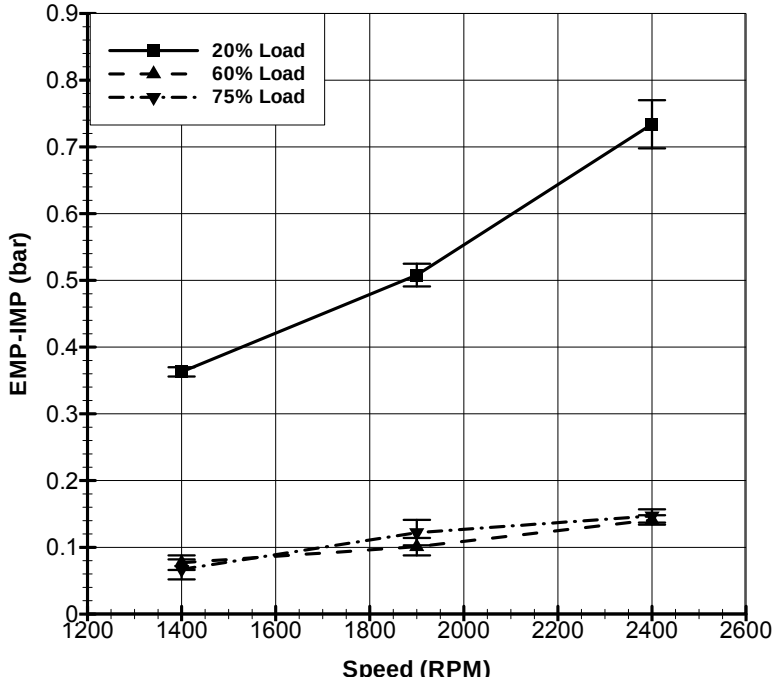

Figure 26: Difference of exhaust and intake manifold pressure versus engine speed for conventional diesel fuel for 20%, 60%, and 75% loads. Max uncertainty ± .036 bar.

Figure 27 shows exhaust manifold temperature or the turbine temperature in (TTI) versus engine speed. The first trend to notice is the exhaust temperature increasing with increasing engine speed for 20% load. On the other hand, the trend is reversed for the 60 and 75% load as exhaust temperatures decrease with increasing speed. The reverse trend can be due to the addition of EGR to the air charge. As the speed increases, more EGR is being mixed with fresh air to lower combustion temperatures for the

control of emissions. Exhaust temperature can also be affected by combustion timing, which was not determined for this study.

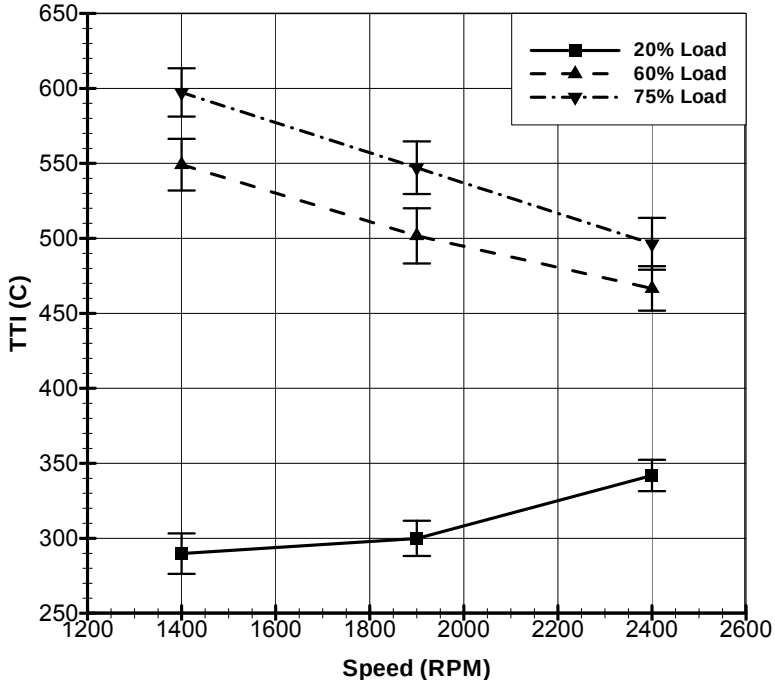

Figure 27: Turbine temperature in versus engine speed for conventional diesel fuel for 20%, 60%, and 75% loads. Max uncertainty ± 18.384°C.

Turbine temperature out (TTO) is the temperature of the exhaust gases after passing through the turbine. The flow of exhaust gas through the turbine results in energy transfer and expansion, thus lowering the temperature of the gas. Figure 28 shows TTO versus engine speed. A similar trend to TTI is noticed for 60 and 75% loads with the temperature decreasing as engine speed increases. Also, at these two loads, TTO is similar with the exception of 1400 rpm where a noticeable difference is seen. At 20% load, the trend follows closely a straight horizontal line with a decrease in

temperature at 1900 rpm. The reason for these trends can be seen from the difference of these two temperatures.

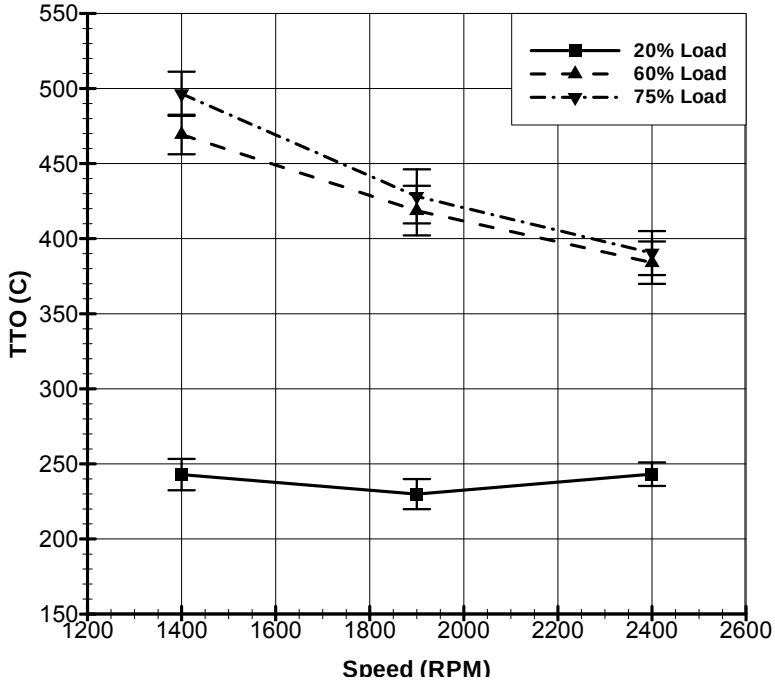

Figure 28: Turbine temperature out versus engine speed for conventional diesel fuel for 20%, 60%, and 75% loads. Max uncertainty ± 17.994°C.

The exhaust temperature difference between TTI and TTO correlates with how much work the turbine is extracting from the exhaust gases. The amount of work extracted from the exhaust is a function of both the temperature and pressure of the exhaust gases. At the same exhaust pressure, the higher temperature exhaust gases will have a higher velocity through the turbine, thus increasing the energy transfer from the exhaust gases to the turbine blades. The difference between TTI and TTO is shown in Figure 29 versus engine speed. At 20% load, the temperature difference increases as

engine speed increases. The temperature in the exhaust manifold or TTI at 20% load is low, thus the exhaust gas velocity through the turbine is small. Compensating for the low exhaust gas temperature the ECM demands the VGT vanes to close to increase EMP. Increasing pressure increases the velocity through the turbine, thus the trend seen of EMP as speed increases at 20% load. At 60% load, the temperature difference at each speed is similar giving a linear trend as engine speed increases. The increase in exhaust manifold temperature and similar pressure to 20% load extract more work from the exhaust gases, thus the larger pressure difference of 60% load. At 75% load, the temperature difference increases from 60% load. The pressure and temperature of the exhaust are larger compared to 60% load, thus giving the increased temperature difference through the turbine.

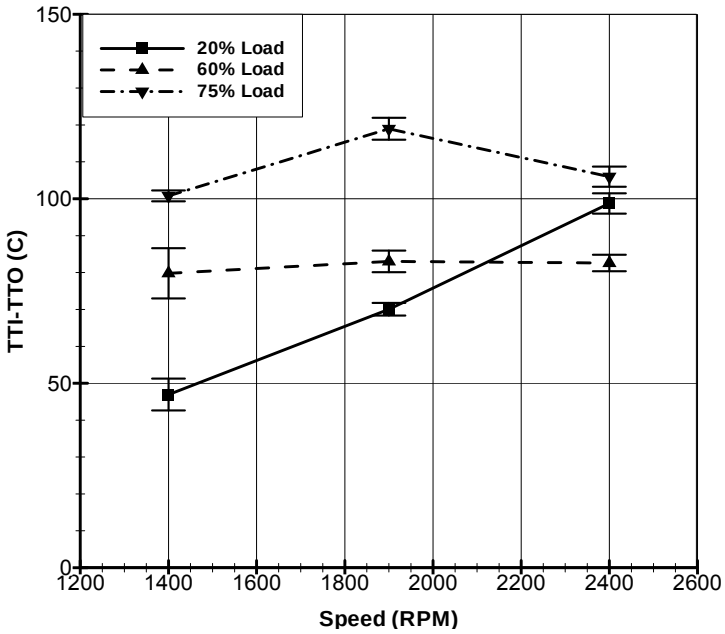

Figure 29: The difference between turbine temperature in and turbine temperature out versus engine speed for conventional diesel fuel for 20%, 60%, and 75% loads. Max uncertainty ± 6.801°C.

The turbine pressure out (TPO) is the pressure after exhaust gases pass through the turbine. TPO is presented in Figure 30 versus engine speed. The pressure is attributed to how much back pressure is seen with flow through the muffler. A general trend of TPO at each load is an increase in TPO as engine speed increases. More generally, however, the pressure difference from the lowest pressure to the highest pressure is negligible.

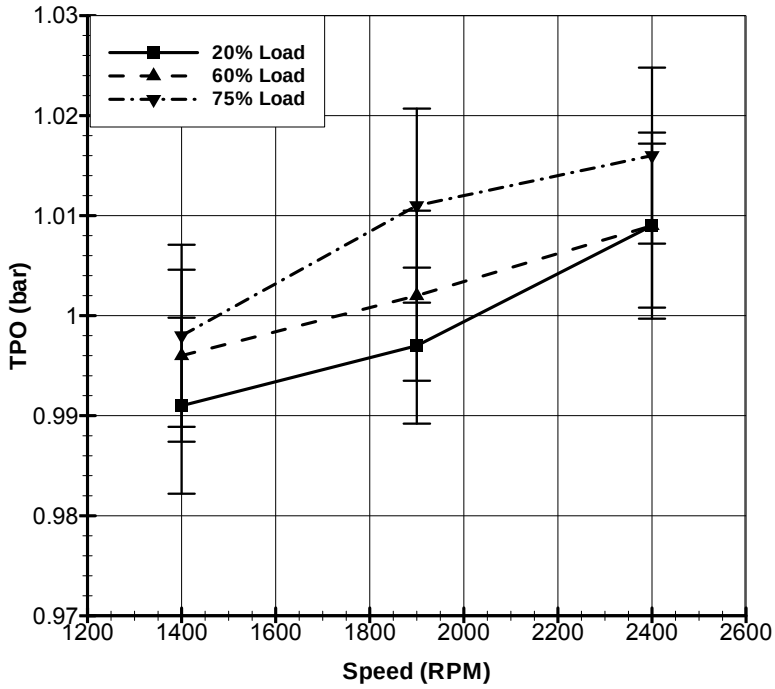

Figure 30: Turbine pressure out versus engine speed for conventional diesel fuel for 20%, 60%, and 75% loads. Max uncertainty ± .01 bar.

3.3 Characterization Differences between Biodiesel and Conventional Diesel

3.3.1 Performance Differences between Biodiesel and Conventional Diesel

The following section of discussion presents the characterization of the differences in engine performance as a result of using biodiesel relative to petroleum diesel. Biodiesel has different fuel properties compared to petroleum diesel such as the lower heating value, density, and cetane number; they are tabulated in Table 2. These fuel properties change the combustion and performance characteristics of biodiesel compared to diesel. The performance characteristic of most significance is the amount of mechanical work produced by the engine, namely torque.

Figure 31 through Figure 33 show the torque production of biodiesel relative to conventional diesel at each respective load versus engine speed. These figures reveal for all loads and engine speeds a decrease in torque production for the engine as a result of using biodiesel. Fundamentally, torque can decrease by altering fuel conversion efficiency (e.g., changes to combustion timing or changes to rates of heat transfer), decreasing fuelling per cycle, increasing pumping work, or increasing friction work. It is assumed that friction work is not changing with the change in fuel. Thus, the torque decrease can be evaluated from any fuel conversion efficiency decrease, fuelling decrease and pumping work increase. The in-cylinder combustion work will not be evaluated directly. The engine facility is not equipped with in-cylinder pressure transducers. Therefore, a pressure versus volume (P-V) diagram could not be generated for the direct evaluation of combustion work and pumping work.

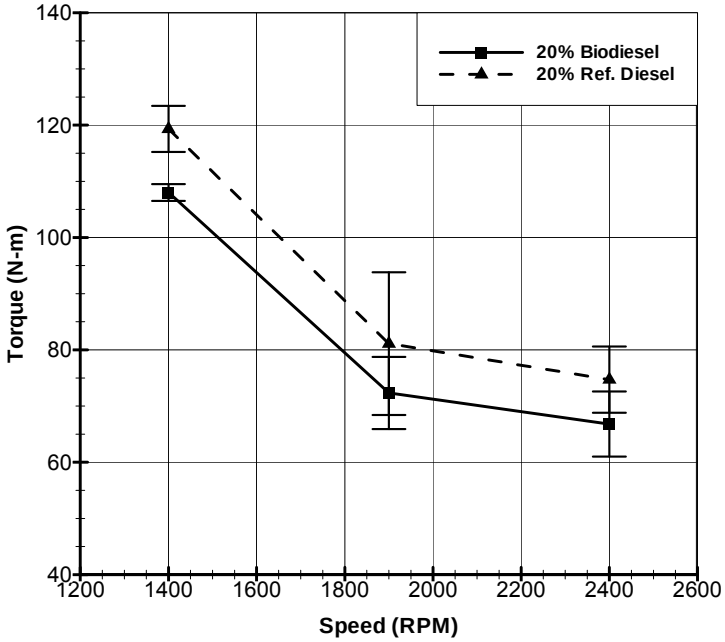

Figure 31: Torque versus engine speed for biodiesel and conventional diesel fuel for 20% load. Max uncertainty ± 12.7 N-m.

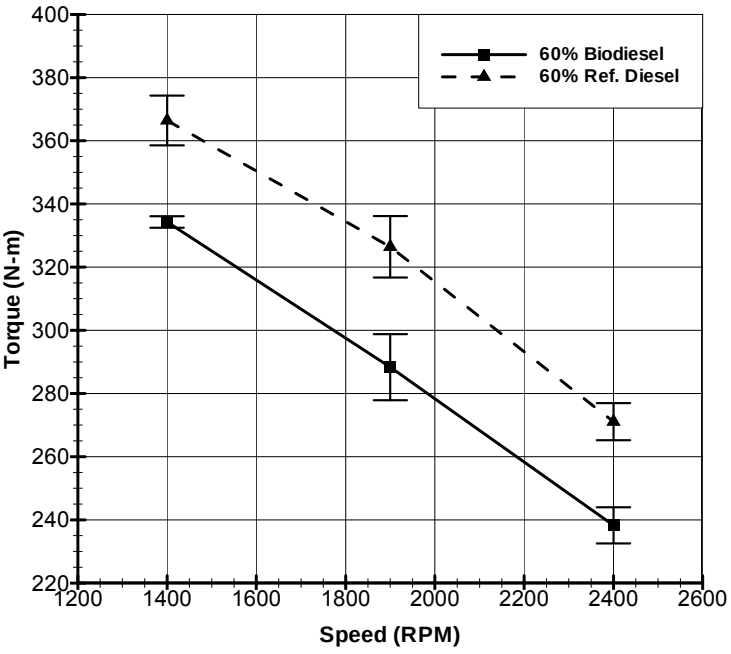

Figure 32: Torque versus engine speed for biodiesel and conventional diesel fuel for 60% load. Max uncertainty ± 10.461 N-m.

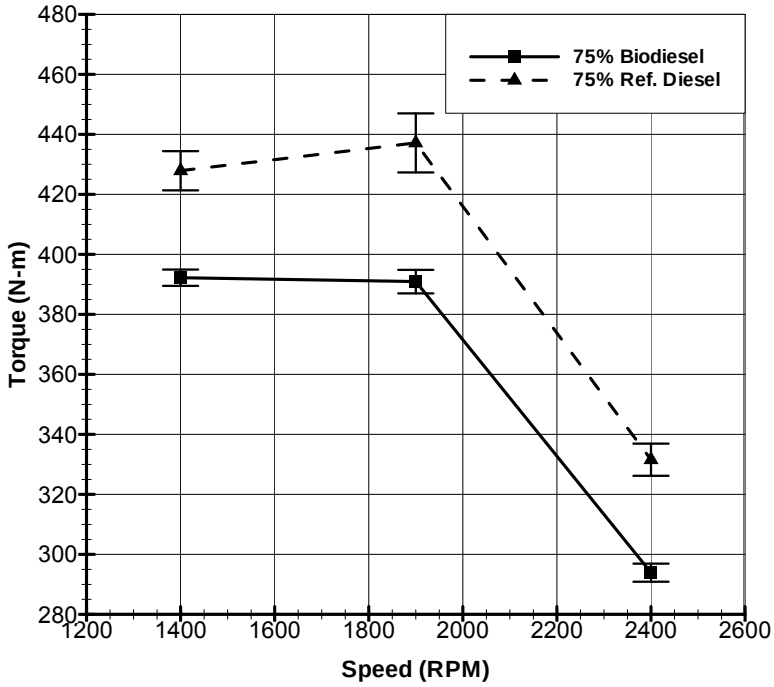

Figure 33: Torque versus engine speed for biodiesel and conventional diesel fuel for 75% load. Max uncertainty ± 9.825 N-m.

Torque differences between biodiesel and conventional diesel will be evaluated by differences in engine performance parameters. The relationship of performance parameters affecting torque are expressed in the following equation:

$$T = \frac{\eta_{fc}\eta_{\upsilon}\rho_{a,i}V_d\left(\frac{F}{A}\right)Q_{LHV}}{4\pi}$$

The performance parameters that affect torque consist of fuel conversion efficiency, volumetric efficiency, intake manifold air density, displacement volume, fuel-air ratio, and the lower heating value of the fuel. These changes will be discussed to establish why torque has decreased by using biodiesel.

The first parameter that affects torque is the displacement volume. The two fuels used in this study are both performed on the same engine and displacement volume does not change between biodiesel and conventional diesel fuel testing. Thus, displacement volume has no effect on the torque differences seen in the comparison of biodiesel and conventional diesel fuel.

A second parameter that affects torque is the energy content of the fuel or the lower heating value. The lower heating value of conventional diesel is 42.240 MJ/kg compared to the heating value of biodiesel of 37.691 MJ/kg. The heating value of biodiesel is considerably less than that of conventional diesel which will produce less work per cycle. Thus, the production of less work per cycle translates into lower torque production. The heating value of the fuel is one parameter attributed to the lower torque production seen with biodiesel fuel.

A third parameter that affects torque is the density of the air in the intake manifold before entering the combustion chamber. The intake manifold air density is a function of the intake absolute manifold pressure, humidity, and temperature. These parameters were evaluated in determining the intake air density. The humidity and barometric pressure set the partial pressure of water vapor in the air. Knowing this partial pressure, one can calculate the pressure of solely the air in the intake manifold. The pressure of air is then used to calculate the air density in the intake manifold. The increased density of the air translates to more mass entering the combustion chamber volume, thus allowing for more fuel to be injected. The more fuel injected translates into a higher torque production.

Figure 34 through Figure 36 show the intake manifold air density of biodiesel relative to conventional diesel at each respective load versus engine speed. At 20% load, the conventional diesel intake air density is slightly higher compared to the intake manifold air density of biodiesel. The biodiesel intake manifold density lies within the conventional diesel uncertainty giving confidence that the slight difference in air density is negligible. Biodiesel intake manifold air density at 60% load is slightly higher than conventional diesel but as seen with 20% load it also lies within the conventional diesel uncertainty. Thus, the 60% load intake manifold air density can be said to be similar. At 75% load, as 60% load, the intake manifold air density can be said to be similar. Therefore, the intake manifold air density is not a parameter affecting the difference in torque seen between fuels.

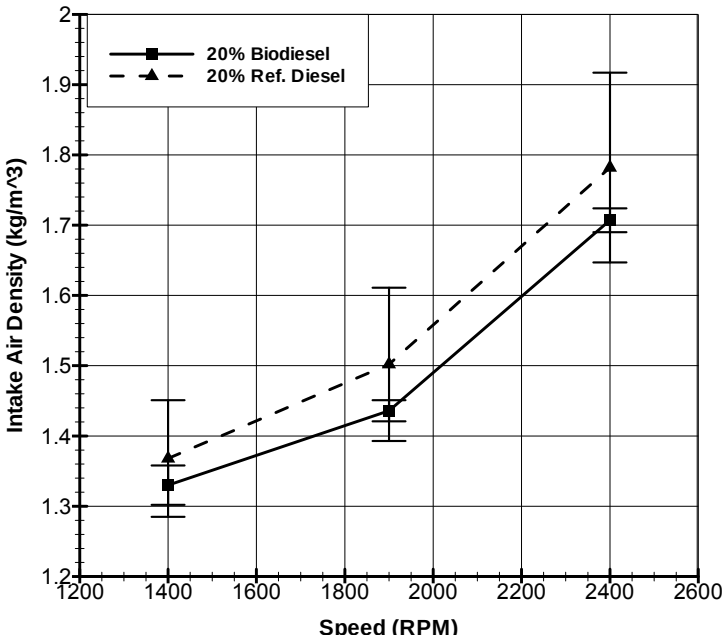

Figure 34: Intake manifold air density for biodiesel and conventional diesel fuel for 20% load. Max uncertainty ± .135 kg/m^3.

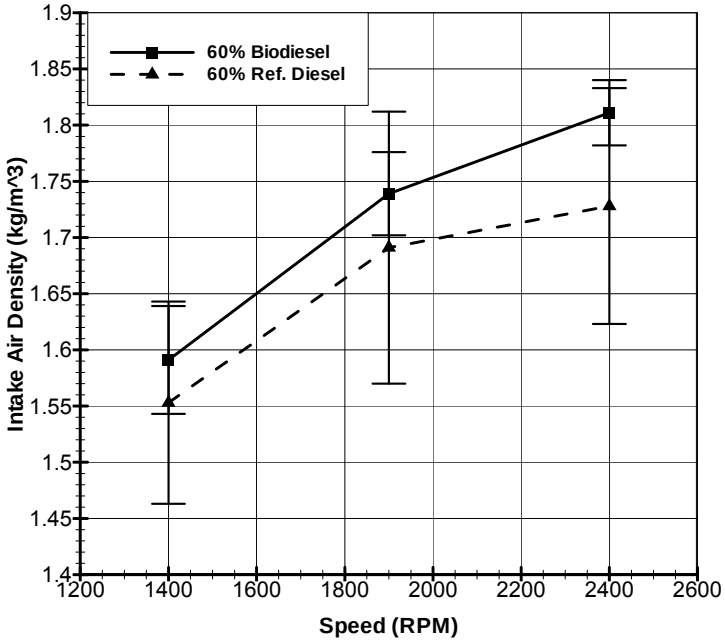

Figure 35: Intake manifold air density for biodiesel and conventional diesel fuel for 60% load. Max uncertainty ± .121 kg/m^3.

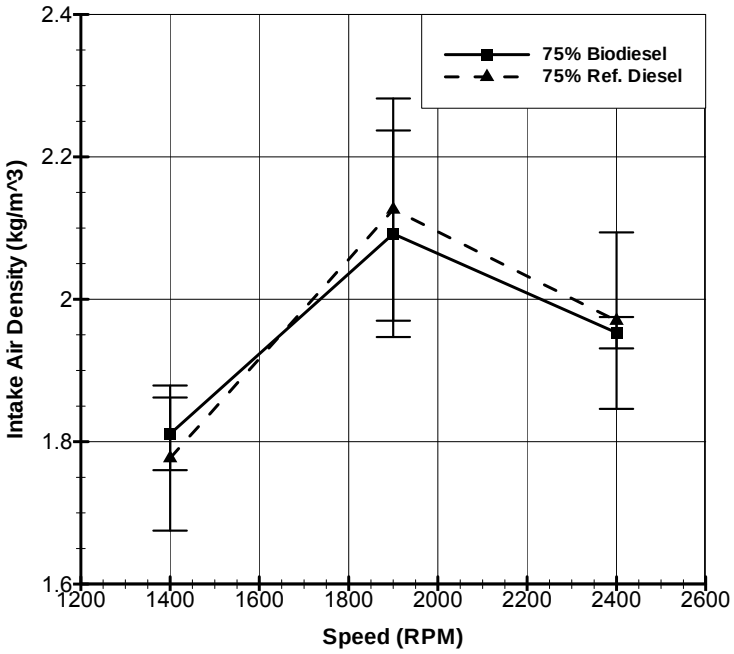

Figure 36: Intake manifold air density for biodiesel and conventional diesel fuel for 75% load. Max uncertainty ± .156 kg/m^3.

Figure 37 through Figure 39 show the intake manifold pressure of biodiesel relative to conventional diesel at each respective load versus engine speed. Notice that IMP trends follow closely the trends of intake air density at all loads of both the biodiesel and conventional diesel fuels. At 20% load, conventional diesel IMP is higher than biodiesel; thus the increased intake air density seen in Figure 34. At 60% load, biodiesel IMP is higher than conventional diesel. This translates into the higher intake air density of biodiesel compared to conventional diesel. The increased uncertainty can be attributed to the humidity and barometric pressure variations of day to day testing. The same trends of IMP at 75% load are seen with intake air density.

A fourth parameter that affects torque is the fuel conversion efficiency. The fuel conversion efficiency is how well the energy supplied to the engine is being released by combustion in the cylinder. Thus, the fuel conversion efficiency is a measure of how well the combustion process converts the fuel energy into work or in this case torque. Fuel conversion efficiency is the ratio of the power produced by the engine to the rate of fuel energy that is supplied to the engine. The rate of fuel energy that is supplied to the engine is a multiplication of the mass flow rate of fuel with lower heating value of fuel.

Figure 40 through Figure 42 show the fuel conversion efficiency comparison between biodiesel and conventional diesel fuel at each load tested. At 20% load, the fuel conversion efficiency of both fuels is similar with conventional diesel being slightly higher. Increasing the load to 60%, the fuel conversion efficiency with conventional diesel has a slightly lower efficiency at 1400 rpm but is slightly higher for the other two engine speeds. At 75% load, a similar trend is seen to 60% load. Looking at these

figures, the fuel conversion efficiency of biodiesel and conventional diesel lie within the uncertainty of each fuel for 1400 and 1900 rpm; giving confidence that the slight difference in fuel conversion efficiency is negligible. Thus, the fuel conversion efficiency for both fuels can be said to be similar. At 2400 rpm, the difference in fuel conversion efficiency is significant, but is minimal. This parameter is therefore not affecting the difference in torque production between the two fuels.

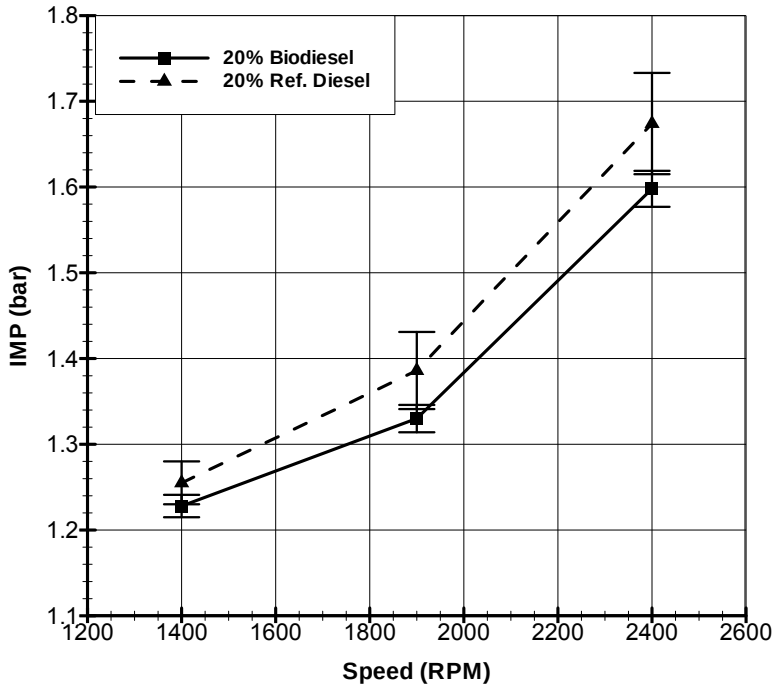

Figure 37: Intake manifold pressure using biodiesel and conventional diesel fuel for 20% load. Max uncertainty ± .059 bar.

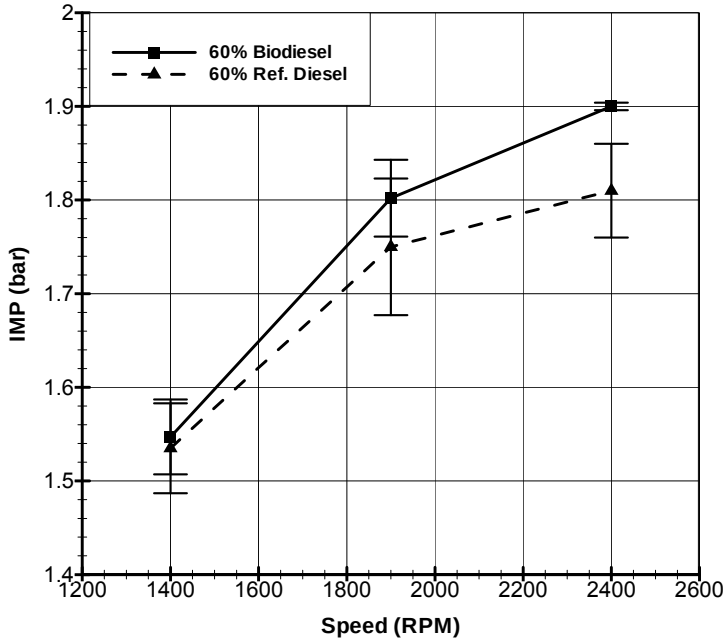

Figure 38: Intake manifold pressure using biodiesel and conventional diesel fuel for 60% load. Max uncertainty ± .073 bar.

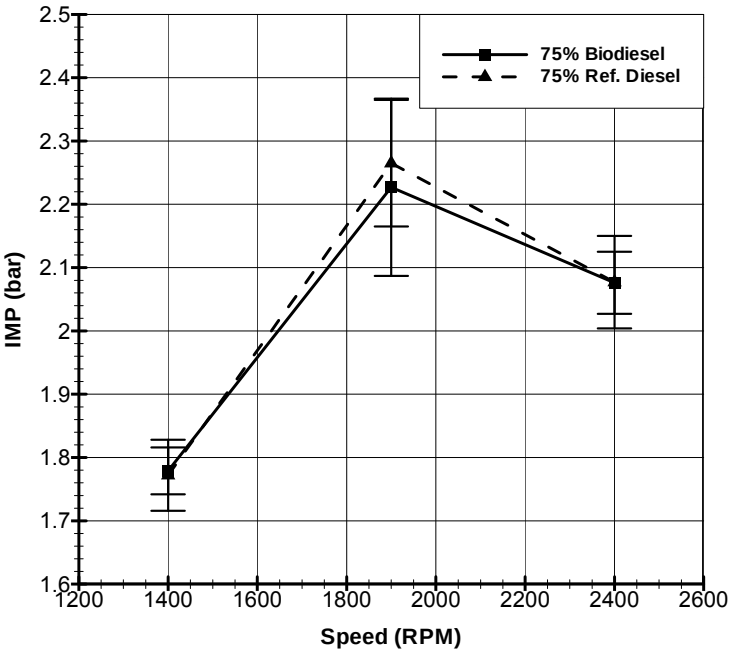

Figure 39: Intake manifold pressure using biodiesel and conventional diesel fuel for 75% load. Max uncertainty ± .14 bar.

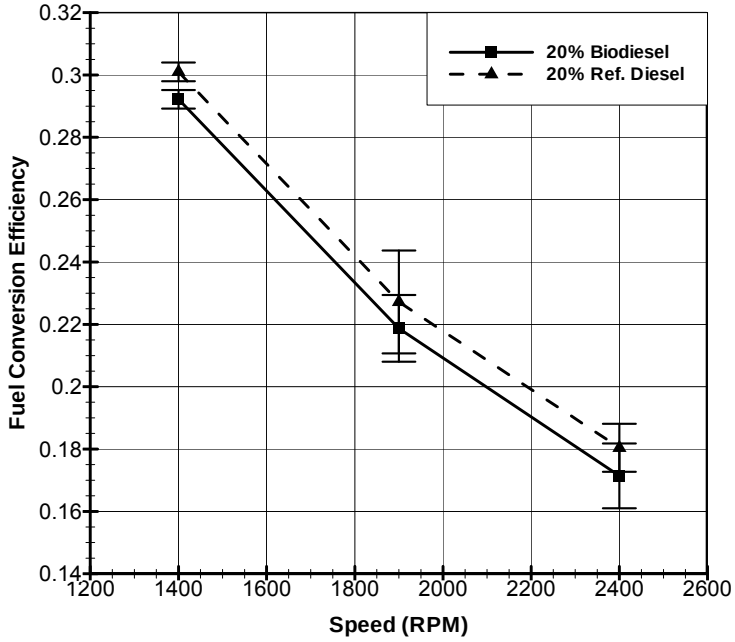

Figure 40: Fuel conversion efficiency for biodiesel and conventional diesel fuel for 20% load. Max uncertainty ± .016.

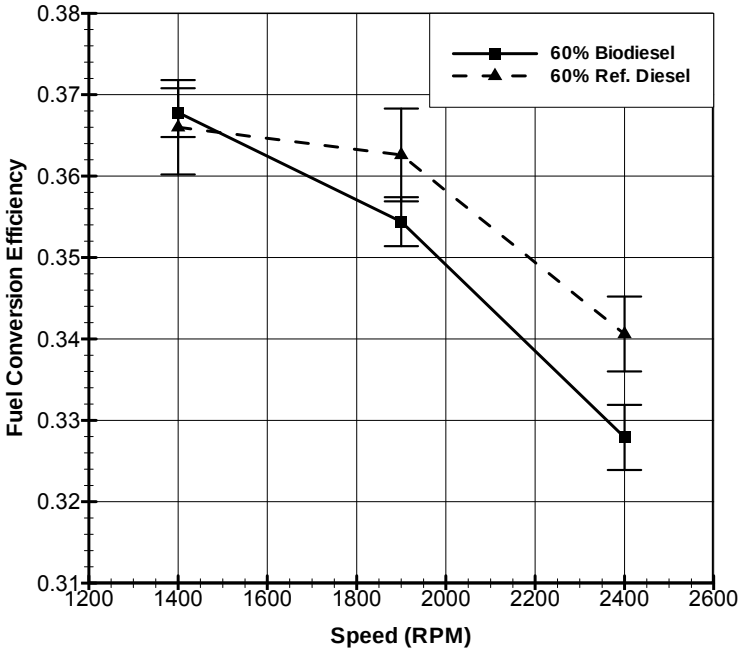

Figure 41: Fuel conversion efficiency for biodiesel and conventional diesel fuel for 60% load. Max uncertainty ± .006.

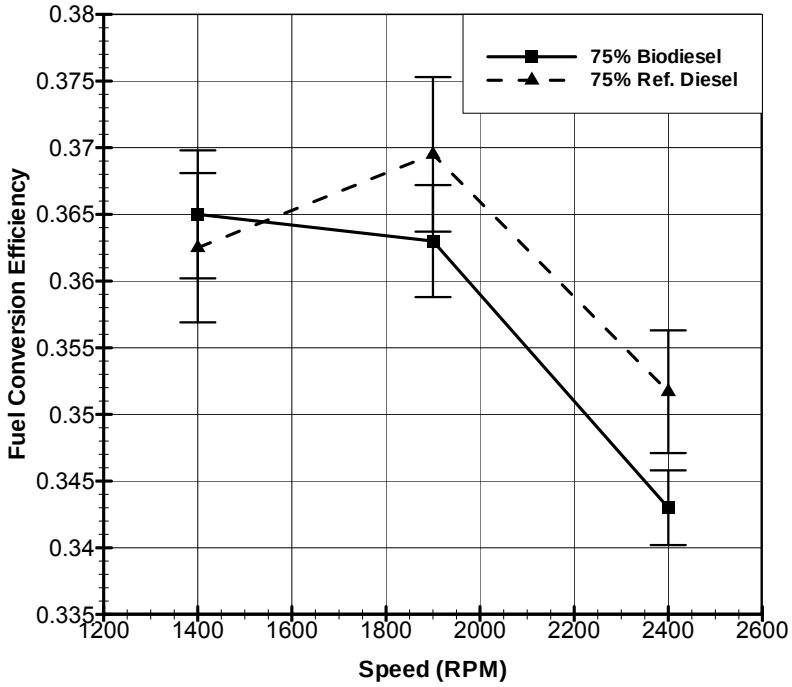

Figure 42: Fuel conversion efficiency for biodiesel and conventional diesel fuel for 75% load. Max uncertainty ± .006.

A fifth parameter that affects torque is the fuel-air ratio. The fuel-air ratio is a ratio of the fuel mass flow to the air mass flow. Thus, the fuel-air ratio gives the amount of mass of fuel in the mixture for a unit mass of air. The stoichiometric fuel-air ratios for biodiesel and conventional diesel differ with biodiesel having the greater fuel-air ratio. Biodiesel requires more fuel per unit mass of air compared to conventional diesel at stoichiometric conditions. An increase in biodiesel fuel-air ratio should be seen in comparison of these fuels to obtain a similar torque production to conventional diesel.

Figure 43 through Figure 45 show the fuel-air ratio comparison between biodiesel and conventional diesel fuel at each load tested. At 20% load, the fuel-air ratio decreases as speed increases with a slight increase from 1900 to 2400 rpm. Also,

biodiesel has a higher fuel-air ratio compared to conventional diesel for the engine speeds tested. The mixture enriches with air as the speed increases to 1900 rpm with the fuel-air ratio increasing slightly as the speed is raised to 2400 rpm. Again, biodiesel fuel-air ratio is higher than conventional diesel for 60 and 70% load. As the speed increases, the ratio decreases meaning the mixture is getting leaner. The difference of fuel-air ratio between both fuels for all loads is not significant. This parameter will not give a significant contribution to the difference of torque production seen between biodiesel and conventional diesel fuel.

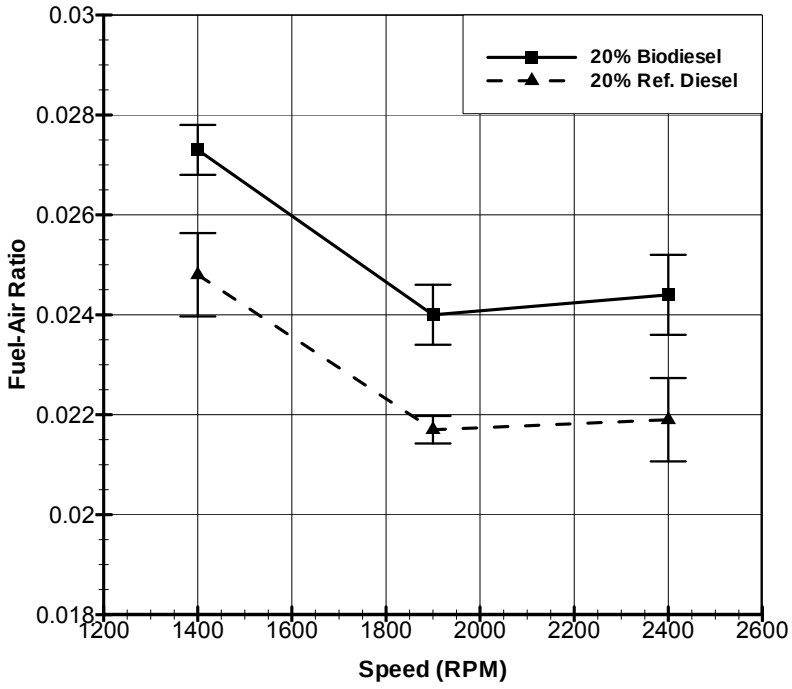

Figure 43: Fuel-air ratio versus engine speed for biodiesel and conventional diesel fuel for 20% load. Max uncertainty ± .00083.

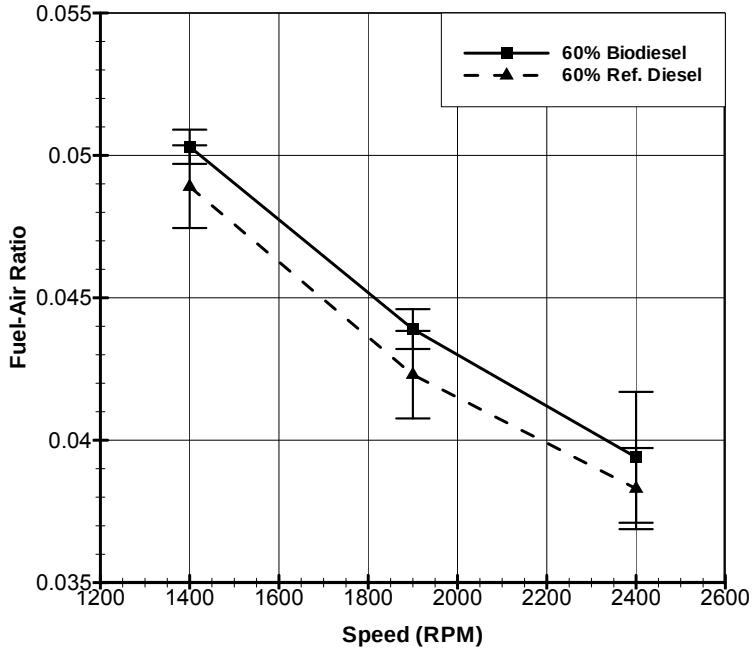

Figure 44: Fuel-air ratio versus engine speed for biodiesel and conventional diesel fuel for 60% load. Max uncertainty ± .00153.

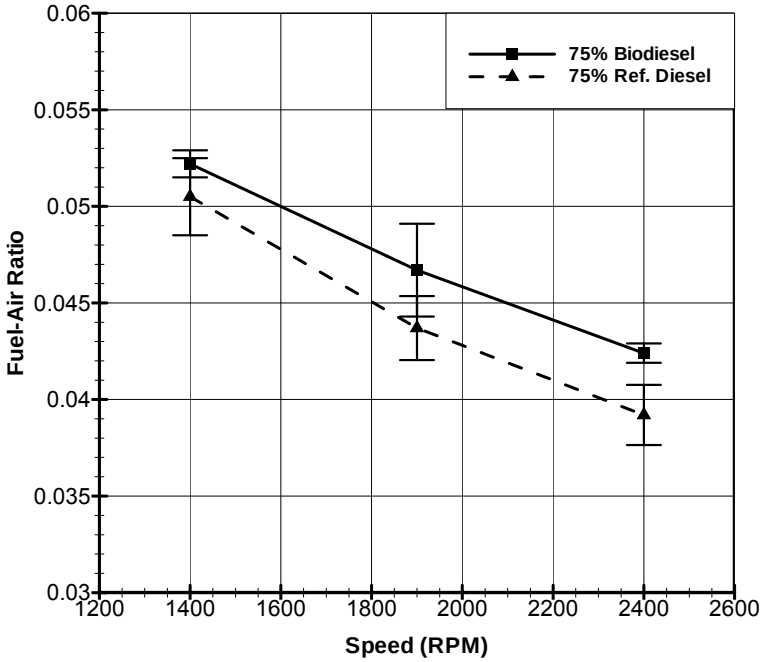

Figure 45: Fuel-air ratio versus engine speed for biodiesel and conventional diesel fuel for 75% load. Max uncertainty ± .00235.

A final parameter that affects torque production is the volumetric efficiency. The volumetric efficiency is measuring how well the engine is inducting air into the cylinder volume. The greater volumetric efficiency the greater amount of fuel can be injected into the cylinder, thus increasing the torque output of the engine.

Figure 46 through Figure 48 show the volumetric efficiency comparison between biodiesel and conventional diesel fuel. At all loads, there is a slight increase in volumetric efficiency from biodiesel by conventional diesel fuel. The slight increase can be said to be negligible due to the uncertainty lying within the biodiesel uncertainty, thus not affecting the difference in torque production.

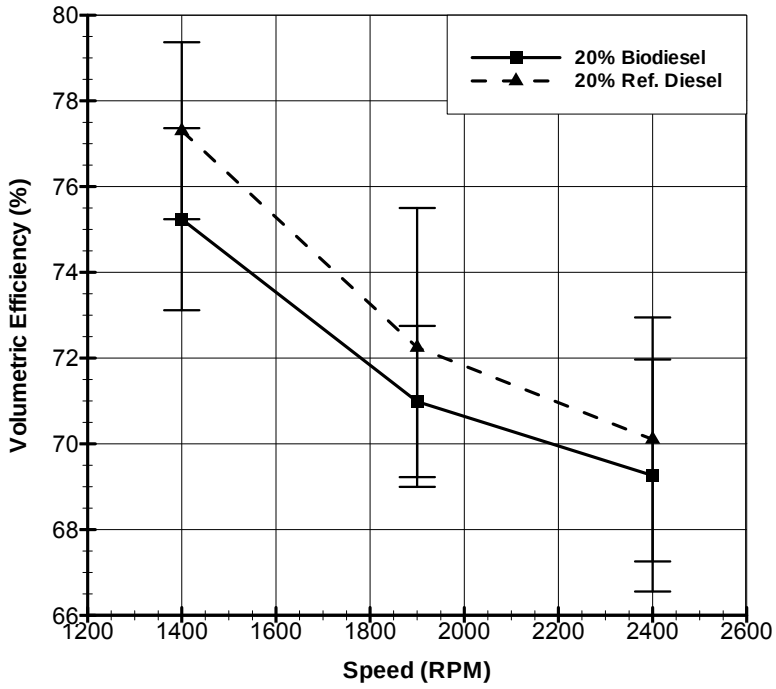

Figure 46: Volumetric efficiency versus engine speed for biodiesel and conventional diesel fuel for 20% load. Max uncertainty ± 3.252%.

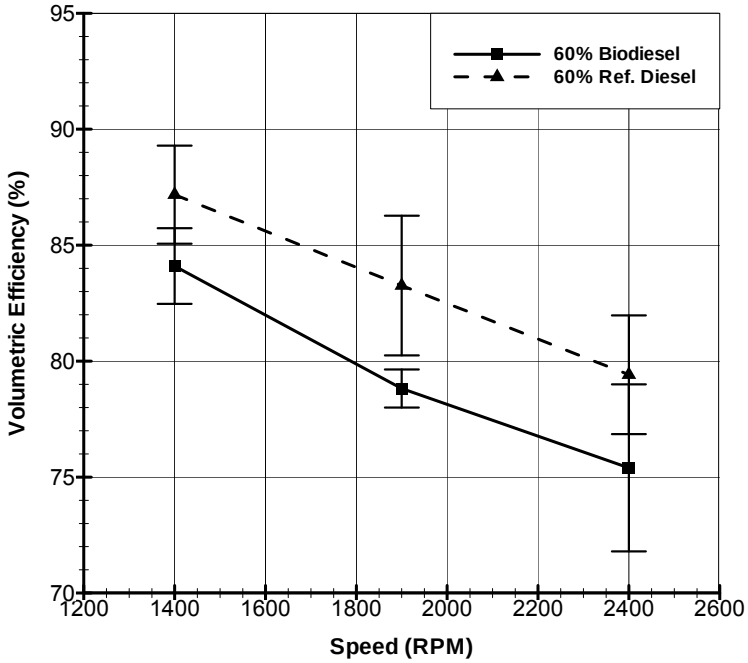

Figure 47: Volumetric efficiency versus engine speed for biodiesel and conventional diesel fuel for 60% load. Max uncertainty ± 3.602%.

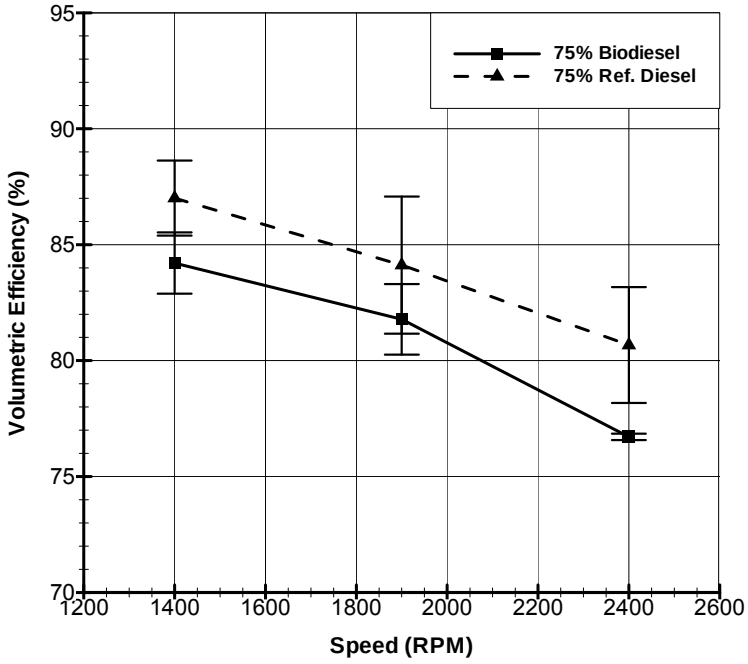

Figure 48: Volumetric efficiency versus engine speed for biodiesel and conventional diesel fuel for 75% load. Max uncertainty ± 2.955%.

Another way fundamentally to decrease torque is to increase the pumping work of the engine. The pumping work is defined as the work transfer between the cylinder gases and the piston during inlet and exhaust of gases. The pumping work transfer will be to the piston or positive if the intake manifold pressure is greater than the exhaust manifold. The opposite is true for negative pumping work; the exhaust manifold pressure is greater than the intake manifold pressure. Again, not having the capability to generate a P-V diagram, an approximation is used for the pumping work of the engine. The pumping work is taken to be the difference between the exhaust manifold and intake manifold pressures.

Figure 49 through Figure 51 show the pumping work comparison of biodiesel and conventional diesel fuel for each respective load. Figure 49 shows a slight decrease in pumping work for biodiesel at 20% load. Though at 1400 rpm, the difference in pumping work is negligible. At 60 and 75 % load, there is a significant increase in the pumping work of biodiesel compared to conventional diesel. Thus, the increased pumping work of biodiesel at 60 and 75% load decreases torque. The reason for the increase in pumping work will be discussed later.

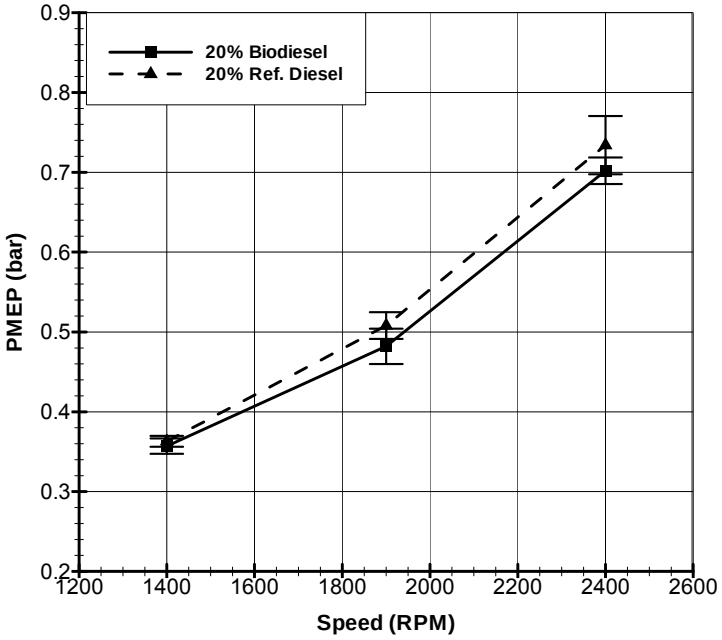

Figure 49: Pumping work comparison of biodiesel and conventional diesel fuel for 20% load. Max uncertainty ± .036 bar.

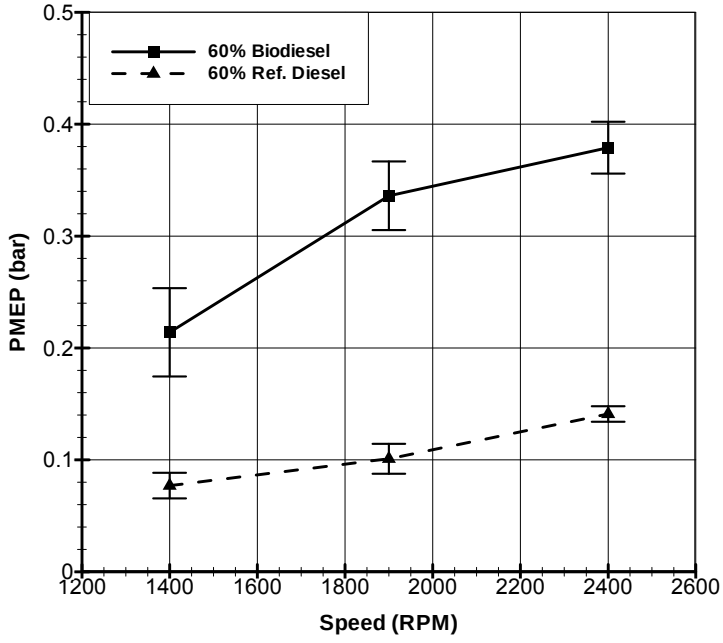

Figure 50: Pumping work comparison of biodiesel and conventional diesel fuel for 60% load. Max uncertainty ± .039 bar.

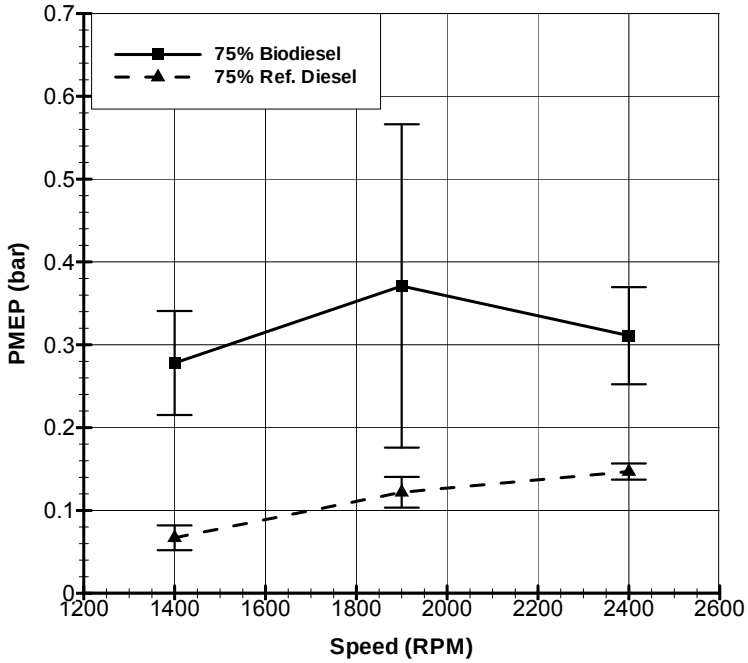

Figure 51: Pumping work comparison of biodiesel and conventional diesel fuel for 75% load. Max uncertainty ± .195 bar.

The final way fundamentally, discussed in this study, to decrease torque is to decrease the fuelling of the engine. Figure 52 through Figure 54 show the fuel flow rate of biodiesel relative to conventional diesel at each respective load versus engine speed. The fuel flow rate for all loads and engines speeds show a slight increase for biodiesel compared to conventional diesel. Thus, one can infer the torque of the biodiesel fuelled engine would be larger than conventional diesel. This, of course, is not true as previously discussed.

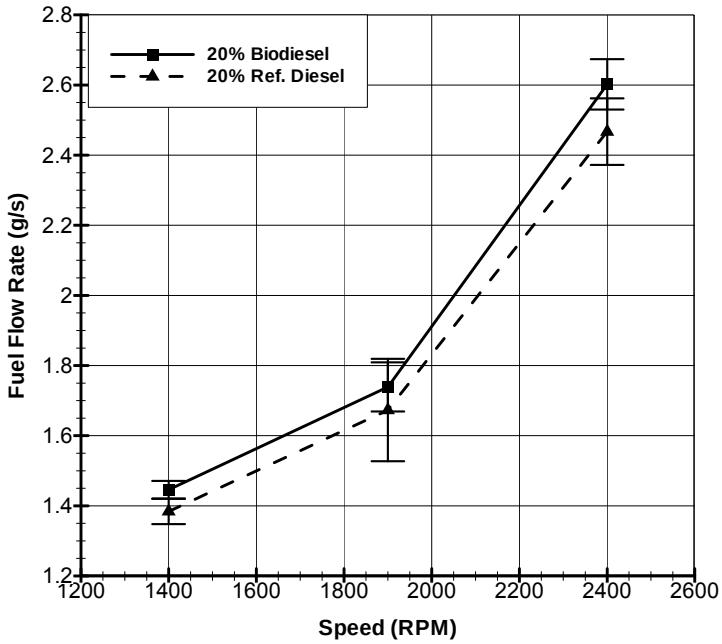

Figure 52: Fuel flow rate comparison for biodiesel and conventional diesel fuel for 20% load. Max uncertainty ± 0.146 g/s.

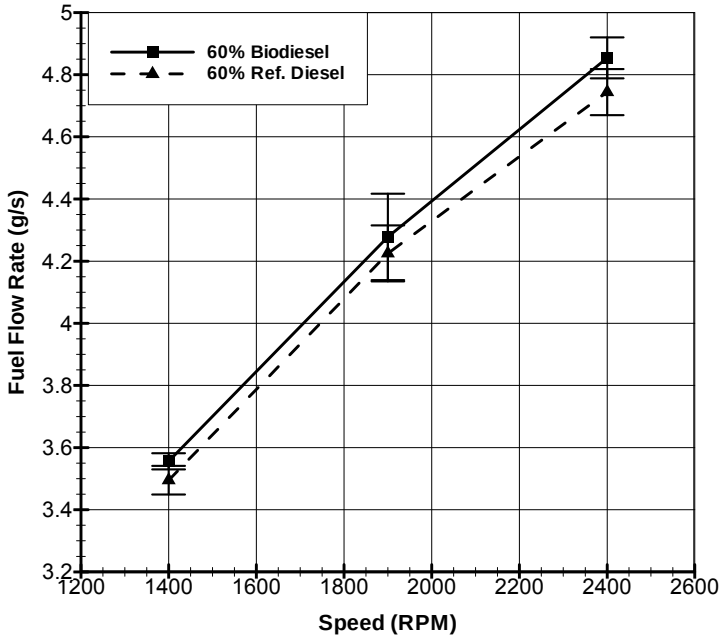

Figure 53: Fuel flow rate comparison for biodiesel and conventional diesel fuel for 60% load. Max uncertainty ± 0.139 g/s.

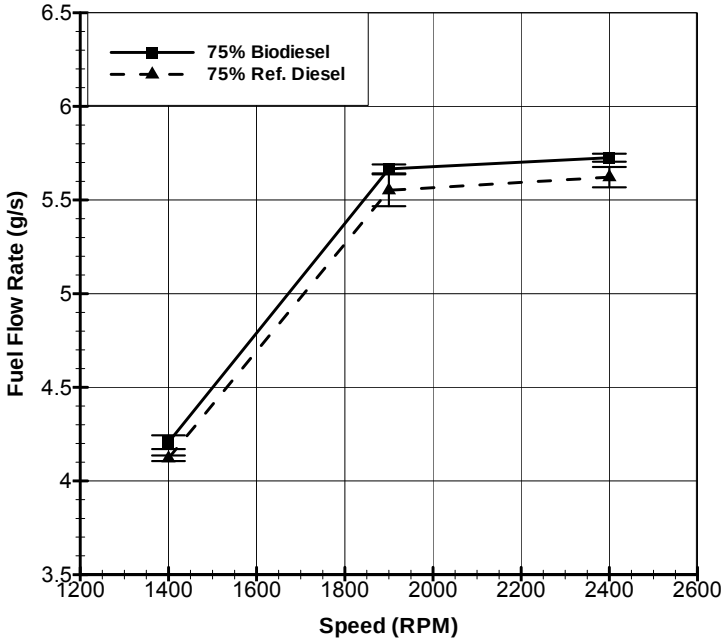

Figure 54: Fuel flow rate comparison for biodiesel and conventional diesel fuel for 75% load. Max uncertainty ± 0.085 g/s.

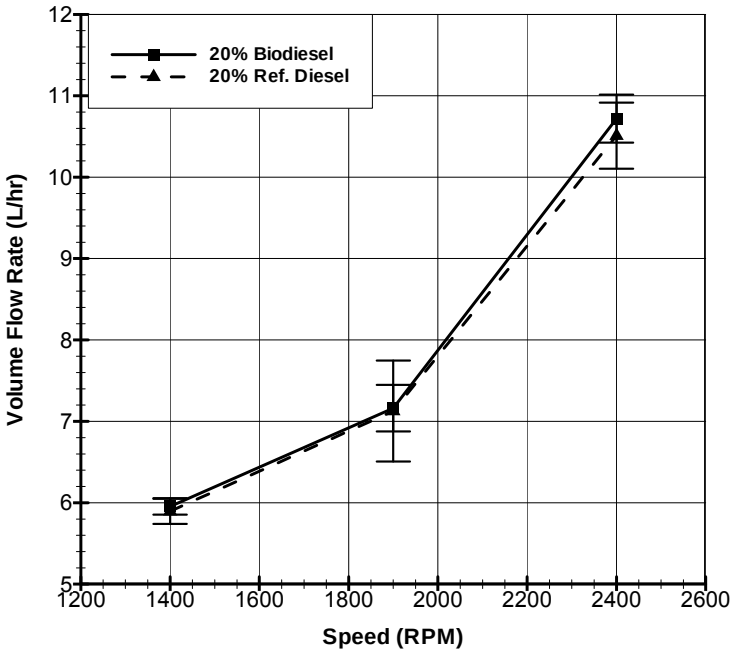

Figure 55: Volume flow rate comparison for biodiesel and conventional diesel fuel for 20% load. Max uncertainty ± 0.621 L/hr.

One explanation for biodiesel fuel flow rate increasing over conventional diesel fuel is the fact that biodiesel has a higher density. Therefore, for the same volume of biodiesel flow as conventional diesel, the biodiesel would have a higher mass flow rate. The fuel flow rate was normalized with density, thus divided by their respective densities to obtain a volume flow rate shown in Figure 55 through Figure 57. The volume flow rates at 20% load are similar with the exception of 2400 rpm with a slight volume flow increase of biodiesel. The 60% load trend is a linear increase in volume flow as engine speed increases with conventional diesel having a slightly higher volume flow. At 75% load, similarly to 60% load, conventional diesel has a slightly higher volume flow. The slight differences in volume flow rates are insignificant; therefore the engine is requiring the same flow for both fuels and is not a factor in decreasing combustion work.

As stated earlier in the performance of conventional diesel, a parameter that measures the efficiency of how well the engine uses the fuel supplied to produce work is BSFC. Figure 58 through Figure 60 show the BSFC of biodiesel relative to conventional diesel at each respective load versus engine speed. Biodiesel BSFC increases over conventional diesel and follows the same trend for all loads and engine speeds. As discussed earlier, the ECM is not demanding a change in fuel flow for biodiesel compared to conventional diesel fuel. Thus, BSFC increases for biodiesel due to the engine producing less power for the same amount of fuel flow.

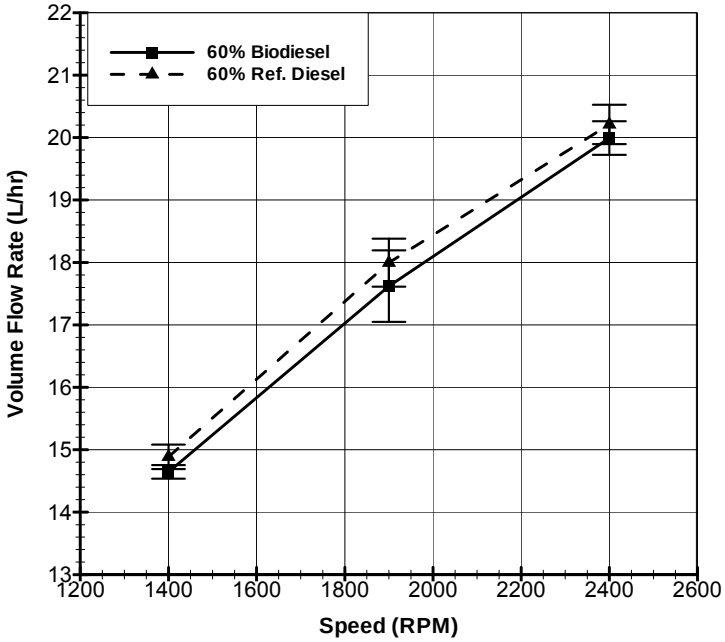

Figure 56: Volume flow rate comparison for biodiesel and conventional diesel fuel for 60% load. Max uncertainty ± 0.573 L/hr.

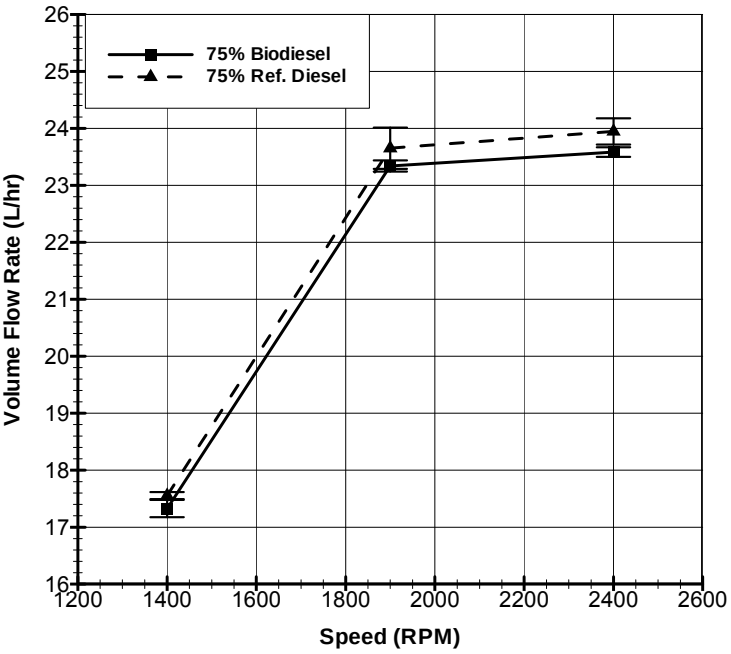

Figure 57: Volume flow rate comparison for biodiesel and conventional diesel fuel for 75% load. Max uncertainty ± 0.363 L/hr.

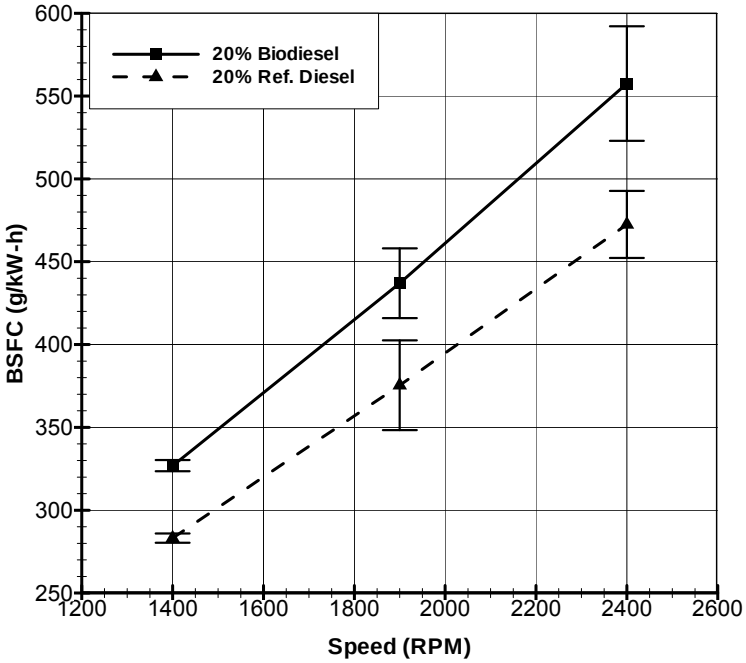

Figure 58: BSFC comparison for biodiesel and conventional diesel fuel for 20% load. Max uncertainty ± 34.586 g/kW-h.

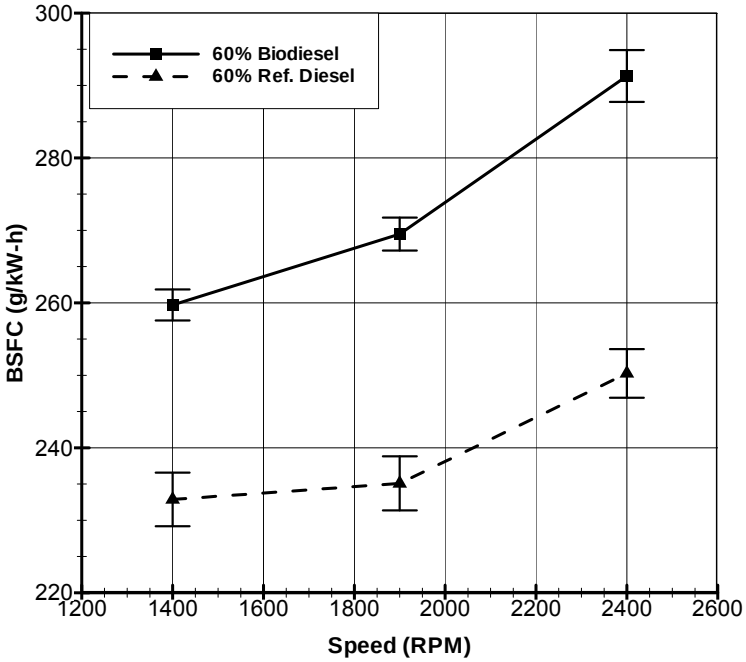

Figure 59: BSFC comparison for biodiesel and conventional diesel fuel for 60% load. Max uncertainty ± 3.579 g/kW-h.

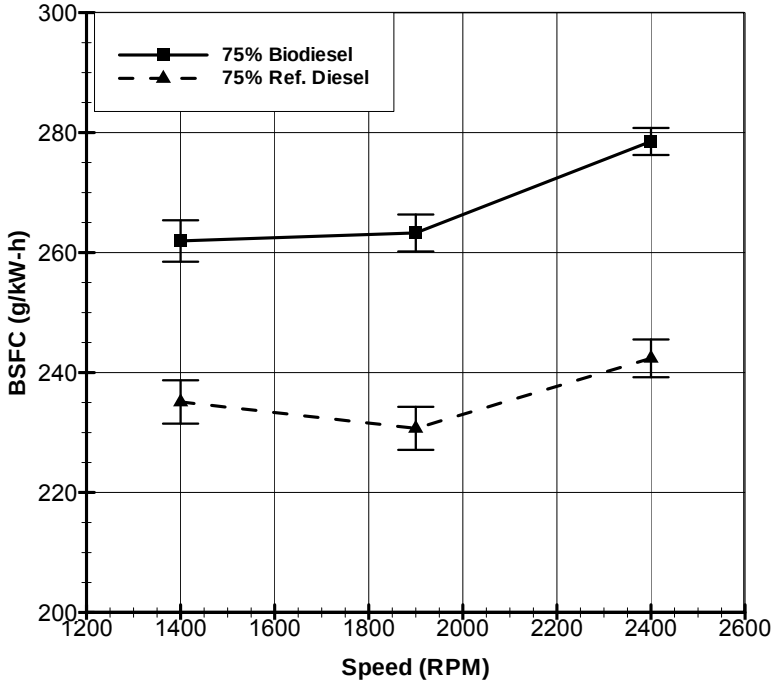

Figure 60: BSFC comparison for biodiesel and conventional diesel fuel for 75% load. Max uncertainty ± 3.61 g/kW-h.

3.3.2 Breathing of Engine

The VGT, as discussed earlier, is an important tool to the breathing of the engine. The VGT sets the exhaust manifold pressure as the ECM demands pressure both to drive EGR and engine performance. The turbine derives its work from the exhaust gases passing through it. The work transfer to the compressor is a function of both the exhaust temperature and pressure of the exhaust gases.

The first parameter that affects the amount of work derived from exhaust gases is temperature. A decrease in temperature at a fixed pressure ratio through the turbine results in a decrease in the velocity to the turbine vanes, thus decreasing the work extracted by the turbine. Figure 61 through Figure 63 show the turbine temperature inlet

(TTI) comparison between biodiesel and conventional diesel. All the loads tested show a decrease in TTI for biodiesel as a result of the decrease in fuel heating value. Therefore, there is a decrease in energy that the turbine can extract from the exhaust gases. At 20% load, the biodiesel TTI is not lowered significantly compared to conventional diesel. Thus, the decrease in energy the turbine can extract is also not as significant. On the other hand, the 60 and 75% load biodiesel TTI is significantly lower than conventional diesel.

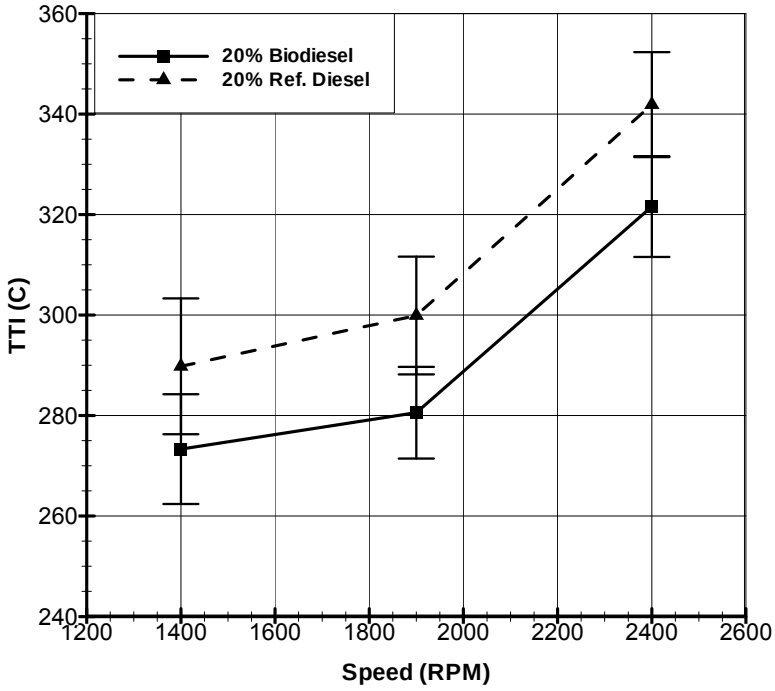

Figure 61: Turbine temperature inlet comparison of biodiesel and conventional diesel fuel for 20% load. Max uncertainty ± 13.156°C.

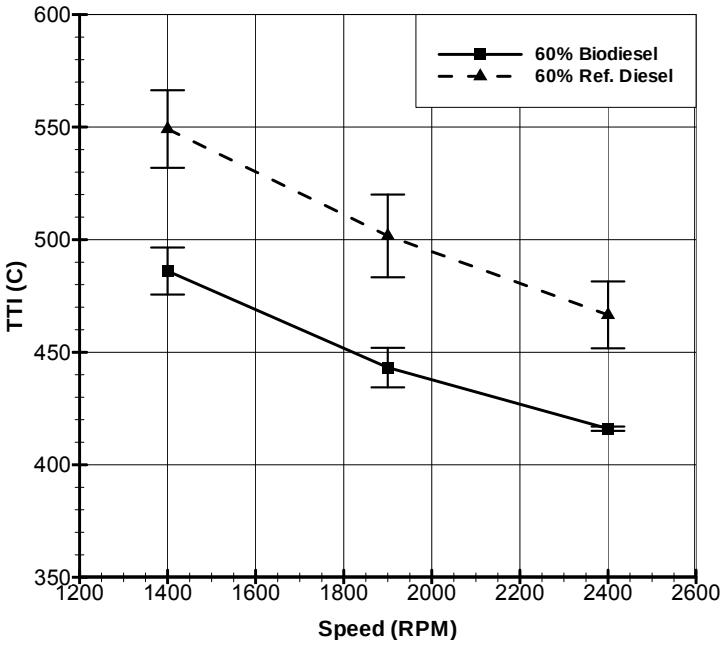

Figure 62: Turbine temperature inlet comparison of biodiesel and conventional diesel fuel for 60% load. Max uncertainty ± 18.384°C.

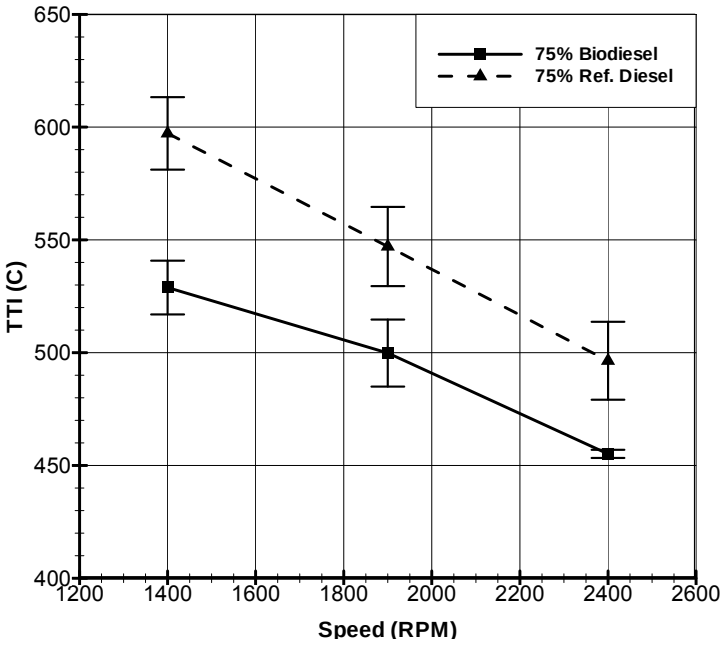

Figure 63: Turbine temperature inlet comparison of biodiesel and conventional diesel fuel for 75% load. Max uncertainty ± 17.541°C.

The second parameter that affects the amount of turbine work derived from exhaust gases is pressure. Figure 64 through Figure 66 show the exhaust manifold pressure (EMP) comparison between biodiesel and conventional diesel at each respective load. At 20% load, biodiesel has a slight decrease of EMP compared to conventional diesel. The slight decrease in EMP can be attributed to the ECM not demanding the VGT vanes to close to increase the EMP. Thus, because the exhaust gas temperature of biodiesel is less than conventional diesel a decrease in pressure is seen at 20% load shown in Figure 64. A reverse trend is seen at both 60 and 75% load with biodiesel EMP increasing compared to conventional diesel. At these two loads, as stated above, biodiesel TTI is significantly less than conventional diesel. Thus, the EMP has to increase to compensate for the lower temperature exhaust flow through the turbine.

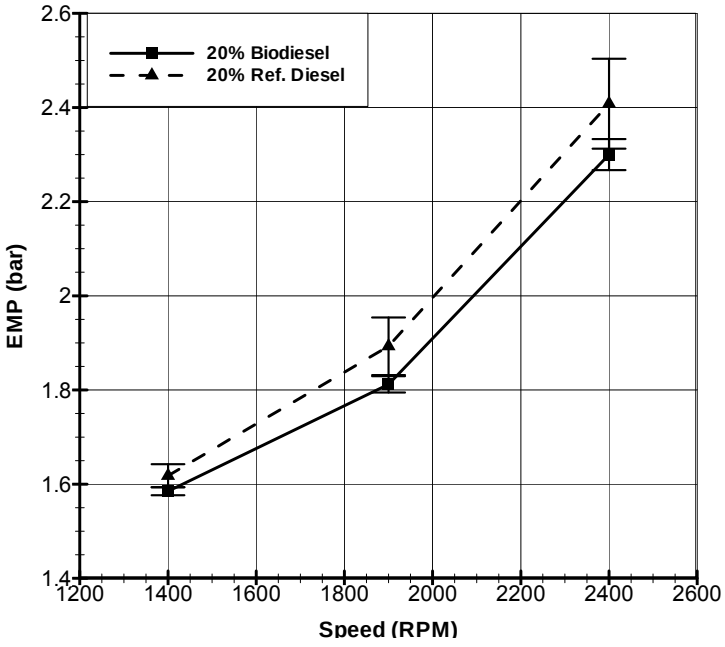

Figure 64: Exhaust manifold pressure comparison of biodiesel and conventional diesel fuel for 20% load. Max uncertainty ± .095 bar.

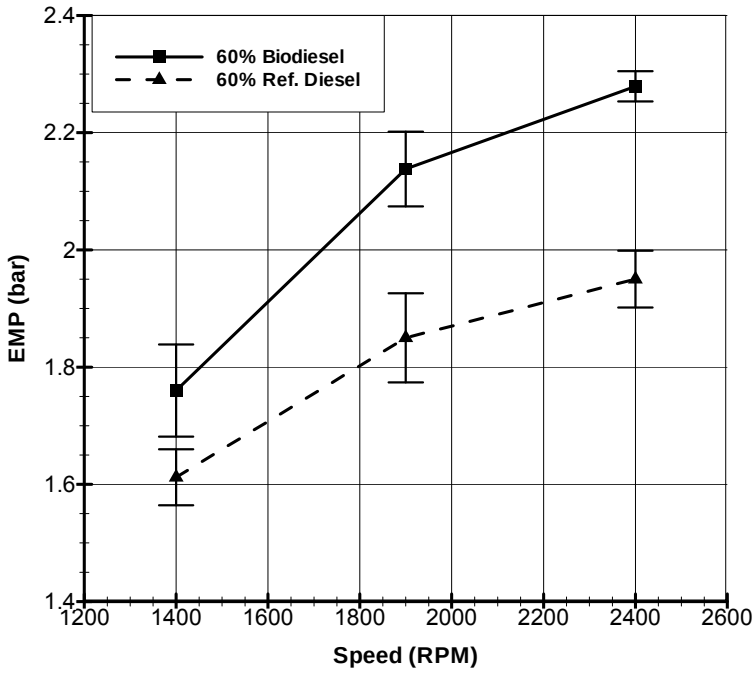

Figure 65: Exhaust manifold pressure comparison of biodiesel and conventional diesel fuel for 60% load. Max uncertainty ± .079 bar.

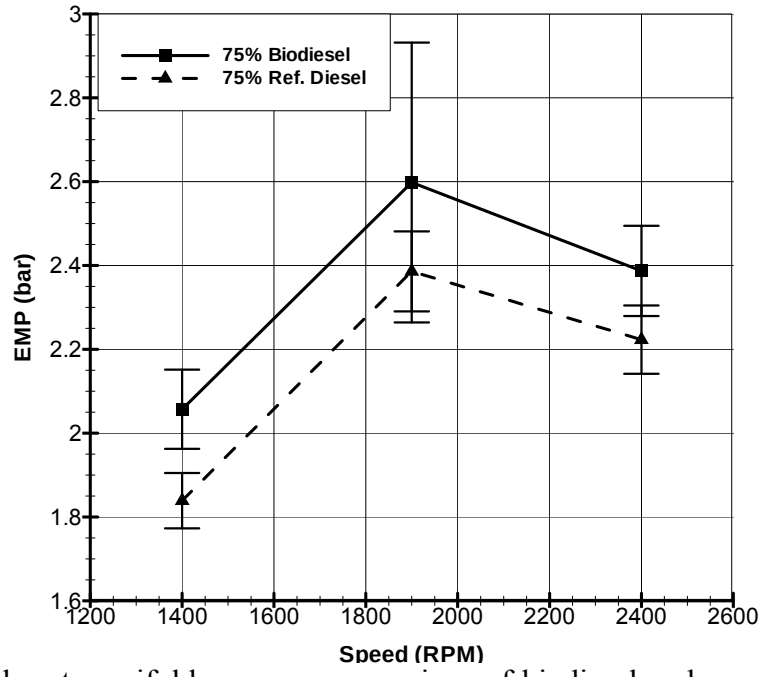

Figure 66: Exhaust manifold pressure comparison of biodiesel and conventional diesel fuel for 75% load. Max uncertainty ± .334 bar.

After exhaust gases pass through the turbine, the exhaust gas temperatures decrease. The decrease in temperature is given by the turbine temperature out (TTO) shown in Figure 67 through Figure 69. The biodiesel TTO, for all loads tested, decrease compared to conventional diesel. The decrease in temperature of biodiesel compared to conventional diesel is attributed to the starting TTI of biodiesel exhaust and the amount of energy extracted from the exhaust stream. Looking at 20% load, the difference in TTO between biodiesel and conventional diesel is not as significant compared to the other two loads tested. This follows the 20% load temperature comparison of TTI. Also, similar to TTI, the 60 and 70% load biodiesel TTO is significantly lower than conventional diesel.

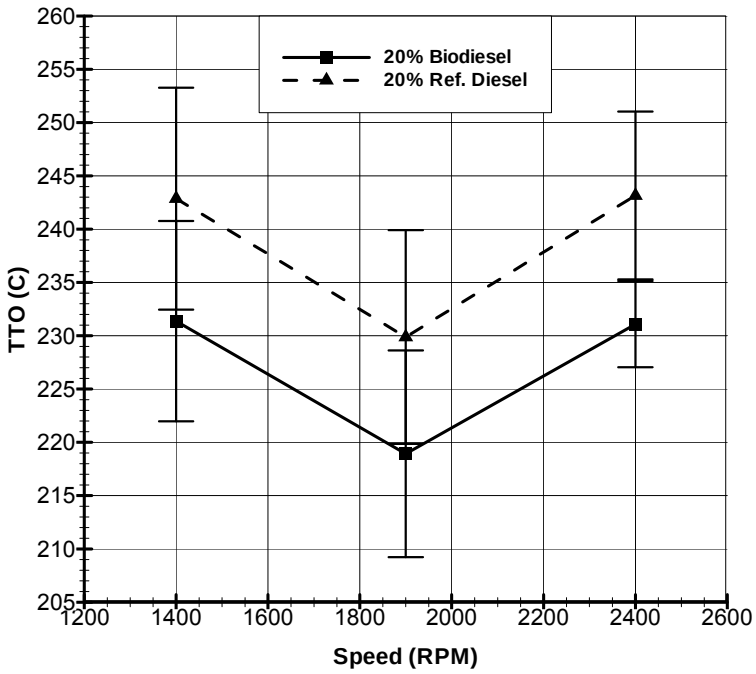

Figure 67: Turbine temperature out comparison of biodiesel and conventional diesel fuel for 20% load. Max uncertainty ± 10.412°C.

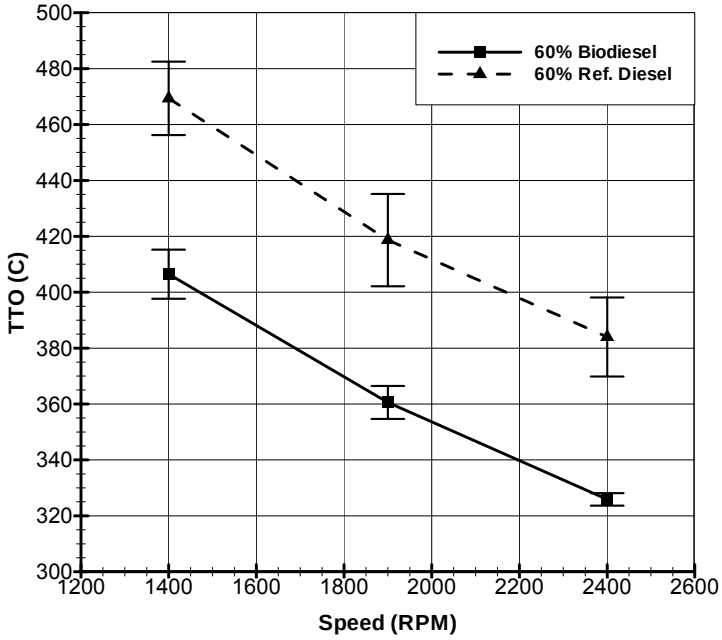

Figure 68: Turbine temperature out comparison of biodiesel and conventional diesel fuel for 60% load. Max uncertainty ± 16.511°C.

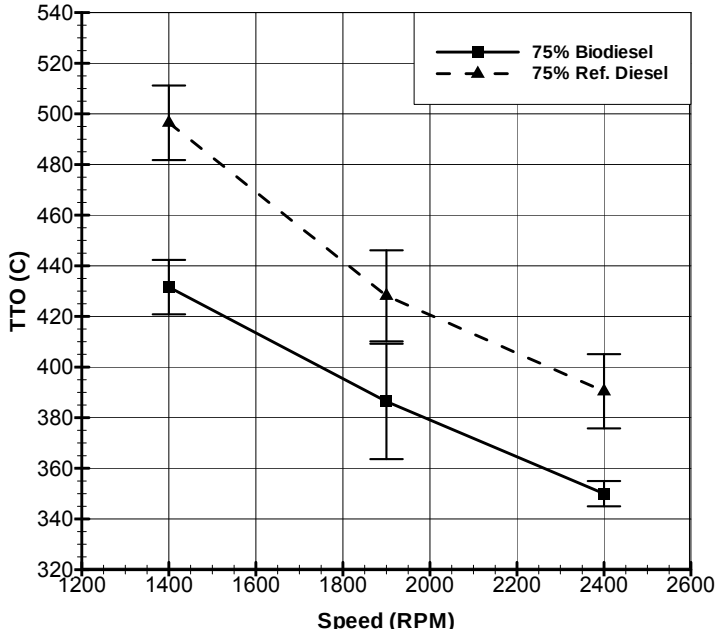

Figure 69: Turbine temperature out comparison of biodiesel and conventional diesel fuel for 75% load. Max uncertainty ± 22.799°C.

The difference between TTI and TTO translates into the energy extracted from the exhaust gases. Figure 70 through Figure 72 show the difference between TTI and TTO. At 20% load, the ECM of the engine should demand the same IMP as conventional diesel and raise the EMP to compensate for the lower TTI. Pressure is directly proportional to temperature, therefore with lower exhaust temps the pressure should decrease in the exhaust manifold. Figure 64 shows biodiesel EMP lower than conventional diesel. The EMP is not being raised for the compensation of the lower exhaust temperature. Thus, the ECM is not demanding any changes at this load. The difference between TTI and TTO shown in Figure 70, therefore, decreases for biodiesel compared to conventional diesel. The decreased difference between TTI and TTO for biodiesel directly affects IMP. Thus, IMP of biodiesel is lower than that of conventional diesel shown in Figure 37.

At 60% load shown in Figure 71, the difference between TTI and TTO is similar for biodiesel and conventional diesel at 1400 and 1900 rpm with a large increase for biodiesel at 2400 rpm. The similarity at these two speeds is due to the ECM demanding an increase in EMP of biodiesel compared to conventional diesel. The increased EMP, shown in Figure 65, translates into an increase in the difference between TTI and TTO which otherwise would have been lower than conventional diesel. Thus, a similarity of IMP at these two speeds. The greater increase in biodiesel EMP at 2400 rpm increases the difference between TTI and TTO, thus increasing biodiesel IMP compared to conventional diesel at this speed.

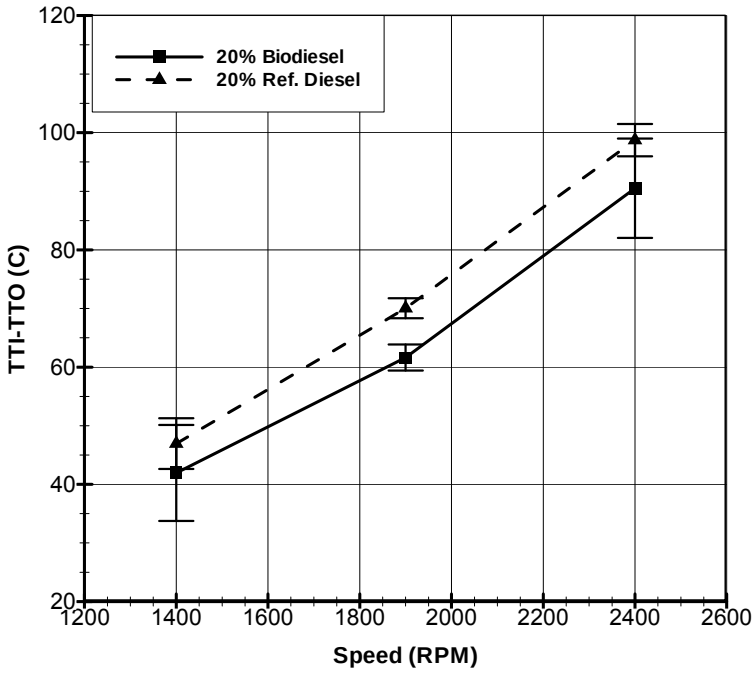

Figure 70: TTI - TTO comparison of biodiesel and conventional diesel fuel for 20% load. Max uncertainty ± 8.475°C.

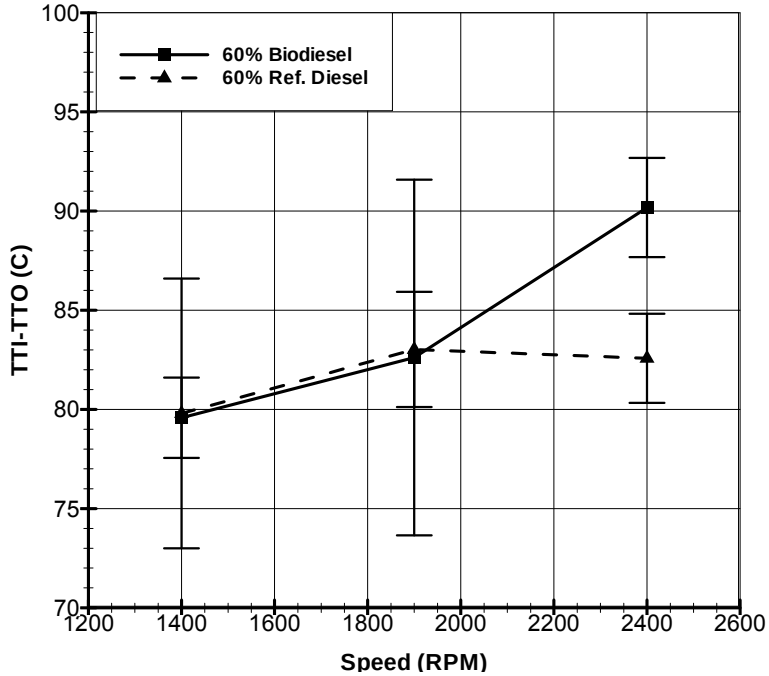

Figure 71: TTI - TTO comparison of biodiesel and conventional diesel fuel for 60% load. Max uncertainty ± 8.976°C.

Figure 72 shows the biodiesel temperature difference between TTI and TTO at 75% load slightly lower than the conventional diesel. Again, the similarity of the temperature difference between TTI and TTO of biodiesel is due to the increased EMP shown in Figure 66. The ECM has demanded the EMP to increase to compensate for the lower TTI, thus achieving a similar IMP for biodiesel compared to conventional diesel fuel.

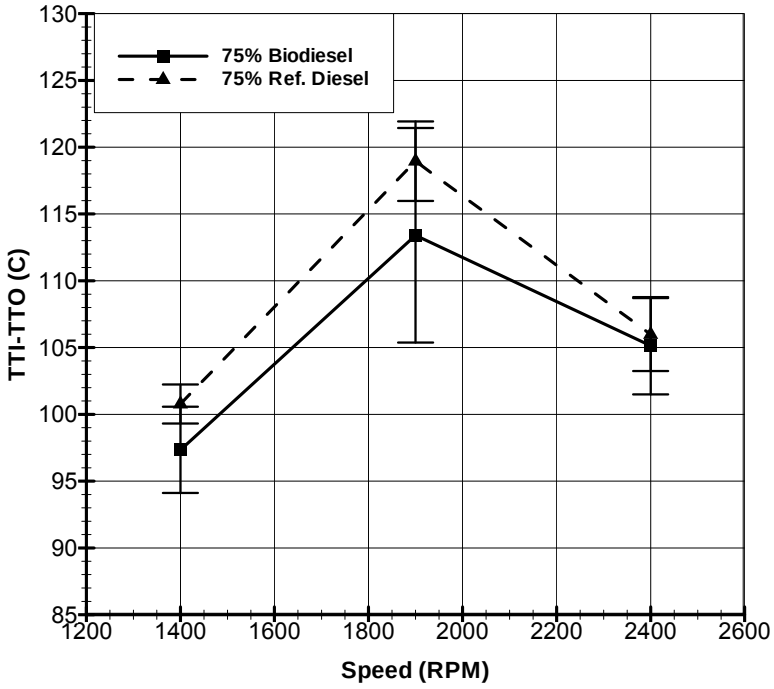

Figure 72: TTI - TTO comparison of biodiesel and conventional diesel fuel for 75% load. Max uncertainty ± 8.028°C.

The work transfer from the turbine to the compressor drives the air flow rate to the VGT. As stated previously, the ECM is demanding the biodiesel IMP to be the same as conventional diesel which translates to the air flow rate induced by the VGT to be the

same. Figure 73 through Figure 75 show the calculated emissions air flow rate comparison between biodiesel and conventional diesel at each respective load. At 20% load the biodiesel air flow rate calculated from emissions data decreases compared to conventional diesel. This small decrease is due, as discussed earlier, to the ECM not demanding the VGT to increase the EMP to compensate for the lower exhaust temperatures. The calculated emission air flow rate at 60 and 75% load for biodiesel is similar to conventional diesel. As with 20% load, the ECM is trying to set the same air flow rate as conventional diesel, thus the similar calculated emissions air flow rates.

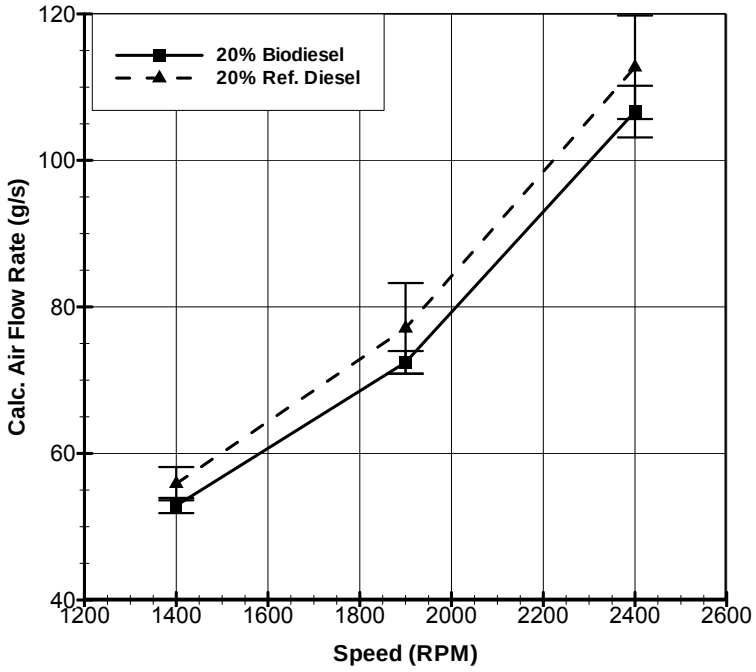

Figure 73: Calculated emissions air flow rate comparison of biodiesel and conventional diesel fuel for 20% load. Max uncertainty ± 7.07 g/s.

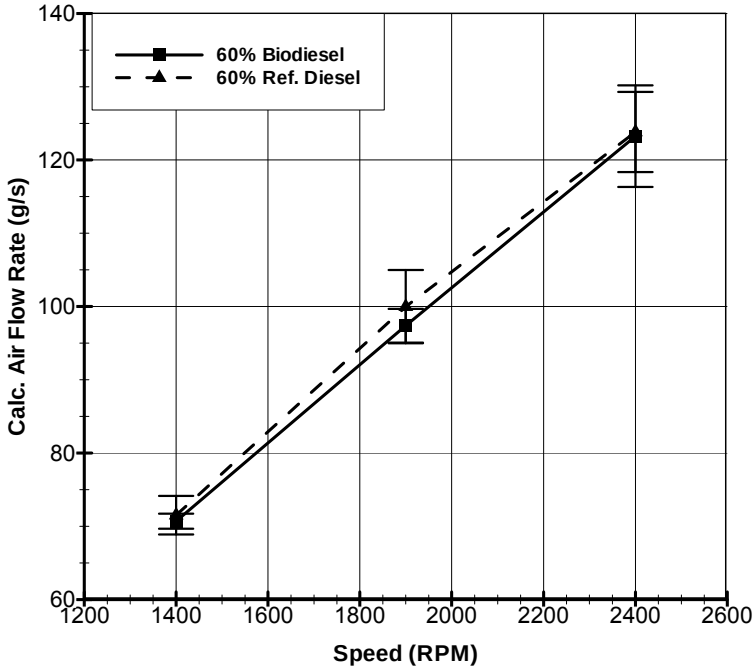

Figure 74: Calculated emissions air flow rate comparison of biodiesel and conventional diesel fuel for 60% load. Max uncertainty ± 6.93 g/s.

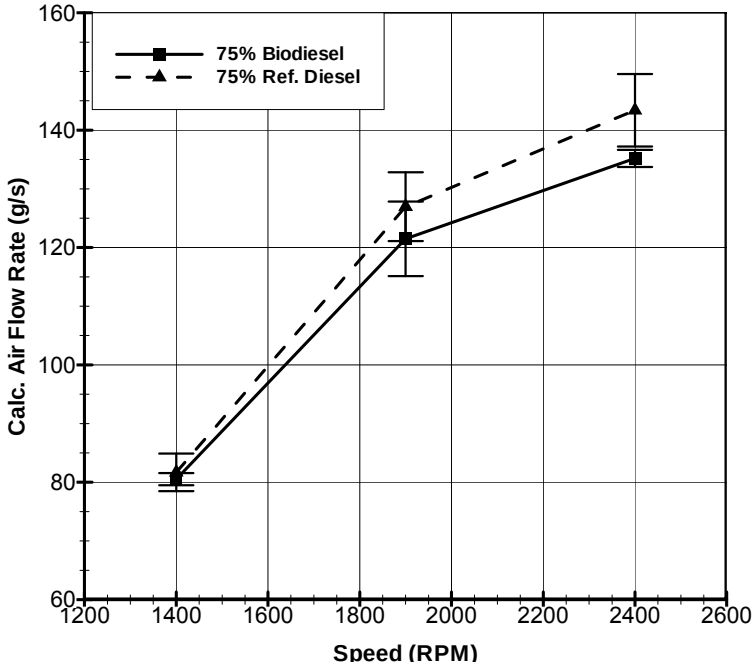

Figure 75: Calculated emissions air flow rate comparison of biodiesel and conventional diesel fuel for 75% load. Max uncertainty ± 6.35 g/s.

The biodiesel compressor pressure out (CPO), as temperature, is similar to conventional diesel. The temperature after the air is compressed is directly proportional to the increase in pressure. Therefore, CTO, shown in Figure 79 through Figure 81, follow the same trends as CPO, shown in Figure 76 through Figure 78.

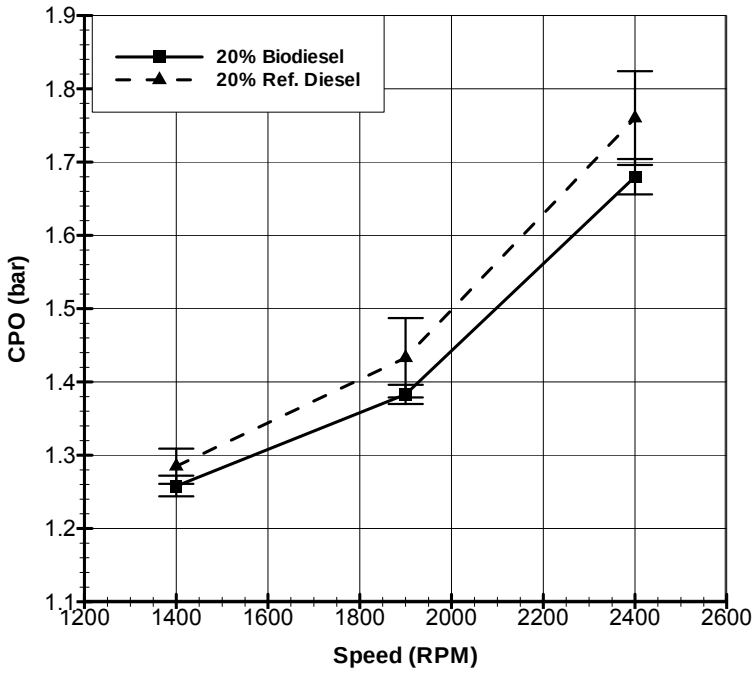

Figure 76: Compressor pressure out comparison of biodiesel and conventional diesel fuel for 20% load. Max uncertainty ± .064 bar.

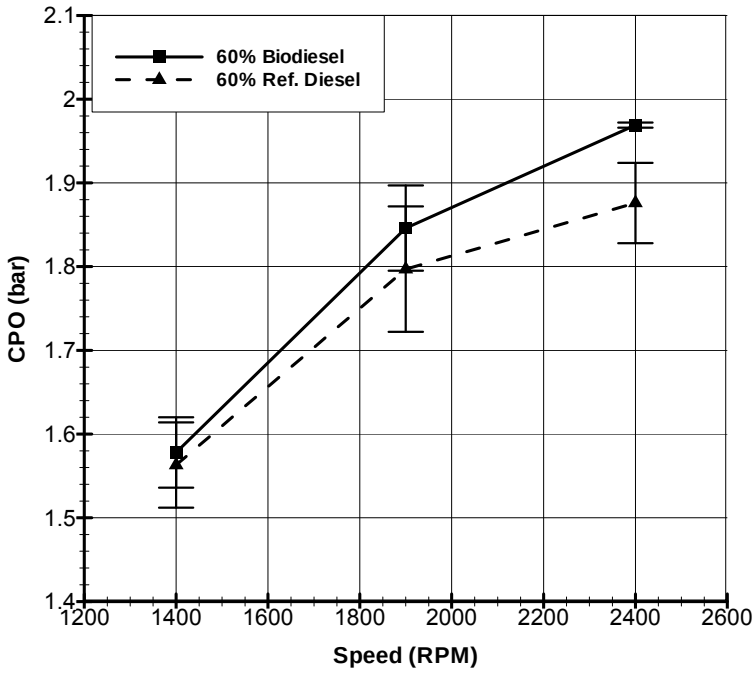

Figure 77: Compressor pressure out comparison of biodiesel and conventional diesel fuel for 60% load. Max uncertainty ± .075 bar.

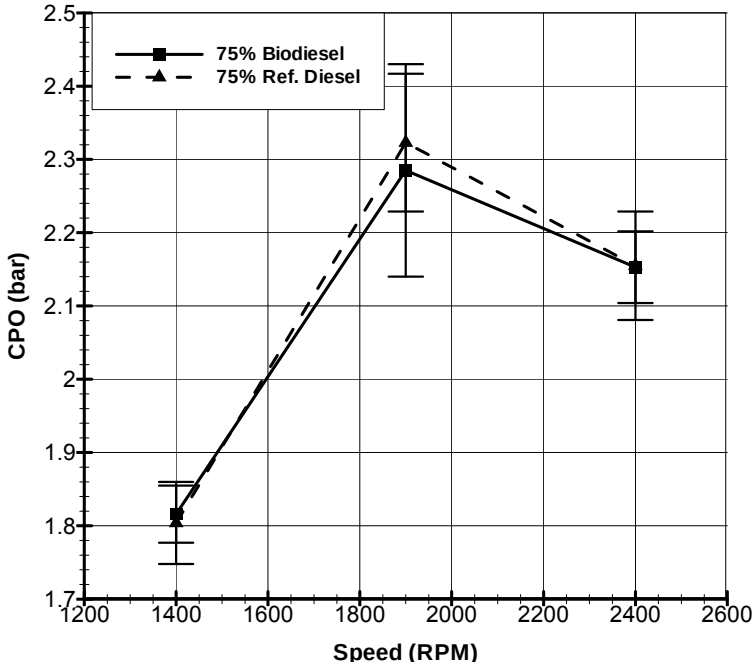

Figure 78: Compressor pressure out comparison of biodiesel and conventional diesel fuel for 75% load. Max uncertainty ± .145 bar.

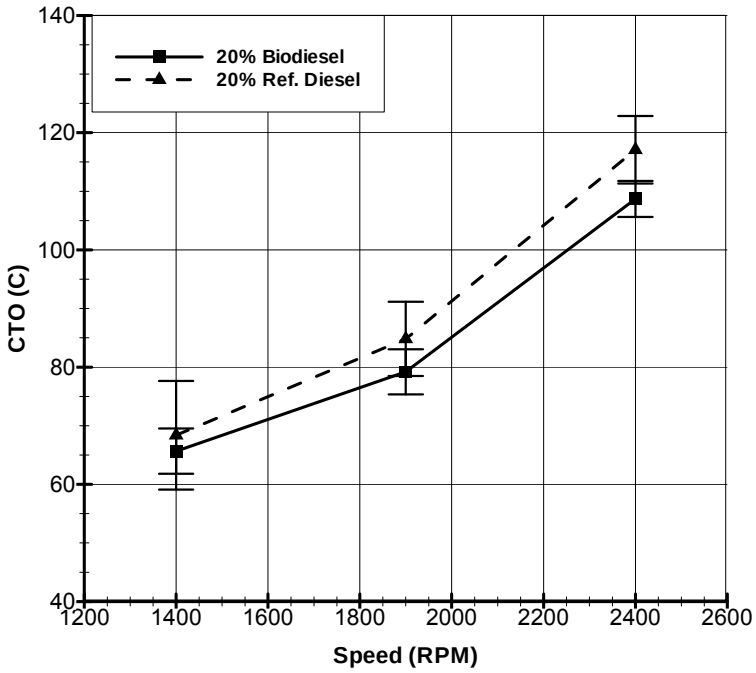

Figure 79: Compressor temperature out comparison of biodiesel and conventional diesel fuel for 20% load. Max uncertainty ± 9.272°C.

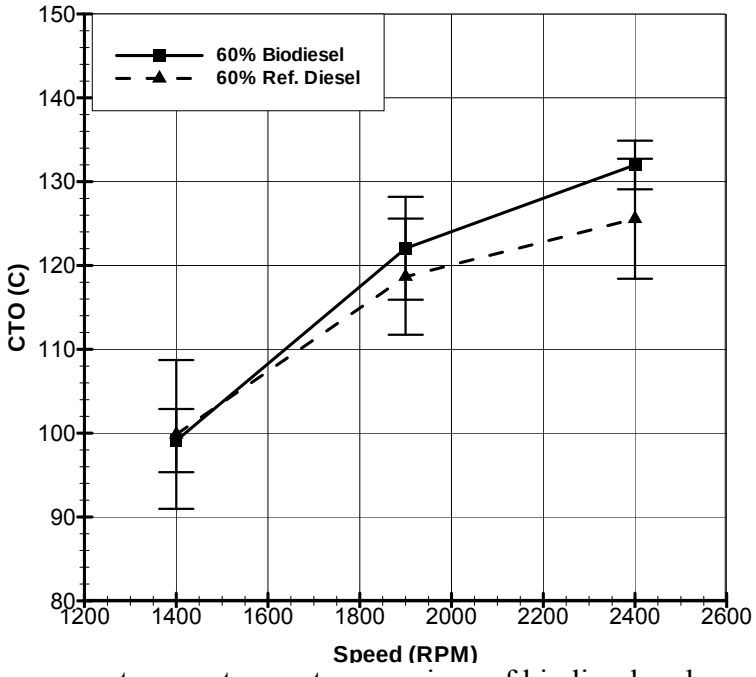

Figure 80: Compressor temperature out comparison of biodiesel and conventional diesel fuel for 60% load. Max uncertainty ± 8.875°C.

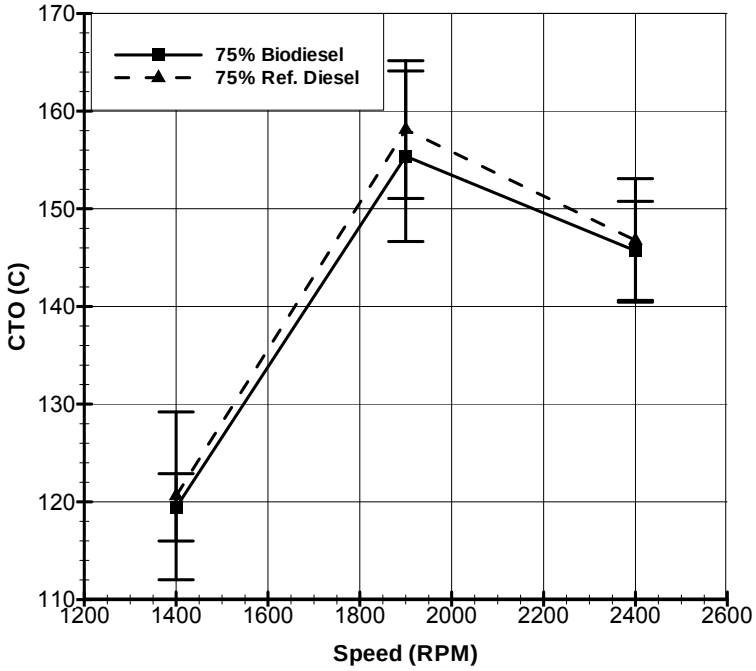

Figure 81: Compressor temperature out comparison of biodiesel and conventional diesel fuel for 75% load. Max uncertainty ± 8.736°C.

Intake manifold temperatures are functions of CTO, air flow rate through the intercooler, and EGR induction. This is not the case for 20% load because of the fact that no EGR flows for this load. The biodiesel IMT at 20% load, as shown in Figure 82, is similar to conventional diesel with a slight decrease in biodiesel at 1900 and 2400 rpm. The uncertainty of both biodiesel and conventional diesel are within each other and can be said to be a negligible temperature difference between the two fuels IMT. At 60% load shown in Figure 83, the trend of IMT should follow CTO. This, in fact, is not true and IMT is reversed with biodiesel decreasing in temperature. The reverse trend could be due to a lower amount of EGR inducted into the intake manifold for biodiesel due to the increase of CPO. The IMT at 75% load trends the same with CTO. The air flow rate at this load is similar; therefore EGR induction is the controlling factor in the

temperature shown in Figure 84. Again, as seen with 60% load, 1400 rpm shows the highest IMT over conventional diesel leading to less EGR being inducted. The higher engine speeds show similar IMT.

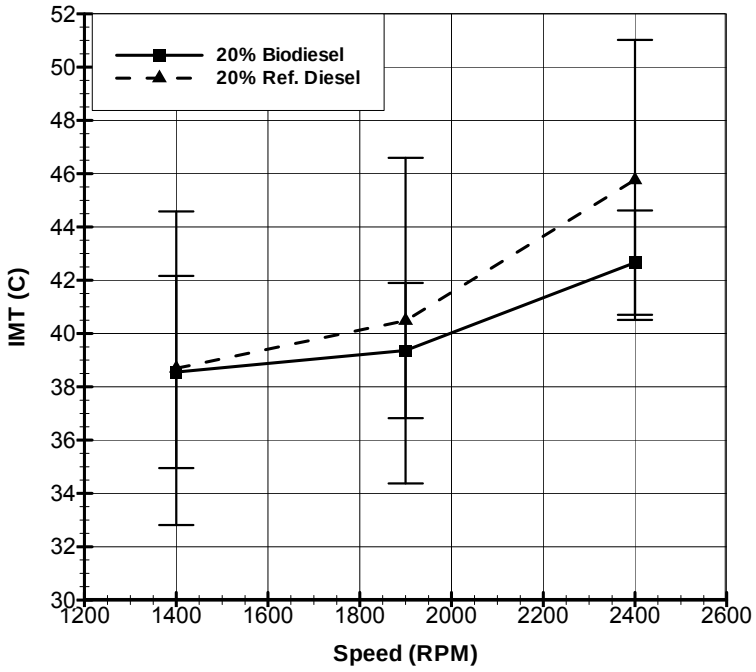

Figure 82: IMT comparison of biodiesel and conventional diesel fuel for 20% load. Max uncertainty ± 6.109°C.

In summary, the engine ECM is demanding the same air flow rate into the engine. The VGT is not able to supply the same air flow due to the lower exhaust temperatures. The VGT compensates for this lower exhaust temperature by changing its vane position. The closing of the vanes increase EMP to drive the compressor speed to induct the same amount of air. The VGT is not always successful at matching the air flow demands.

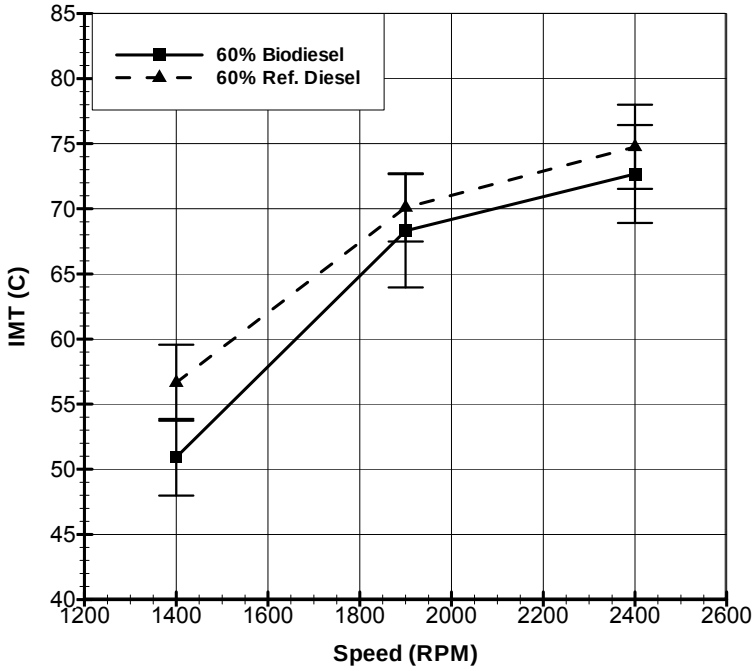

Figure 83: IMT comparison of biodiesel and conventional diesel fuel for 60% load. Max uncertainty ± 4.348°C.

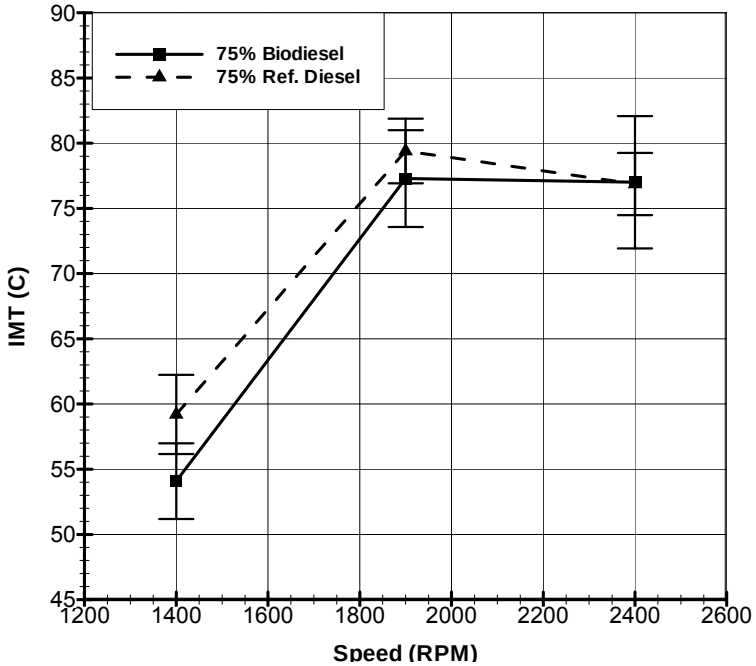

Figure 84: IMT comparison of biodiesel and conventional diesel fuel for 75% load. Max uncertainty ± 5.07°C.

4. SUMMARY AND CONCLUSION

4.1 Summary

In the wake of fossil fuel depletion, attention has been paid to using alternative renewable fuels and shifting away from the use of petroleum based fuels. Alternative fuels, such as the oil/fat derived fuels (biodiesel) used in this study, are now extensively being researched for the development of engines that will utilize them. A major research push is to study biodiesel emissions, particularly the increase in NO_x, due to global warming and air quality. In studying biodiesel, engine performance is also a major assessment tool for the viability of biodiesel becoming a mainstream energy source to power diesel engines.

In researching the background for this paper, as stated above, the major research push has been studying the emissions from biodiesel combustion particularly NO and its formation. Various papers have given performance parameters, such as torque and power. They have given these performance parameters to decrease within a 5-10% range compared to petroleum diesel. Because of the limited view on the performance of biodiesel fuelled diesel engines, this study focuses an approach to characterize the performance of a medium-duty diesel engine fuelled with biodiesel and petroleum diesel. Measurements were taken of manifold pressure and temperature, fuel flow, air flow, and torque to evaluate the differences in performance of each fuel within a John Deere 4.5 liter 4 cylinder direct injection engine with exhaust gas recirculation, common rail fuel injection, and variable turbo-charging.

The engine ECM does not distinguish between fuels thus demands the same performance of the engine regardless of the fuel. The lower exhaust from biodiesel causes the ECM to compensate for this decrease and demands the VGT to change its vane position. The change in vane position increases EMP which increases the compressor speed to induct the same amount of air. The ECM and VGT are not always successful in matching the performance.

4.2 Conclusions

In conclusion, the objective of this research study has been satisfied and the performance of the medium-duty diesel engine has been characterized using biodiesel and petroleum diesel fuel. The specific major conclusions of this research study are:

- A reduction in torque and power are seen with the use of biodiesel in fuelling a medium-duty diesel in comparison to conventional diesel. The torque and power reduction of the engine using biodiesel was about 10% compared to conventional diesel.
- Engine performance parameters consisting of fuel conversion efficiency, volumetric efficiency, intake manifold air density, displacement volume, fuel-air ratio, and the lower heating value of the fuel were evaluated to establish why torque decreased using biodiesel. The performance parameter determined to decrease torque is its heating value. The heating value of biodiesel is lower than that of petroleum diesel. All other parameters did not significantly change with biodiesel compared to petroleum diesel, thus not significantly changing the torque production of the engine.

- Another parameter evaluated that affects torque is the pumping work of the engine. At 60 and 75% load the pumping work for biodiesel is increased compared to conventional diesel. The increased pumping work decreases torque production for biodiesel.

4.3 Future Work

The objective of this study has been reached and the knowledge gained from it is the first step into gaining knowledge of biodiesel combustion in a medium-duty diesel engine. Future work to further characterize the differences between biodiesel and conventional diesel are as follows:

1. Knowing that fuelling an engine with biodiesel produces less torque, a more detailed work through in-cylinder pressure measurements can determine the in-cylinder characteristics of biodiesel compared to conventional diesel.
2. Measure the differences in changing injection timing and its effects on performance of the engine with biodiesel. In combination, use in-cylinder pressure data to determine optimum injection timing for biodiesel to obtain an optimum performance out of the engine.
3. In relation to injection timing, different type of injectors with different spray patterns and pressure can be used to evaluate fuel-air mixture mixing in the cylinder with different timings to compare the optimum setup of an engine using biodiesel to maximize performance as well as emissions.

REFERENCES

1. Heywood, J., 1988, *Internal Combustion Engine Fundamentals*, McGraw-Hill, New York, pp. 1-41.

2. Canacki, M., 2007, "Combustion Characteristics of a Turbocharged DI Compression Ignition Engine Fueled with Petroleum Diesel Fuels and Biodiesel," Bioresource Technology, **98**, pp. 1167-1175.

3. Agarwal, A., 2007, "Biofuels (Alcohols and Biodiesel) Applications as Fuels for Internal Combustion Engines," Progress in Energy and Combustion Science, **33**, pp. 233-271.

4. Demirbas, A., 2007, "Importance of Biodiesel as Transportation Fuel," Energy Policy, **9**, pp.4661-4670.

5. Demirbas, A., 2005, "Biodiesel Production from Vegetable Oil via Catalytic and Non-Catalytic Supercritical Methanol Transesterification Methods," Progress in Energy and Combustion Science, **31**, pp. 466-487.

6. Hess, M., Haas, M., Foglia, T., 2007, "Attempts to Reduce NO_x Exhaust Emissions by Using Reformulated Biodiesel," Fuel Processing Technology, **88**, pp. 693-699.

7. Korres, D., Karonis, D., Lois, E., Linck, M.,Gupta, A., 2008, "Aviation Fuel JP-5 and Biodiesel on a Diesel Engine," Fuel, **87**, pp. 70-78.

8. Proc, K., Barnitt, R., Hayes, R., Ratcliff, M., McCormick, R., Ha, L., Fang, H., 2006, "100,000-Mile Evaluation of Transit Buses Operated on Biodiesel Blends (B20)," SAE Paper No. 2006-01-3253.

9. Cheng, A., Upatnieks, A., Mueller, C., 2006, "Investigation of the Impact of Biodiesel Fuelling on NO_x Emissions Using an Optical Direct Injection Diesel Engine," International Journal of Engine Research, **7**, pp. 297-318.

10. Canakci, M., Van Gerpen, J., 2003, "Comparison of Engine Performance and Emission for Petroleum Diesel Fuel, Yellow Grease Biodiesel, and Soybean Oil Biodiesel," Transactions of the American Society of Agricultural Engineers, **46**, pp. 937-944.

11. Grabowski, M., McCormick, R., 1998, "Combustion of Fat and Vegetable Oil Derived Fuels in Diesel Engines," Progress in Energy and Combustion Science, **24**, pp. 125-164.

12. 2006, “Technical Manual, Powertech Plus 4.5L and 6.8L Diesel Engines CTM320 [CD-ROM],” Waterloo, IA: John Deere & Company.

13. Esquivel, J., Tompkins B.T., Jacobs T.J., 2008, “The Development of a Diesel Engine Experimental Research Facility for Biodiesel Combustion Studies.” Paper presented at the 2008 Technical Meeting of the Central States Section of The Combustion Institute, Tuscaloosa, Alabama.

14. Stivender, D., 1971, “Development of a Fuel Based Mass Emission Measurement Procedure,” SAE Paper No. 710604.

15. Heywood, J., 1988, *Internal Combustion Engine Fundamentals*, McGraw-Hill, New York, pp. 100-160.

16. Heywood, J., 1988, *Internal Combustion Engine Fundamentals*, McGraw-Hill, New York. pp. 712-747.

17. Ferguson, C., Kirkpatrick, A., 2001, *Internal Combustion Engines*, John Wiley & Sons, New York, pp. 334-349.

APPENDIX A

CALCULATIONS

The following appendix shows sample calculations of parameters that are used for this study. They go through the assumptions taken to calculate the parameters.

Power:

$$P = 2\pi NT$$

$$P = 2\pi * \left(\frac{rev}{\min} * \frac{1\min}{60\sec} \right) * \left(ft \cdot lbs * \frac{1kN \cdot m}{737.56\, ft \cdot lbs} \right) = \frac{kN \cdot m}{\sec} = \frac{kJ}{s} = kW$$

Fuel Conversion Efficiency:

$$\eta_f = \frac{P(kW)}{\dot{m}_f\,(g/s) * Q_{LHV}\,(MJ/kg)} = \frac{kJ}{\sec} * \frac{\sec}{g} * \frac{kg}{MJ} * \frac{1000g}{1kg} * \frac{1MJ}{1000kJ}$$

BMEP:

$V_d = 4.5L * \frac{231in^3}{3.7854L} = in^3$, $n_r = 2$ for 4 stroke cycle; 1 for 2 stroke cycle

$$BMEP = \frac{n_R * 75.4 * T(ft - lbs)}{V_d} = \frac{lb}{in^2} * \frac{.06895bar}{1 \, lb/in^2} = bar$$

PMEP:

$$EMP(bar) - IMP(bar) = bar$$

BSFC:

$$BSFC = \frac{\dot{m}_f}{P} = \frac{g}{\sec} * \frac{1}{kW} * \frac{3600\sec}{hr}$$

Volumetric Efficiency:

$$\eta_v = \frac{2\dot{m}_a}{\rho_{a,i} V_d N} = \frac{g}{\sec} * \frac{m^3}{kg} * \frac{1}{L} * \frac{\min}{rev} * \frac{3.7854L}{1gal} * \frac{264.2gal}{1m^3} * \frac{1kg}{1000g} * \frac{60\sec}{1\min}$$

Cycle Fuel and Air Flow:

$$m_{cycle} = \frac{\dot{m} * n}{N/60} = \frac{g}{s} * \frac{2rev}{cycle} * \frac{\min}{rev} * \frac{60\sec}{1\min} = \frac{g}{cycle}$$

Volumetric Flow Rate:

$$\dot{V}_f = \frac{\dot{m}}{\rho} = \frac{\frac{g}{s} * \frac{1kg}{1000g}}{\frac{kg}{m^3}} = \frac{m^3}{s} * \frac{1000L}{1m^3} * \frac{3600s}{1hr} = \frac{\dot{m} * 3600 * 1000}{1000 * \rho} = \frac{3600 * \dot{m}}{\rho} = \frac{L}{hr}$$

LHV Calculation of Biodiesel:

Assumption of Biodiesel Formula from References [2,3] is $C_{18.74}H_{34.43}O_2$.

$$C_{18.74}H_{34.43}O_2 + a(O_2 + 3.76N_2) \rightarrow bCO_2 + cH_2O + dN_2$$

C: $18.74 = b$

H: $34.43 = 2c$ $\quad c = 17.215$

O: $2 + 2a = 2b + c$ $\quad a = 26.348$

N: $7.52a = 2d$ $\quad d = 99.067$

$$C_{18.74}H_{34.43}O_2 + 26.348(O_2 + 3.76N_2) \rightarrow 18.74CO_2 + 17.215H_2O + 99.067N_2$$

$$MW_{C_{18.74}H_{34.43}O_2} = 291.62 \frac{kg_{fuel}}{kmol_{fuel}} \qquad MW_{H_2O} = 18.02 \frac{kg_{fuel}}{kmol_{fuel}}$$

$$\frac{m_{H_2O}}{m_{fuel}} = \frac{17.215 kmol_{H_2O} * MW_{H_2O}}{1 kmol_{fuel} * MW_{C_{18.74}H_{34.43}O_2}} = 1.064$$

$$LHV = 17325.78 \frac{Btu}{lb} - 1050\left(\frac{m_{H_2O}}{m_{fuel}}\right) = 16208.6 \frac{Btu}{lb}$$

or

$$16208.6 \frac{Btu}{lb} * \frac{1055.056J}{1BTU} \frac{1kJ}{1000J} * \frac{1MJ}{1000kJ} * \frac{2.204lb}{1kg} = 37.691 \frac{MJ}{kg}$$

LHV Calculation of Reference Fuel:

Hydrogen Wt % = 13.1%

Carbon Wt% = 86.9%

Find x of chemical formula of fuel from Wt%

$$CH_x + a(O_2 + 3.76N_2) \rightarrow bCO_2 + cH_2O + dN_2$$

$x = \frac{y_H}{y_C}$ Find the mol fraction of both Hydrogen and Carbon

$$MW_{fuel} = \frac{1}{\frac{mf_H}{MW_H} + \frac{mf_C}{MW_C}} = \frac{1}{\frac{.131}{1.008} + \frac{.869}{12.01}} = 4.943 \frac{kg_{fuel}}{kmol_{fuel}}$$

$$y_H = mf_H * \frac{MW_{fuel}}{MW_H} = .131 \frac{kg_H}{kg_{fuel}} * \frac{4.943 \frac{kg_{fuel}}{kmol_{fuel}}}{1.008 \frac{kg_H}{kmol_H}} = .642 \frac{kmol_H}{kmol_{fuel}}$$

$$y_C = mf_C * \frac{MW_{fuel}}{MW_C} = .869 \frac{kg_C}{kg_{fuel}} * \frac{4.943 \frac{kg_{fuel}}{kmol_{fuel}}}{12.01 \frac{kg_C}{kmol_C}} = .358 \frac{kmol_C}{kmol_{fuel}}$$

$$x = \frac{.642 \frac{kmol_H}{kmol_{fuel}}}{.358 \frac{kmol_C}{kmol_{fuel}}} = 1.796$$

$$CH_{1.796} + a(O_2 + 3.76N_2) \rightarrow bCO_2 + cH_2O + dN_2$$

C: $1 = b$

H: $1.796 = 2c$ $\quad c = .898$

O: $2a = 2b + c$ $\quad a = 1.449$

N: $7.52a = 2d$ $\quad d = 5.448$

$$CH_{1.796} + 1.449(O_2 + 3.76N_2) \rightarrow CO_2 + .898H_2O + 5.448N_2$$

$$MW_{CH_{1.796}} = 13.82 \frac{kg_{fuel}}{kmol_{fuel}} \qquad MW_{H_2O} = 18.02 \frac{kg_{fuel}}{kmol_{fuel}}$$

$$\frac{m_{H_2O}}{m_{fuel}} = \frac{.898 kmol_{H_2O} * MW_{H_2O}}{1 kmol_{fuel} * MW_{CH_{1.796}}} = 1.17$$

$$LHV = 19393.689 \frac{Btu}{lb} - 1050\left(\frac{m_{H_2O}}{m_{fuel}}\right) = 18165.189 \frac{Btu}{lb}$$

Or

$$18165.189\frac{Btu}{lb}*\frac{1055.056J}{1BTU}\frac{1kJ}{1000J}*\frac{1MJ}{1000kJ}*\frac{2.204lb}{1kg}=42.240\frac{MJ}{kg}$$

Gross Heat of Combustion (HHV):

Reference Fuel: $$19393\frac{Btu}{lb}*\frac{1055.056J}{1BTU}\frac{1kJ}{1000J}*\frac{1MJ}{1000kJ}*\frac{2.204lb}{1kg}=45.095\frac{MJ}{kg}$$

Biodiesel Fuel: $$17325.78\frac{Btu}{lb}*\frac{1055.056J}{1BTU}\frac{1kJ}{1000J}*\frac{1MJ}{1000kJ}*\frac{2.204lb}{1kg}=40.287\frac{MJ}{kg}$$

Density of Intake Air:

Barometric Pressure: $740mmHg*\frac{.01bar}{7.501mmHg}=.987bar$

Relative Humidity: $\phi=\frac{p_v}{p_g}$

p_v = actual vapor pressure p_g = saturation pressure at the same temperature

Mole Fraction: $y_v=\frac{p_v}{p_{atm}}$ $P_{air}=P_{IMP}-y_vP_{IMP}-y_{CO_2}P_{IMP}$

Humidity Ratio: $\omega=.0622\frac{p_v}{p_a}=0.622\frac{p_v}{P-p_v}=0.622\frac{\phi p_g}{P-\phi p_g}$

Calculation using EES:
Obtain the humidity ratio using temperature, pressure, and relative humidity at atmospheric conditions.
Solve for p_g using the humidity ratio equation.
Knowing relative humidity and p_g, the vapor pressure is calculated.
The mole fraction of vapor in the air can now be calculated from the division of vapor pressure by total atmospheric pressure.
The pressure of the air in the intake manifold can now be solved by multiplying the mole fraction of vapor to the intake manifold pressure. This is the vapor pressure in the intake manifold. When EGR is demanded by the ECM, CO_2 inducted into the intake manifold is also accounted for in the pressure of air in the intake manifold. The partial pressures of vapor and CO_2 can now be taken from the total pressure of the intake manifold to give the pressure of air in the intake manifold.
The density now can be solved two ways, either by the ideal gas assumption or by EES. Using EES, input the intake manifold temperature and the pressure of air into the density function of Air_ha.

APPENDIX B

HEATING VALUE ANALYSIS

Table 5: Gross Heating Value Analysis
Parr 6200 Calorimeter
Results:

Sample	B-100	REFDIESEL
Replicate 1	Sample ID: BIO-S1 Weight: 0.4778 Fuse: 15.0000 Sulfur: 0.0000 Init. Temp.: 26.3244 Jacket Temp.: 30.0098 EE Value: 2397.8270 Spike Weight: 0.0000 Acid: 10.0000 Temp. Rise: 1.9170 Gross Heat: 17222.893Btu/lb	Sample ID: REFD-S1 Weight: 0.4869 Fuse: 15.0000 Sulfur: 0.0000 Init. Temp.: 24.9227 Jacket Temp.: 30.0111 EE Value: 2397.8270 Spike Weight: 0.0000 Acid: 10.0000 Temp. Rise: 2.2047 Gross Heat: 19451.181 Btu/lb
Replicate 2	Sample ID: BIO-S2 Weight: 0.4918 Fuse: 15.0000 Sulfur: 0.0000 Init. Temp.: 24.6200 Jacket Temp.: 29.6200 EE Value: 2397.8270 Spike Weight: 0.0000 Acid: 10.0000 Temp. Rise: 1.9877 Gross Heat: 17352.413 Btu/lb	Sample ID: REFD-S2 Weight: 0.4852 Fuse: 15.0000 Sulfur: 0.0000 Init. Temp.: 25.8150 Jacket Temp.: 30.0463 EE Value: 2397.8270 Spike Weight: 0.0000 Acid: 10.0000 Temp. Rise: 2.1899 Gross Heat: 19387.339 Btu/lb
Replicate 3	Sample ID: BIO-S3 Weight: 0.4899 Fuse: 15.0000 Sulfur: 0.0000 Init. Temp.: 22.7987 Jacket Temp.: 29.9321 EE Value: 2397.8270 Spike Weight: 0.0000 Acid: 10.0000 Temp. Rise: 1.9857 Gross Heat: 17402.034 Btu/lb	Sample ID: REFD-S3 Weight: 0.5177 Fuse: 15.0000 Sulfur: 0.0000 Init. Temp.: 25.7773 Jacket Temp.: 29.9612 EE Value: 2397.8270 Spike Weight: 0.0000 Acid: 10.0000 Temp. Rise: 2.3305 Gross Heat: 19342.546 Btu/lb
Average Gross heating Value (Btu/lb)	17325.780	19393.689

Analyzed at:Bio Energy Testing and Analysis Laboratory
Department of Biological and Agricultural Engineering
109 Price Hobgood Building
Texas A&M University
College Station, TX 77843

APPENDIX C

ENGINE AND DYNO OPERATING PROCEDURE

- Check SAE side of dyno to see if SAE engine shaft is connected. Make sure to disconnect SAE engine if connected.
- Start generator of dyno by pulling the handle to the start position and waiting a few seconds and then pushing the handle back to the run position.
- Check dyno speed encoder to make sure it has not pulled out. Rotate back if it has pulled out and rotate lock nuts until tight.
- Open exhaust outlet port next to the test engine bed by lifting it up. Close after engine is turned off.
- Connect fuel system and make sure once engine key is turned to the first notch that the fuel pump is working and the pressure gauge reads about 7 psi.
- Start PXI1010 and SCXI chassis powers, there should be two switches and both need to be turned on.
- Turn on and boot up the main computer.
- Double click on JacobsDynoControllerSS.vi in the folder “Jacobs” on the desktop.
- Go to Operate → Switch Execution Target. At this point the strain gauge signal has to be verified as working correctly.
- Click on configure → Expand Data Neighborhood → Right Click on the name in the configuration tree and select Test. Start on the first strain gauge and continue down the line with the next two. The first strain gauge will test at about an offset of 69. Once the three are tested go back to the first one and it should read about 0.
- Select DAQ::3 RT Engine on PXI-7030 and make sure “Reset Device” is checked and click “OK”.
- After the reboot procedure, reopen JacobsDynoControllerSS.vi.
- Go to operate → Download application
- On the screen at the lower left hand of the page, set the visual switch to a down position and click icon below it to manual. The dyno load will be set in the box marked “Manual IF”.
- Click the run (or arrow) button.
- Start engine and allow warming up for about 2-3 minutes before engaging clutch.
- Engage PTO clutch.
- Set desired speed to 1200 RPM on engine controller by pushing the up (or bunny) button.
- The set speed should now be lowered until the percentage load on the engine controller display reads about 30%.
- Allow engine to warm up to about 130°F before commencing testing.

VITA

Jason Esquivel received his Bachelor of Science degree in mechanical engineering from The Florida State University in 2002. After a short stint in the work force, he decided to pursue a Master of Science degree in mechanical engineering. He entered the mechanical engineering program at Texas A&M University in the September 2004 and was awarded a fellowship by The National Consortium for Graduate Degrees for Minorities in Engineering and Science (GEM). He received a Master of Science in mechanical engineering from Texas A&M University in 2008. His research interests include thermodynamics and combustion of alternative fuels with a specific application to internal combustion engines.

Mr. Esquivel can be reached at Texas A&M University, Mechanical Engineering Department, College Station, TX 77843. His email is esqui317@aol.com.